INFORMATION TO USERS

This manuscript has been reproduced from the microfilm master. UMI films the text directly from the original or copy submitted. Thus, some thesis and dissertation copies are in typewriter face, while others may be from any type of computer printer.

The quality of this reproduction is dependent upon the quality of the copy submitted. Broken or indistinct print, colored or poor quality illustrations and photographs, print bleedthrough, substandard margins, and improper alignment can adversely affect reproduction.

In the unlikely event that the author did not send UMI a complete manuscript and there are missing pages, these will be noted. Also, if unauthorized copyright material had to be removed, a note will indicate the deletion.

Oversize materials (e.g., maps, drawings, charts) are reproduced by sectioning the original, beginning at the upper left-hand corner and continuing from left to right in equal sections with small overlaps. Each original is also photographed in one exposure and is included in reduced form at the back of the book.

Photographs included in the original manuscript have been reproduced xerographically in this copy. Higher quality 6" x 9" black and white photographic prints are available for any photographs or illustrations appearing in this copy for an additional charge. Contact UMI directly to order.

Finite element analysis of cellular structures subjected to wave loads

Bakır, Bahadır Sadık, Ph.D.

Iowa State University, 1993

Finite element analysis of cellular structures subjected to

wave loads

by

Bahadır Sadık Bakır

A Dissertation Submitted to the

Graduate Faculty in Partial Fulfillment of the

Requirements for the Degree of

DOCTOR OF PHILOSOPHY

Department: Civil and Construction Engineering
Major: Civil Engineering (Structural Engineering)

Approved:

In Charge of Major' Work

For the Major Department

For the Graduate College

Iowa State University
Ames, Iowa

1993

TABLE OF CONTENTS

ACKNOWLEDGEMENTS

I would like to express my sincere appreciation to my advisors, Dr. Terry J. Wipf and Dr. Lowell F. Greimann, not only for their excellent guidance, but also for their encouragement, support and understanding throughout this study.

I am thankful to Dr. Fouad S. Fanous, for his guidance regarding ANSYS finite element package and for serving in my graduate committee. I would like to thank the other members of my graduate committee, Dr. Robert A. Lohnes and Dr Loren W. Zachary, for their time, wisdom and courtesy.

I would like to extend my sincere thanks to my colleague and friend, Rama K. Challa, for his contributions regarding parts of this study.

I am thankful to my parents for their guidance and encouragement throughout my career. I am indebted to my daughter, Bahar, for being an endless source of joy. Finally, I would like to express my deep gratitude to my wife, Ufuk Bakır, for her continuous encouragement, understanding and patience during all these years.

1. INTRODUCTION

1.1. Background

Cellular cofferdams, in general, are double wall structures constructed of interlocking steel sheet piles forming the cells which are filled with geomaterials, most often of the granular type. Originally, they were developed as temporary structures to exclude water from an excavation to provide a dry construction environment. Later they were used increasingly as permanent structures retaining water, soil or both. The combination of fill and cells of steel sheet piles, which individually are unstable, make cofferdams a unique type of structure which is capable of withstanding lateral loads. Relatively large displacements which are an inherent characteristic of cellular structures do not hinder their performance. Common geometries of cells include circular, cloverleaf and diaphragm as shown in Figure 1.1.

The study presented here covers a part of a project initiated to investigate the failures in a cellular cofferdam breakwater which was built in 1934 as a permanent structure near Calumet Harbor in Lake Michigan near Chicago, Illinois. Significant damage over some of the cells was observed after a storm in February 1984 [1]. The project was conducted by the Structural Division of the Civil and Construction Engineering Department at Iowa State University starting in 1988. The sponsor was the Chicago District, Army Corps of Engineers.
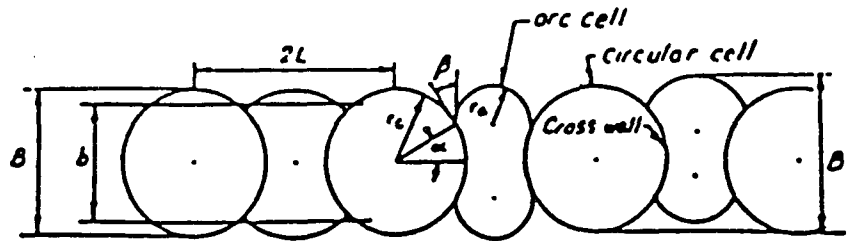
a. Circular Cofferdam
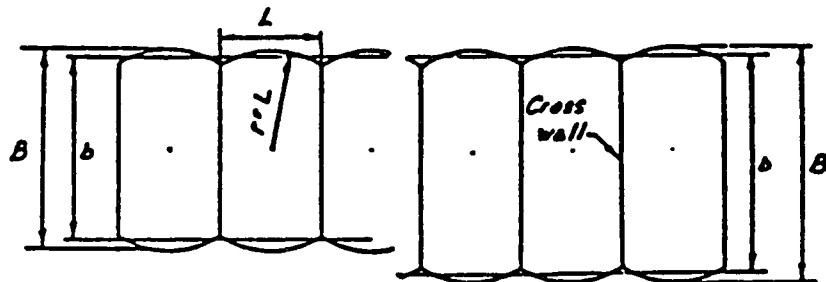
b. Diaphram Cofferdam
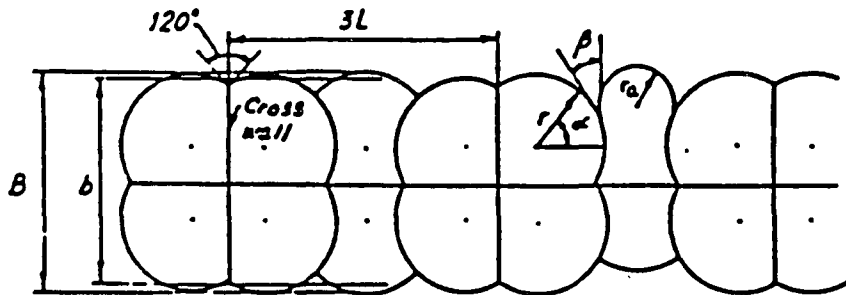
c. Cloverleaf Cofferdam

Legend

b   equivolent width of cellular cofferdom; width of fictitious
    straight-wall cofferdom of some plan area or section
    modulus generally b=0.8B to 0.9B
B   total width of cellular cofferdom
L   average distance between cross wall
r   radius of circular cell wall, diaphrom wall, or cloverleof wall
    as shown

Figure 1.1   Common cell configurations (Lacroix   et al. [11]).

The objectives of the project were to examine the possible failure modes and to evaluate the present condition of the structure as the basis for future rehabilitation [2].

The project had four major parts (see Figures 1.2 and 1.3):

1. Instrumentation and Data Acquisition: A system of strain gauges and data acquisition equipment was installed on two of the cells. The data could instantaneously be downloaded to a personal computer at the base station located at Iowa State University during storms that caused considerable wave action over the breakwater.

2. Force Field Estimation: Wave forces were determined by wave pressures theories. The properties of the waves were chosen in accordance with the direction-dependent local wave data.

3. Finite Element Modelling and Application: The structural analysis of the breakwater was conducted using a two-dimensional finite element model. The stress fluctuations in the sheet piles were determined for the wave pressures generated in the previous step.

4. Laboratory Testing: Sheet pile specimens were subjected to cyclic loads of different magnitude until failure. The data was used in conjunction with the finite element analysis to predict sheet pile failures
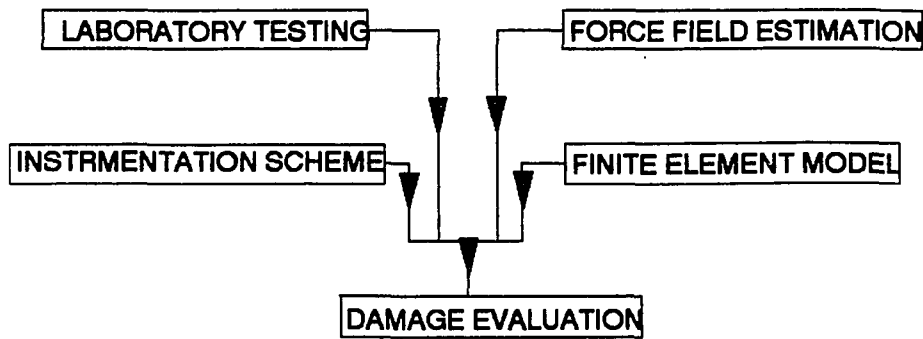
Figure 1.2 Overall solution approach.
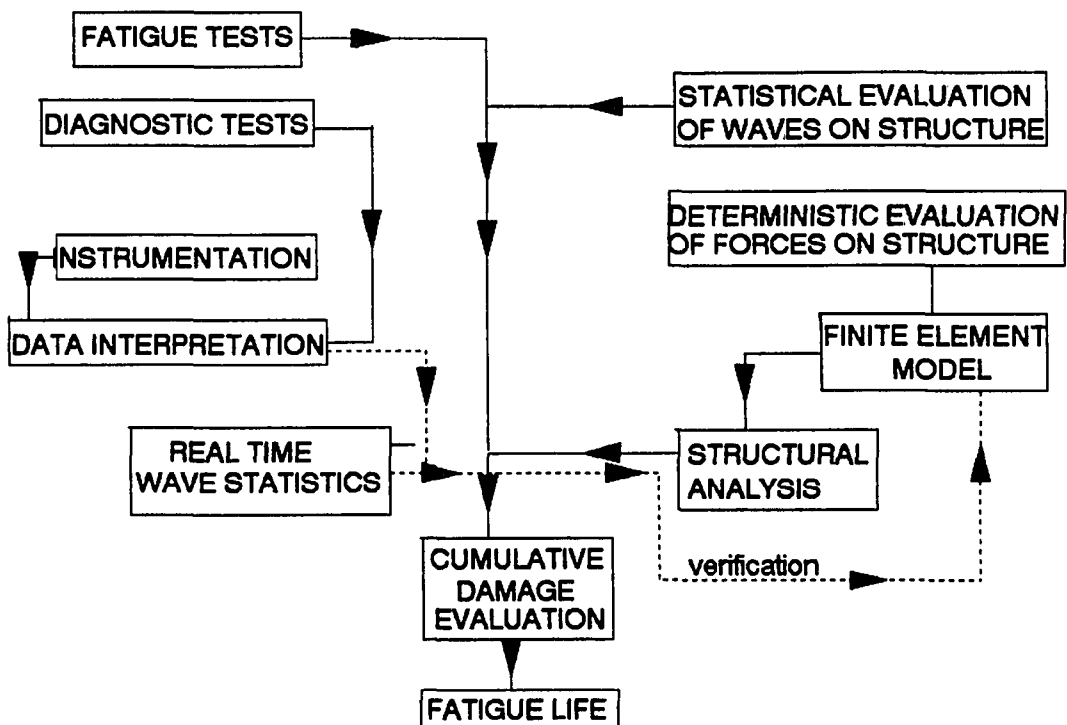
Figure 1.3 Project flow chart.

due to fatigue.

Use of cofferdams as breakwater structures is rather uncommon. No available information exists in the literature on either cofferdam performance under wave action or reported damage similar to the cell failures at the Calumet Harbor Breakwater. The instrumentation system installed over the structure provided an excellent opportunity to understand the behavior of the structure under wave action and to test the capabilities of the available methods under wave loads. Also, since the indications suggested that the most likely reason for the cell failures was metal fatigue, a methodology was developed to provide data for fatigue analysis and service life assessment.

The study described herein undertakes the finite element modelling and application part (Part 3) of the above project. The input data for the study is provided by the force field estimation part (Part 2) and the results are verified with the recorded data for the first part (Part 1).

1.2. Objective

The overall objective of this study was to determine the interlock forces caused by the wave action on the Calumet Harbor Breakwater.

1.3. Failures at the Calumet Harbor Breakwater
1.3.1. Description of the breakwater structure

The Calumet Harbor breakwater was built in 1934 to mitigate and contain the damage due to wave action on the

Calumet Harbor in Lake Michigan, near Chicago, Illinois. The
location of the structure is shown in Figure 1.4. The
breakwater was built in two sections, reaches A and B, which
formed an attached breakwater built of timber cribs, and reach
C, the detached breakwater built of steel sheet pile cells.
In this study, the structural behavior of the steel sheet pile
cells in reach C will be investigated.

Reach C of the breakwater consists of 131 stone-filled
steel sheet pile cells of diaphragm type with a width of 41
ft. at their widest point. The diaphragm walls are 38 ft. 3
in. apart. The cross-sectional elevation and plan views of
the breakwater are illustrated in Figure 1.5. Type PSA23
steel sheet piles, 46 ft. long, are used in the construction.
The structure is founded on clay and sand at lake bottom and
the cell fill consists of quarry run topped by bedding stones
and concrete capping stones. Toe protection is ensured on
both the lake side and the harbor side by a berm, topped by
stone riprap.

1.3.2. Structural damage and site observations

Significant damage to the structure was recorded during a
storm in February 1984. Three cells, located about 600 ft.
from the east end of the breakwater, failed (Figures 1.6, 1.7,
1.8). In October 1984 an inspection by Corps of Engineers
personnel revealed split piles at the intersection of two
cells and settled capstones as shown in Figures 1.9 and 1.10.
The sheet piles were repaired by welding, and protective stone

N

ILLINOIS

IND

CHICAGO DISTRICT
STONE STORAGE
DOCK

CALUMET RIVER

GAP 1700'

REACH A

2562'

PORT AUTHORITY

REACH B

ATTACHED
BREAKWATER

(TIMBER CRIB)

2492'

CHICAGO
AREA
CONFINED
DISPOSAL
FACILITY

GAP 616'

LAKE MICHIGAN

REACH C

DETACHED
BREAKWATER

(SHEET PILE)

5007'

COAST GUARD
STATION

MONITORED CELL LOCATIONS

LIGHT HOUSE
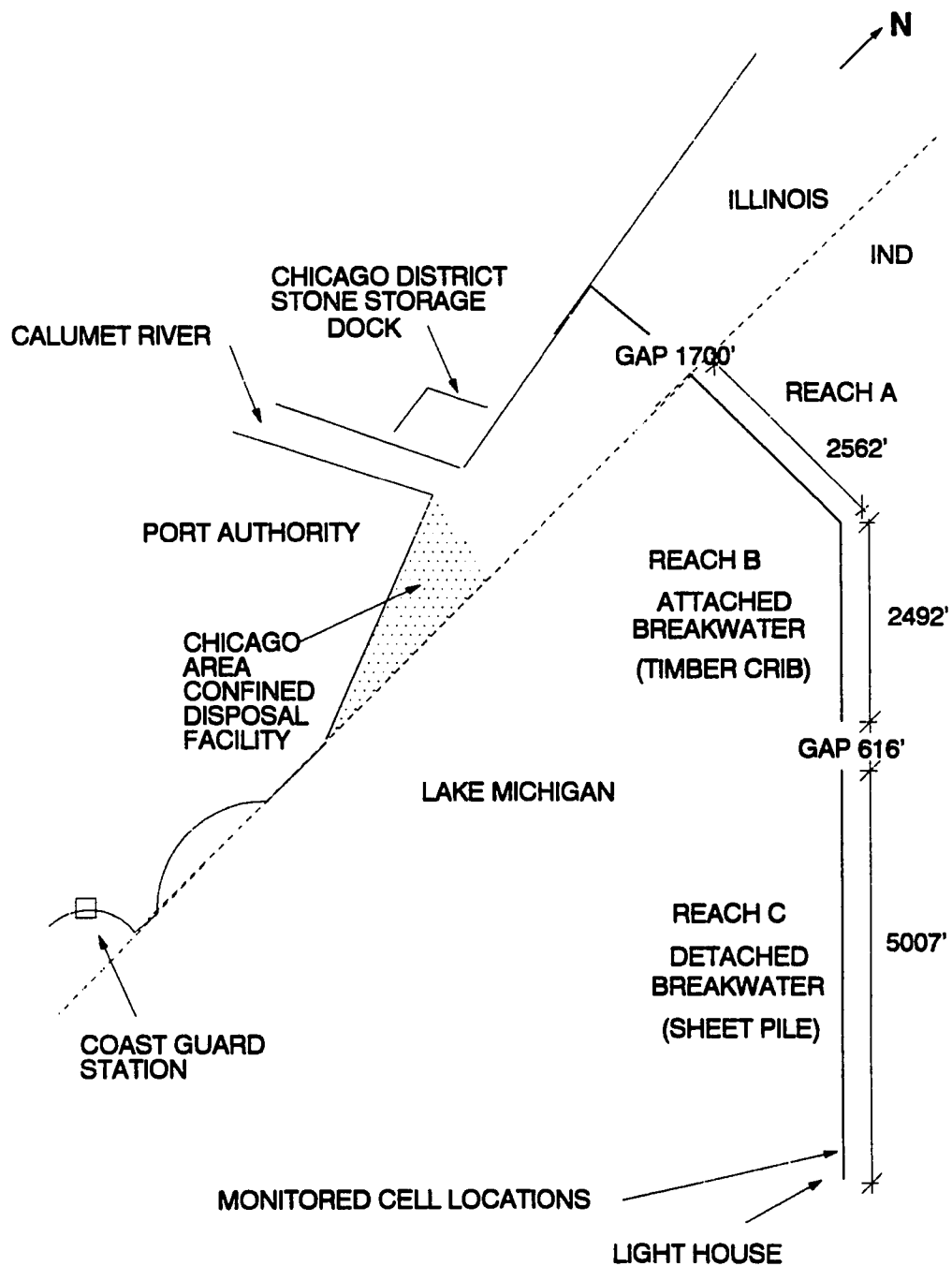
Figure 1.4 Location of Calumet Harbor breakwater.

Y - DIAPHRAGM

CELL WALL

DIAPHRAGM
WALL

CELL WALL

41'-1"   31'

38'-3"

PLAN VIEW

CAPSTONE

6'

LWD

BEDDING STONE

QUARRY RUN STONE FILL

19'

TOE PROTECTION
(BERM)

12'

3'   SAND

6'

CLAY
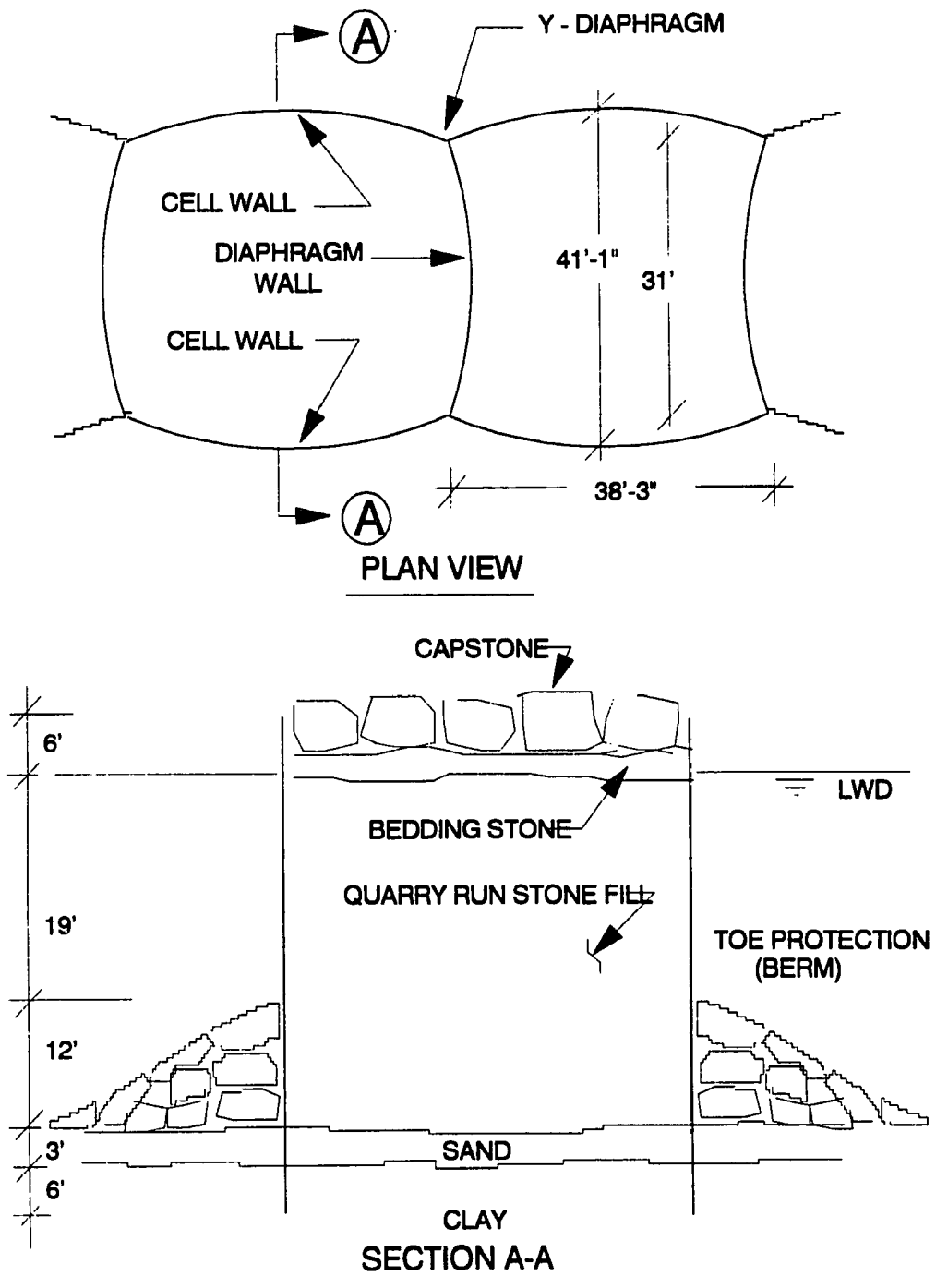
SECTION A-A

Figure 1.5   Sectional elevation and plan view of breakwater
cells.
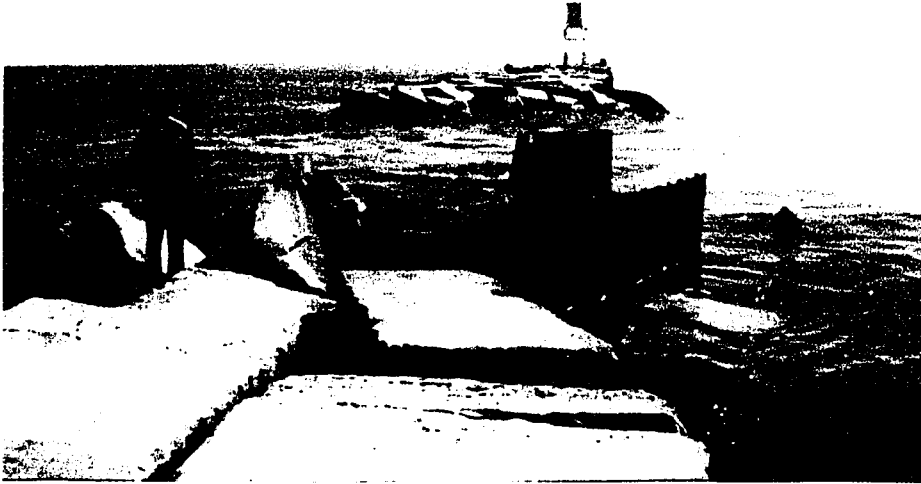
Figure 1.6   View towards Southeast end of the breakwater
             indicating failed cells.

Figure 1.7   View towards Northwest end of the breakwater
             indicating failed cells.

Figure 1.8   A view of the failed cells during a reconnaissance
              survey
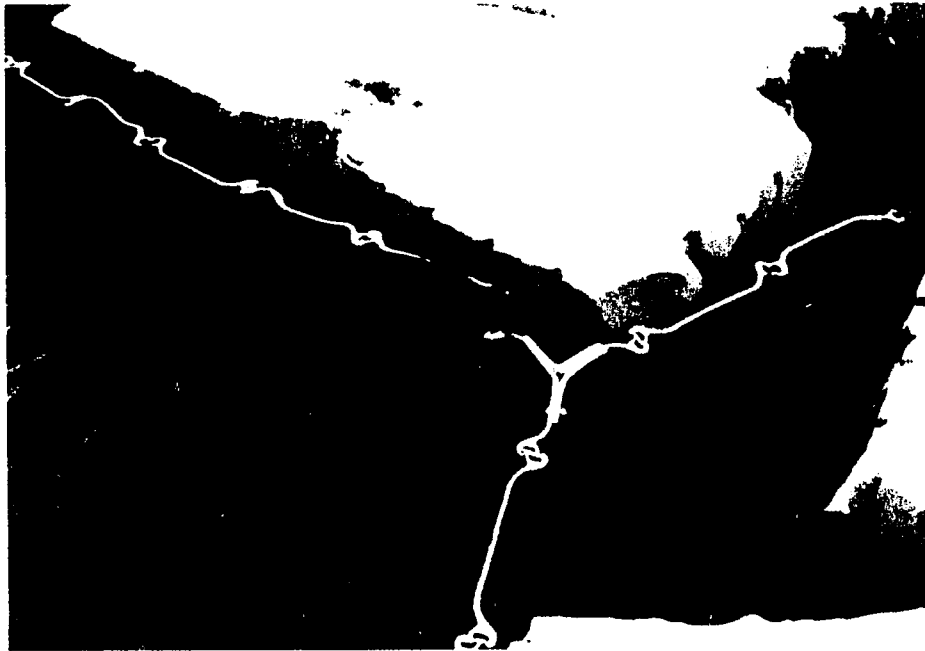
Figure 1.9   Photograph of a cell indicating split piles at a Y-
              intersection

Figure 1.10 View of the structure towards Southeast end
indicating settled capstones.

was placed to create a rubble mound in the gap created by the failed sheet-piles. The rubble mound is shown in Figure 1.11.

Other recorded instances of damage to the structure include ship impact damage in 1957 and failure of a cell diaphragm in 1957. Intermittent repairs were made to the structure for the tears that occurred in the cell walls and diaphragm.

Some of the piles had slight damage on top possibly due to either hard driving or from impact during the handling of the large capstones. At several places where the sheet piles have been curled over from hard driving, the webs have a fracture crack extending down a few inches from the top. These cracks appear to be dormant.

The cells appear to be bulged out and almost all of the sheet piles exhibit dishing even above the still water level which is the characteristic deformation of shallow arc type piles. Such deformations indicate that the sheet piles have been subjected to interlock forces above the recommended working strength of 3000 lb/in. This does not indicate, however, imminent failure since the piles have an ultimate strength of 12000 lb/in. As a direct result of bulging of the cells, fill has settled considerably at some locations. Detailed records in the past have shown settlements up to 3 ft. on the lake side, with very little, if any, on the harbor side [1].

Figure 1.11   Photograph of rubble mound created at cells 115
and 116.

1.3.3.Failure analysis

A design value of 3000 lb/in was used as the maximum allowable interlock tension for the type of piles (PSA23) in the Calumet Harbor breakwater construction. This value is rather conservative under static loading conditions. It includes a safety factor of 4 over the ultimate interlock strength of 12000 lb/in. During wave action, each wave exerts alternating positive and negative pressures from crest to trough on the lakeward face. A net lakeward hydrostatic force accompanying the crest position is also exerted on the sheet piles by the water inside the cell. After over 50 years of service, tens of millions of cycles of loading has been exerted on the sheet pile. Metal fatigue begins to be a very serious hazard at fairly modest stress levels after this many cycles [3]. The foregoing discussion suggests that the primary reason for the failures in the sheet pile was metal fatigue.

The observations indicate that stresses over 3000 lb/in. design value have been experienced by the cell interlocks in the breakwater. The possible levels of interlock forces during a storm action were analyzed by the Army Corps of Engineers employing conventional methods as summarized in the Reconnaissance Report [1]. In this analysis, a lateral earth pressure coefficient of 0.3 was selected rather than 0.4 as recommended by Terzaghi, reasoning the internal strength of the fill would be fully mobilized, as hinted by the observed

cell deformations. In addition, only the hydrostatic pressure effects of an approximately 20 ft. wave over the structure was considered. The results indicate that the over stresses in interlocks may be as high as 70% above the 3000 lb/in. design value. Also it was argued that the piling on the lake side were subjected to cyclic loading in cantilever action causing strain hardening in the piles and aggravating the over stress condition of the piles. Although this behavior is shown in the calculations to create high stresses, cantilever action would create horizontal cracking in the sheet piles which can neither directly cause the cell failures nor corresponds to the observed crack pattern on the sheetpiles.

Swatek was also consulted by the Army Corps of Engineers about the cell failures of the breakwater. His view was that the most probable cause of failure was the cantilever action of the unsupported top edges of sheet piles which exerted excessive forces on the Y-sections and caused cracks that lead to bursts in the piling. He also mentioned that the steel sheet piles would have lower impact values at the cold temperatures of the Lake Michigan in the winter season as indicated by Charpy tests [1].

Other possible failure modes related with external stability like sliding, cell overturning or foundation failure can confidently be eliminated since the tops of all the sheet piles remain at the original elevations. No visible movement of the top occurred and the horizontal alignment of the

structure is quite good.

The cumulative effects of the wave action on the structural condition of the breakwater over the decades had to be assessed. During major wave activity, hydrostatic and hydrodynamic forces cause additional incremental deformations of the sheet piles. The fill material is remolded and compacted by the wave induced motions and the gravitational forces. In other words, the fill is resettled and compacted after every storm. This behavior should be expected to be more dominant on the lake side and in the upper levels of the structure where wave forces are rather effective. This conclusion is supported by the observed settlement pattern of the fill. Considering the consequences of cumulative wave effects, in-situ earth pressures acting over the sheet piles may be quite different from those resulting from static loads alone. Therefore, a more reliable rationale other than the conventional approach is required to assess the interlock force levels for the breakwater.

1.4. Analysis and Design of Cofferdams

Presently, there exist two fundamentally different approaches for the analysis and design of cellular structures. Conventional methods, the majority of which were developed 3 to 5 decades ago, are semi-empirical. Finite element methods, which have been developed in the past 15 years provide considerable advantages by incorporating material nonlinearities and interaction effects among the structural

components.

1.4.1. Conventional design theories

Historically, the basis for the design of cellular

structures is essentially semi-empirical. Theoretical models

and design methods were originally proposed by Pennoyer [4]

and were later modified and extended by Terzaghi [5].

Alternative design concepts and modifications have been

proposed by Cummings [6], Krynine [7], Hansen [8], Department

of the Navy [9] and Schroeder and Maitland [10].

Conventional design approaches for cellular structures

involve consideration of internal and external stability.

External stability requires adequate safety factors against

sliding and overturning. Internal stability considers safety

against bursting of interlocks and shear of cell fill. The

methods for design have been discussed by Terzaghi [5],

Lacroix et al. [11], Dismuke [12], Schroeder and Maitland [10]

and U.S. Army Engineer Waterways Station [13].

Experience with cellular cofferdams over time has proven

that cell failures are most often related to the interlock

tension issue. Even though these problems were, in general,

attributed to faulty fabrication or inadequate design of T-

and Y-sections, the nature and magnitude of interlock tension

and the use of proper factor of safety remains a matter of

concern. Conventional methods compute the interlock forces by

assuming that the cellular structure behaves as a thin walled

cylinder, subjected to gravity loads from the cell fill and

surcharge. Empirical rules indicate that the interlock force increases linearly with depth from the top to a point one-quarter of the free standing height of the cell above the dredge line [11]. Restraint due to embedment is assumed to result in zero interlock force at or near the dredge line.

The choice of a lateral earth pressure coefficient remains to be rather speculative in the conventional approach as different design methods suggest values in a range from 0.3 to 0.5. These two values limit the earth pressure variation on the sheet piles between the active and the at rest conditions for a fill material having 30° internal friction angle. Furthermore, each method suggests different pressure distribution patterns. Predictions of interlock tensions differ significantly. A similar argument exists for the analysis of shear failure of the cell under lateral loading. Each conventional method assumes different positions for the failure surface as well as different values of lateral earth pressure coefficient.

Based on large scale model tests, Schroeder and Maitland [10] have indicated that the external stability consideration is redundant and should be discontinued. According to their work, internal failure in a typical cell takes place before conditions for external failure are reached. Therefore, it is adequate to consider internal safety in designing such structures.

1.4.1.1. Interlock tension   Design for interlock
tension has been discussed by Terzaghi [5], Lacroix et al.
[11], and Schroeder and Maitland [10]. Different procedures
predict different lateral earth pressure distributions and
magnitudes on the cell walls. Pressure diagrams from four
different design procedures for calculating the interlock
forces are presented in Figure 1.12.

The Terzaghi and Corps of Engineers Methods predict that
the lateral earth pressure increases down to the dredge line
and assume a lateral earth pressure coefficient as 0.4 and
0.5, respectively. The lateral earth pressure in the TVA
method increases down to three-fourth of free cell height
above dredge line and then decreases to zero at dredge line.
The lateral earth pressure coefficient is taken as the active
pressure coefficient. The Schroeder and Maitland method takes
a plane of fixity below the dredge line and assumes the
maximum lateral earth pressure occurs at a height of one-third
of the height from the point of fixity to top of the cell (see
Figure 1.12).

For a comparison of these methods consider a circular
cofferdam cell with cell diameter of 40 ft, free cell height
of 40 ft, depth of embedment 10 ft, cell fill with unit
weight and internal friction angle of 120 pcf and 30°,
respectively, and water level at 10 ft from the top of the
cell. The predictions of interlock forces by the various
methods for this sheet pile cell are shown in Figure 1.13.

TERZAGHI METHOD

$P = K\sigma_v'$ at H

$K = 0.4$

TVA METHOD

$P = K_a\sigma_v'$ at $0.75H$

$K_a = \tan^2 (45-\frac{\phi}{2})$

U.S. ARMY CORPS OF ENGRS METHOD

$P = K\sigma_v'$ at H

$K = 0.5$

SCHROEDER & MAITLAND METHOD

$P = K\sigma_v'$ at $\frac{2}{3}H'$

$H' = H+d'$

$d' = 5$ ft.
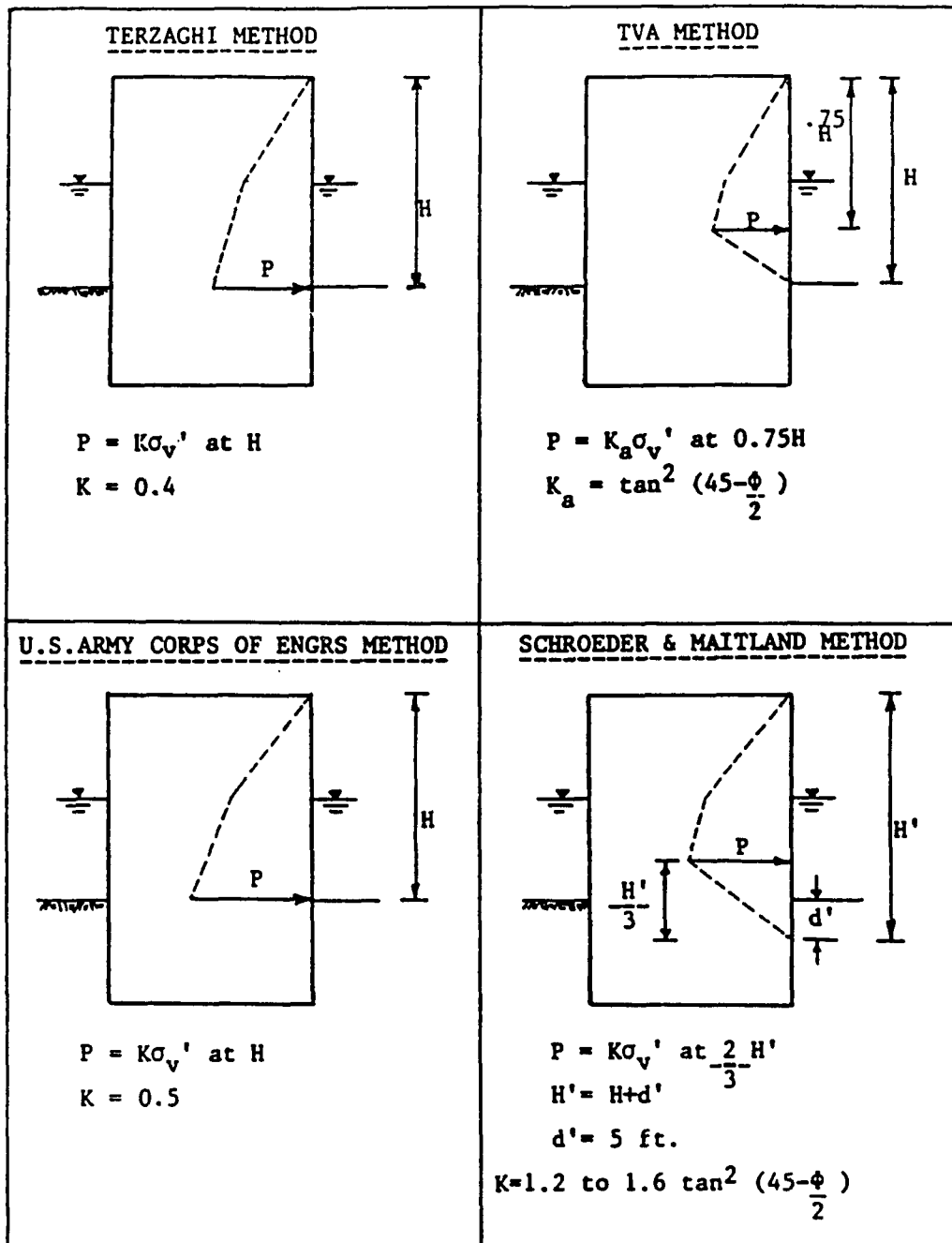
$K=1.2$ to 1.6 $\tan^2 (45-\frac{\phi}{2})$

Figure 1.12 Conventional analyses methods for interlock force (Shannon and Wilson [26]).
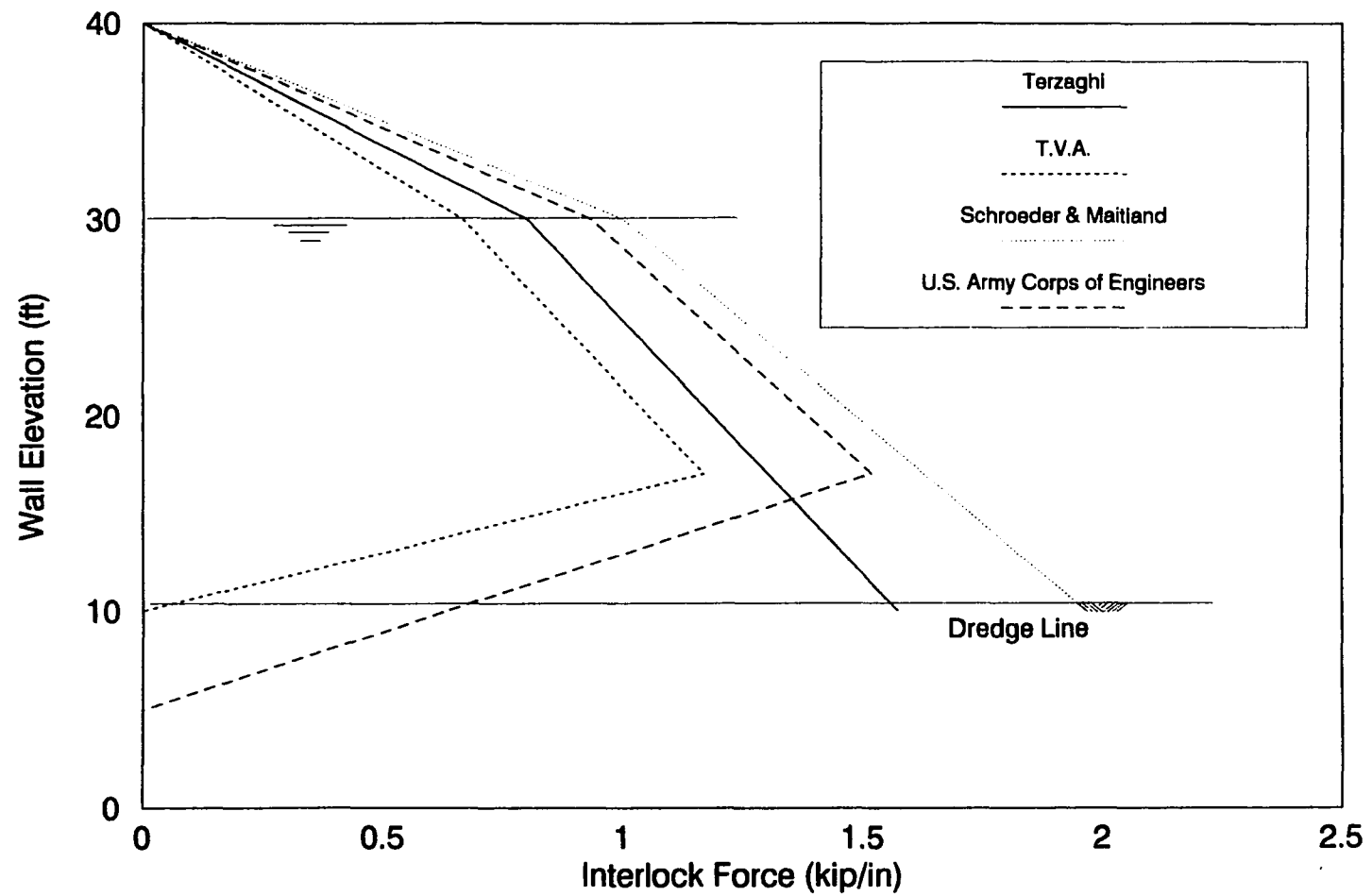
Figure 1.13   Comparison of interlock force predictions by
various methods.

The lateral earth pressure in any portion of a circular cell can be converted to interlock tension by:

$$t = pr \qquad (1.1)$$

where,

t = interlock force per unit length

p = earth pressure on the sheet piles

r = radius of cell

Cellular cofferdams having various configurations (see Figure 1.1) can also be idealized as fictitious rectangular cells with an average diaphragm wall spacing of L as shown in Figure 1.14 [14]. In this case, Equation 1.1. becomes

$$t = pL \qquad (1.2)$$

An alternative equation, the TVA secant equation [15], especially intended for use near the arc connection, is

$$t = pL(\sec\theta) \qquad (1.3)$$

where θ is the angle measured from the cofferdam axis to the connecting pile as shown in Figure 1.15.

<u>1.4.1.2. Shear in cell fill</u>   According to Terzaghi's formulation [5], the cofferdam could fail by shearing the fill material along a vertical plane at the center of the cell under excessive lateral load action as shown in Figure 1.16. Although his original derivations refer to cofferdams on rock, he indicated that results of such an analysis were not greatly different for structures on rock or on sands and proposed that
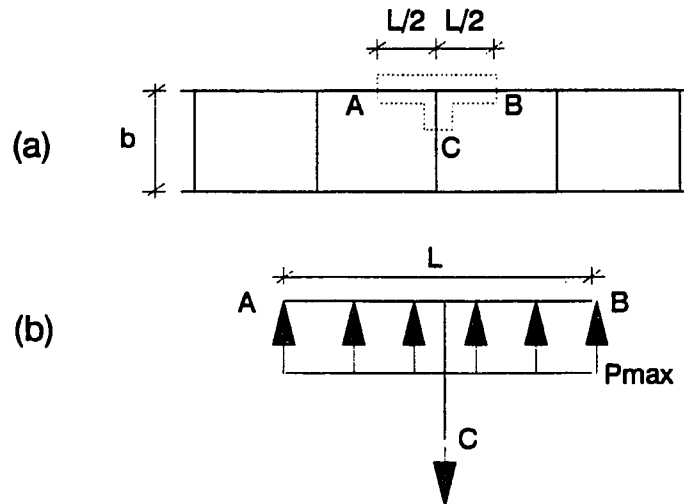
Figure 1.14   Geometry and free body for derivation of Swatek's
               equation: (a) portion of equivalent cofferdam
               selected for analyses, (b) free body of unit
               depth into plane of figure.
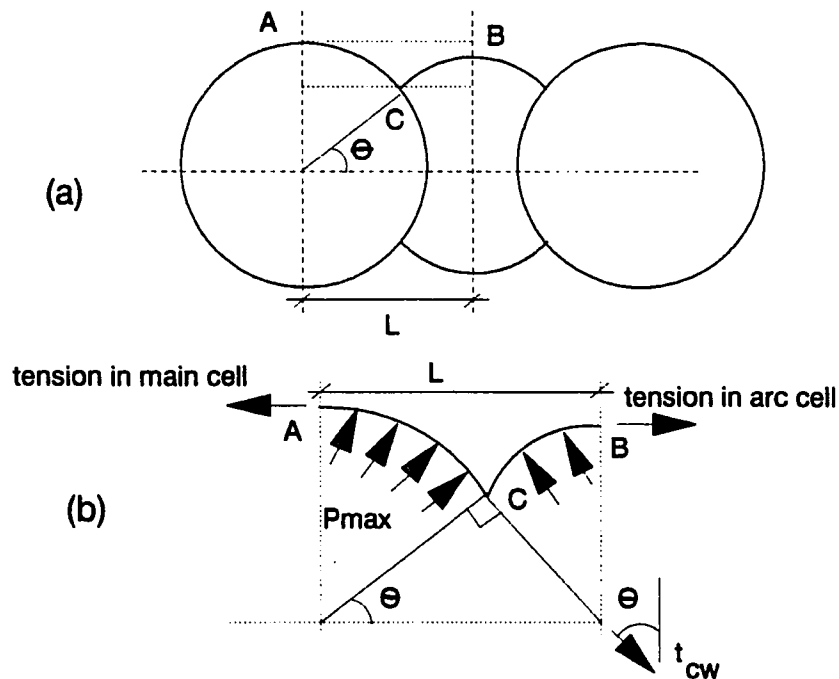
Figure 1.15   Geometry and free body for derivation of TVA-
               secant equation: (a) region selected for
               analyses, (b) free body of unit depth into plane
               of figure.

the rules developed would apply to other cases as well.

In his vertical shear formulation, Terzaghi assumed a straight line distribution of pressure on the cofferdam base (Figure 1.16). The applied overturning moment, M, is equal to

$$M = \frac{2b}{3}Q \qquad (1.4)$$

in which Q is the total force represented by each triangle of the base pressure diagram. By equilibrium, Q is also the applied shear force on the g-h plane. Solving for Q:

$$Q = \frac{3M}{2b} \qquad (1.5)$$

The shearing resistance on the vertical g-h plane is expressed as:

$$\acute{S} = P_c \tan\phi \qquad (1.6)$$

where,

   P_c = earth pressure on the g-h plane per unit length of

   cofferdam, and

   ϕ = coefficient of internal friction of cell fill.

The expression for P_c is:

$$P_c = \frac{1}{2}\gamma K H^2 \qquad (1.7)$$

where

   γ = unit weight of cell fill

   H = height of cell

   K = coefficient of lateral earth pressure at center line
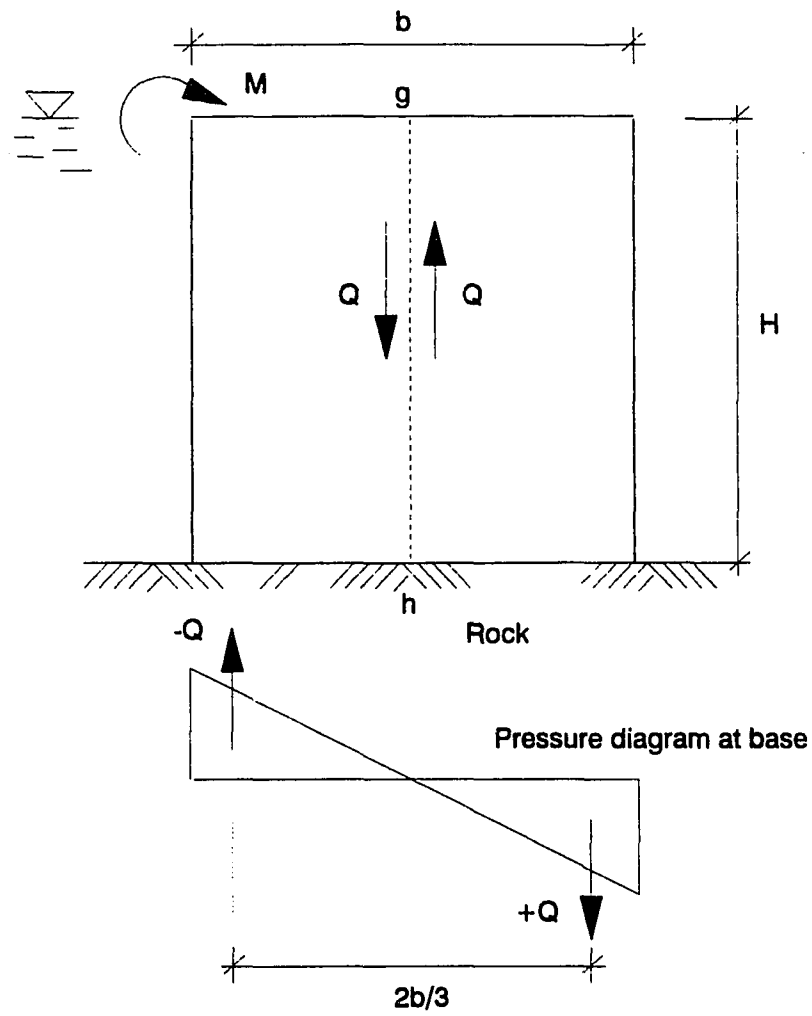
Figure 1.16   Illustration of Terzaghi's vertical shear method.

of cell

Combining Equations 1.6. and 1.7, the resistance of the fill against shearing on g-h plane is:

$$S' = \frac{1}{2}\gamma KH^2\tan\phi \qquad (1.8)$$

The total tension in the interlock on g-h plane is:

$$T = \frac{1}{2}K\gamma H^2 r \qquad (1.9)$$

where,

r = radius of cell

The total frictional resistance against slippage at the interlock is:

$$Tf = \frac{1}{2}\gamma H^2 r f \qquad (1.10)$$

where,

f = coefficient of interlock friction.

Circular cells contain two cross walls per cell and the length of each cell is 2L. The diaphragm type contains one cross wall per cell and the length of each cell is L (Figure 1.1). Hence, the resistance to shearing along g-h plane contributed by the interlock friction per unit length is:

$$S'' = T\frac{f}{L} = \frac{1}{2}\gamma KH^2\frac{r}{L}f \qquad (1.11)$$

The total average shearing resistance S is given by:

$$S = S' + S'' = \frac{1}{2}\gamma KH^2 (\tan\phi + \frac{r}{L}f)$$ (1.12)

The ratio r/L is usually close to unity so that approximately:

$$S = \frac{1}{2}\gamma KH^2 (\tan\phi + f)$$ (1.13)

The corresponding factor of safety:

$$F_s = \frac{S}{Q} = \gamma \frac{bH^2}{3M} K(\tan\phi + f)$$ (1.14)

Terzaghi estimated that the value of lateral earth pressure coefficient, K, for the middle part of the fill in the cell, ranged between 0.4 to 0.5. A typical safety factor F_s is taken equal to or greater than 1.25 and 1.5 for temporary and permanent structures, respectively.

The concept of vertical shear failure has been a quite controversial issue since it was introduced by Terzaghi, in part due to the assumption of a vertical failure surface, and in part due to the suggested lateral earth pressure coefficient. Concern about the assumption of a vertical shear surface was first voiced by Pennoyer [16], who analyzed several cofferdams that performed well using Terzaghi's vertical shear formulation and found that only 60 percent of the cases were predicted to be stable by this formulation. Alternative methods which assume different internal failure surfaces were subsequently proposed (Figure 1.17). Krynine [7] suggested that the failure surface should be curved and

Load → Failure Surface

KRYNINE (1945)

Load →

Failure Surface

HANSEN (1957)

Load →

Failure Surfaces

CUMMINGS (1957)
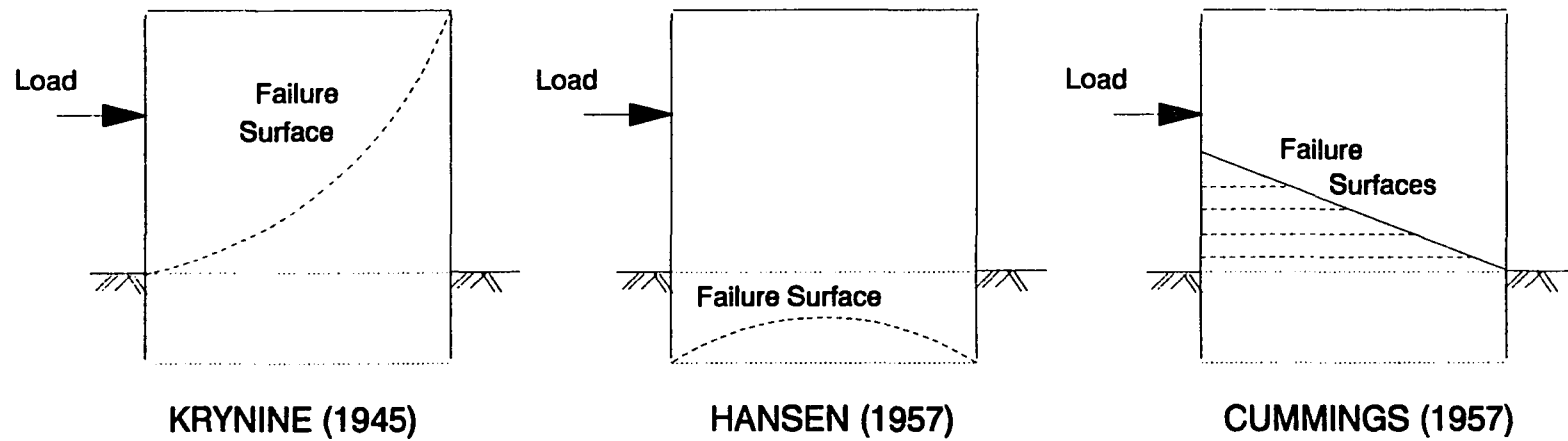
Figure 1.17 Suggested failure surfaces by various authors.

follow a path from the dredge line elevation of the outboard sheet up to the top of the inboard sheet. This failure mechanism provides a correlation between the width of the cell and the resistance against shear. Hansen [8] proposed a failure surface of the logarithmic spiral shape that is located at the bottom of the fill and connecting the inboard and outboard walls of the cell. Later, in a simplified version of this approach, Cummins [6] proposed a method of analysis based on the horizontal shear concept. In this approach, the failure surfaces could be taken as straight horizontal shear planes through the cell fill.

Conventional design methods mentioned in the preceding paragraphs are rules based largely on simplified behavioral modes or observations during small-scale laboratory model tests. In an attempt to provide data on the behavior of cellular structures at failure or near failure, Schroeder and Maitland [10,17] performed a series of large scale tests of cellular structures. The results of these tests are interesting since they provide grounds to examine the predictions of proposed failure forms. In the tests, sharply defined terraces formed at the surface of the cell fill, along with slippage in the sheet pile interlocks in the middle and inboard portions of the cell at failure. The overall failure pattern is closest to the original Terzaghi vertical shear mechanism. Nevertheless, it was apparent that the lateral earth pressure value, K, recommended by Terzaghi for the

vertical shear method, was quite low. A more appropriate value of lateral earth pressure coefficient was suggested near unity which is about twice the original value assumed by Terzaghi.

Schroeder and Maitland also reported that the cell deformations were excessive at the point where the failure mechanism was clearly observed. The lateral displacements at the top levels of sheet piles approached 50 percent of the cell height. Therefore, if deformations are to be kept to reasonable levels, relatively larger safety factors should be applied for overturning resistance.

1.4.1.3. Critique of conventional approach

The stages of construction and subsequent lateral or surcharge loads create incremental effects in the structure. Due to the plastic nature of the geomaterials and the nonlinear interaction effects between the cell and fill, the final outcome of these incremental effects is sequence dependent. The conventional approach provides a solution for the surcharge load effects only and does not consider sequence dependence and lateral load effects. Following placement of back fill behind a cofferdam, for example, field and laboratory investigations show that the interlock force on the loaded side is reduced, while it increases in the unloaded side by about 25 percent [18]. The maximum interlock force design condition is usually for a case where a surcharge load acts on the structure.

The conventional design methods were broadly criticized for being overconservative and modifications based on laboratory work and site observations have been proposed in the past two decades [10,11,17]. Nevertheless, shortcomings can not be properly dealt with within the limitations of conventional approach. The essential deficiency is that the relationship between deformations and stresses which actually exist in a cofferdam structure is not a part of the conventional methods. Considering that the cofferdams are characteristically highly flexible structures, an approach that does not consider deformations can lead to unrealistic evaluations.

1.4.2. Finite element analysis capabilities

Developments in the finite element method make it possible to deal effectively with problems involving soil-structure interaction. Using the finite element method, the entire soil-structure system can be modeled and information regarding displacements as well as stresses can be obtained. Furthermore, the method has the ability to deal with geometric and loading irregularities as well as behavioral complexities of the materials.

The finite element method has been applied to the cofferdam problem over the past 15 years. The application has constantly been improved with the addition of new element types to represent the specific properties of cofferdam structure and more representative models for the fill and

foundation soils that incorporate their nonlinear-plastic characteristics. The finite element method offers the possibility of predicting cofferdam behavior by accounting for many of the aspects of the structural system that elude conventional procedures. It can be particularly useful for the proper assessment of the structural response for taller and permanent structures which require a more careful evaluation or for lateral loads for which no provisions exist in the conventional theories.

Both two and three-dimensional models, each with advantages and drawbacks, can possibly be used. The three-dimensional model provides the means for accurately accounting for the complex geometry of the cellular structures. However, it is computationally expensive and would require tedious modeling work. It remains impractical for most applications at present. Basically three different two-dimensional model versions have been proposed for the cofferdam problem [19]. Although each of these models are only suitable for specific applications, they are more easily applied than three-dimensional versions.

Kittisatra [20] pioneered the application of the finite element method to cofferdams by analyzing the cell filling problem using an axisymmetric model (Figure 1.18). He assumed that the cell was a perfect pressure vessel, the soil was a linearly elastic medium and that no relative deformation could take place between the fill and the cell walls. Although this

AXISYMMETRIC
MODEL

HORIZONTAL
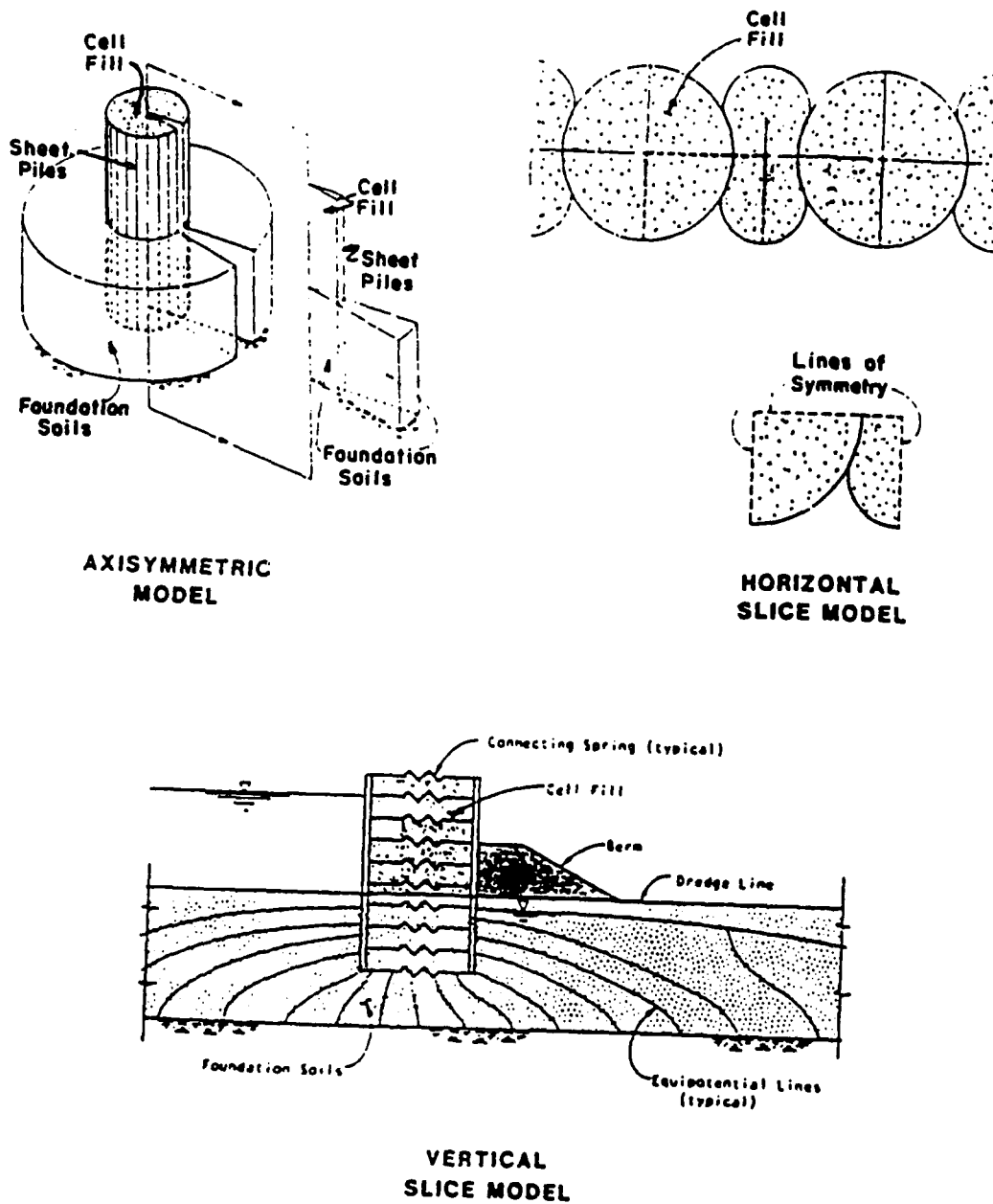SLICE MODEL

VERTICAL
SLICE MODEL

Figure 1.18   Two-dimensional finite element models [26].

was an interesting study, the results were far from being realistic due to the oversimplified assumptions involved in the model.

The vertical slice analysis with the assumption of plane strain conditions was introduced by Clough and Hansen [21] (Figure 1.18). This model was capable of analyzing nonaxisymmetric loads. It was applied to simulate a series of construction processes including cell filling, dewatering and interior excavation at the Willow Island cofferdam located on the Ohio River. The model consists of a two wall structure connected by springs and filled with soil. One-dimensional slip elements are located between fill elements and the walls to allow for relative movements along the boundaries. Spring stiffnesses were determined by considering an isolated individual cylindrical cell subjected to internal pressure. The total stiffness of the cell was assigned to springs distributed over the height of the cell. One dimensional slip elements which allow for relative movements along the boundaries were located between the soils and the sheetpile wall to model the surface contact. These elements had the capability to transmit the normal and shear (cohesive and/or frictional) forces between surfaces. The cell fill and foundation soils were modeled as a nonlinear medium according to a model developed by Clough and Duncan [22,23]. Stevens [24] later contributed to the vertical slice model by suggesting that the spring stiffnesses should be reduced for

possible initial slack and interlock yielding so that the predictions were more realistic.

The generalized plane-strain model, which was suggested by Rossow [19], provides a means of analyzing the interaction between cells. The basic idea is to analyze a horizontal section cut through the cofferdam at a series of different elevations using a generalized plane-strain technique. A constant strain is assumed to exist in the out-of-plane direction, generated by the vertical gravity loads above the plane [25]. The generalized plane strain model provides data on interlock tension and cell deformations for the main and arc cells, the common wall, and the critical Y-section where the two cells are joined. This model is unable to account for the lateral support of the foundation soils and thus is applicable only for the upper two-thirds or so of the cells where the dredge line effects have little influence. However, since maximum interlock tensions generally occur about the level of the lower one-third point, this does not constitute a major drawback.

Beginning in the early 1980s, the replacement process of the Lock and Dam 26 on the Mississippi River involved construction of one of the largest system of cellular cofferdams ever built. Since the U.S. Corps of Engineers was concerned with contradictions between existing design techniques for cofferdams and wanted to reduce embedments and eliminate the need for costly high-strength sheet piles along

the common wall, a large-scale instrumentation program was
instituted for the first stage cofferdam [19]. The two-
dimensional finite element modeling techniques discussed
previously in this section were applied to simulate the
construction process starting with cell filling [19,26].
Thus, it was possible to compare the observed behavior to the
two-dimensional finite element results. Comparisons of the
two-dimensional finite element results with the recorded data
indicated that the cofferdam behavior was reasonably predicted
by the two-dimensional finite element models through the
construction stages including cell filling, berm placement and
dewatering.

Clough et al. [19] presented the E-ratio concept in the
analysis of the Lock and Dam 26 replacement based on Stevens'
previous assessment of increased flexibility of interlocks in
the horizontal direction. E-ratio refers to the reduced
modulus of the sheetpiles in the circumferential direction
with respect to that of steel in the vertical direction. Due
to the uncertainties in the assumptions, the analyses were
performed with a range of E-ratio values of 1.0, 0.1, and
0.03. Also, it was judged that after filling, since much of
the interlock deformation and sheet pile realignment would
have occurred, an E-ratio of 1.0 was assumed applicable for
loading after filling. However, this assumption is not
supported by the load deflection curve for the piles used in
that structure. For the stress levels existing in the sheet

piles after filling, the load-deflection curve indicates much lower values of the circumferential modulus. This assumption results in a stiffer cell and, thus, smaller deformations in the analysis steps following loading. Comparisons of interlock forces after cell filling predicted by classical methods and finite element models in the Lock and Dam 26 study [19] are shown in Figure 1.19.

1.5. Overview of Approach

To accomplish the objective in Section 1.2., the following steps are performed in the course of this study:

1. Model the structure with both two and three dimensional finite element models.

2. Determine the interlock tension levels in the sheet piles immediately after construction.

3. Predict the cumulative effects on the earth pressures and interlock tension levels in the sheetpiles as a result of the wave action on the structure during its service life.

4. Analyze the fluctuating interlock forces under wave action.

5. Verify the results of the finite element models by comparisons with the recorded data.

6. Compare the interlock force levels in Steps 2, 3 and 4 with the predictions of the conventional approach.

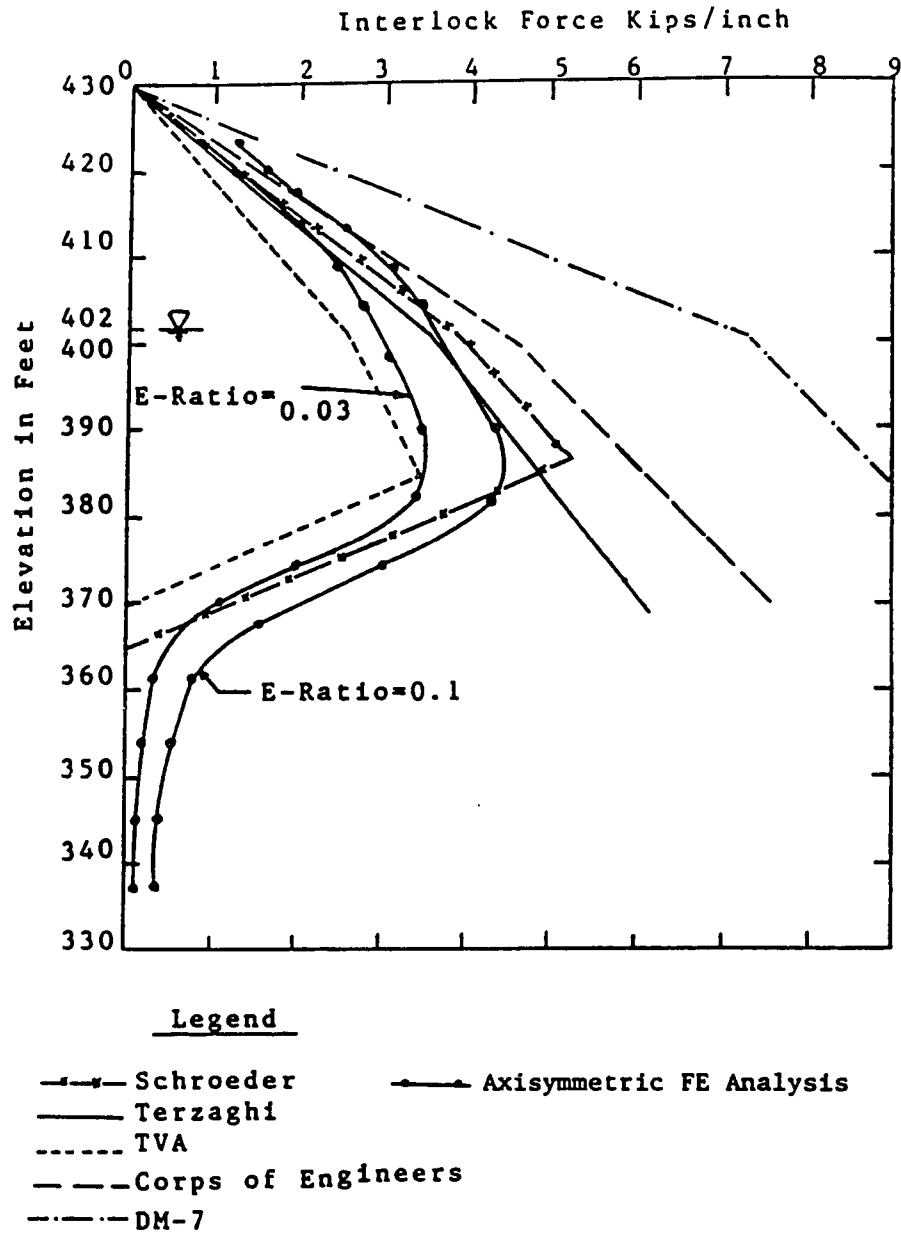7. Compare two and three-dimensional model results.

Figure 1.19   Comparison of interlock forces predicted by methods at the end of cell filling (Clough and Kuppusamy [1985]).

2. FIELD INSTRUMENTATION

2.1. Background

The field instrumentation of the Reach C of the breakwater structure was done in two phases; phase I of the instrumentation was installed in winter 1988-89 and phase II during winter 1989-90. Phase I of the instrumentation was discussed in an interim report submitted to the Corps of engineers [27]. In this Chapter the phase II portion of the field operation is discussed along with brief information related to the equipment and installation procedure.

2.2. Field Instrumentation

The instrumentation system was designed to allow the collection of the data to be controlled at ISU facilities in Ames, Iowa. A schematic diagram of the instrumentation system is shown in Figure 2.1. The instrumentation installed during phase II consisted of the following four parts:

1. Thirteen strain gauges and a pressure transducer.

2. A data acquisition system (DAS) consisting of a CR-7 control module.

3. A communications system consisting of radio frequency, antenna, UHF radios, and phone modems.

4. Microcomputer at ISU to maintain communications protocol, control the data acquisition, and act as a storage module for the collected data.

Figure 2.2 shows the locations of the strain gauges on
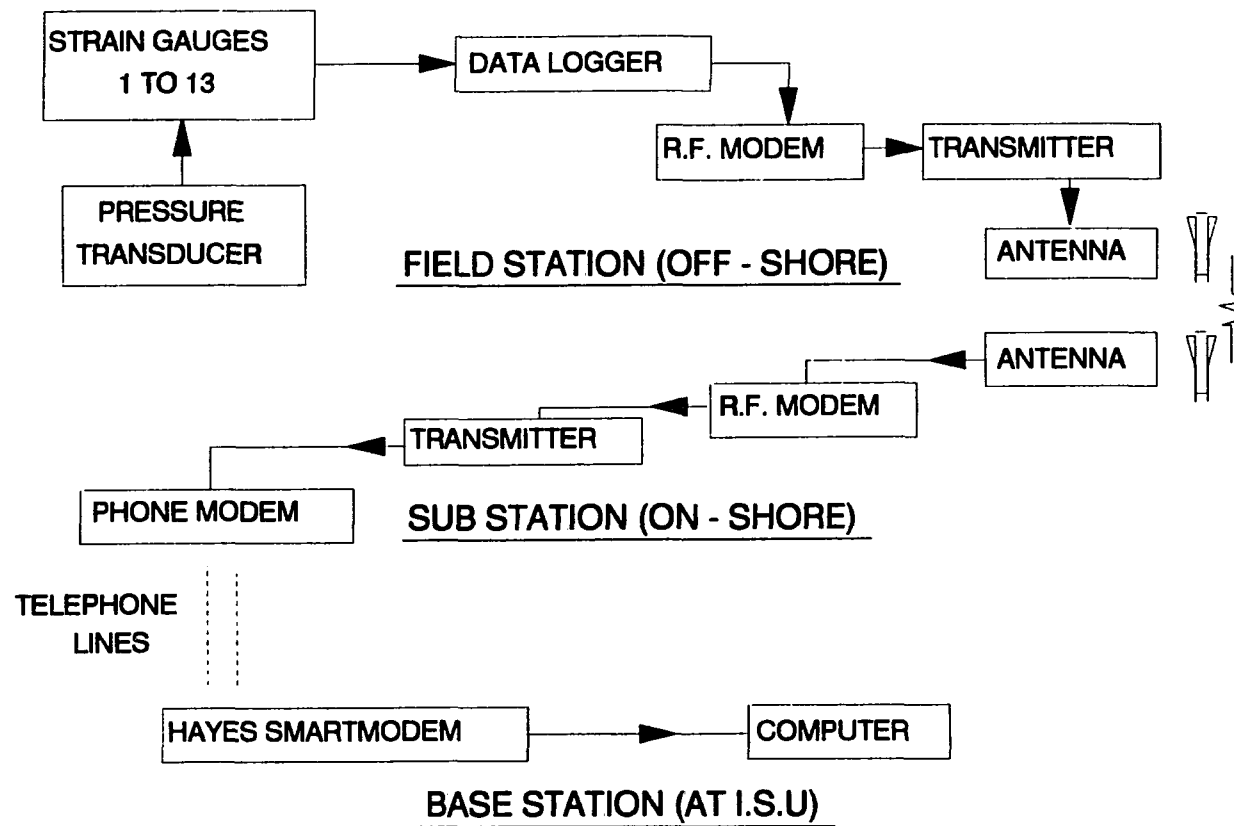
Figure 2.1 Schematic diagram of instrumentation scheme.

INSTRUMENTED CELLS   LIGHT HOUSE LOCATION

PLAN OF THE S.E. END

S.G.5, S.G.11   (B)   (A)   S.G.2, S.G.12, S.G.13

S.G.10   S.G.1   S.G.7

S.G.6

S.G.9   S.G.8

(B)   (A)

PLAN VIEW OF STRAIN GAUGE LOCATIONS

41

S.G.5   3'
LWD
10'
S.G.11

SECTION B - B

S.G.2   1.5'

13'
S.G.12

21'
S.G.13

SECTION A - A
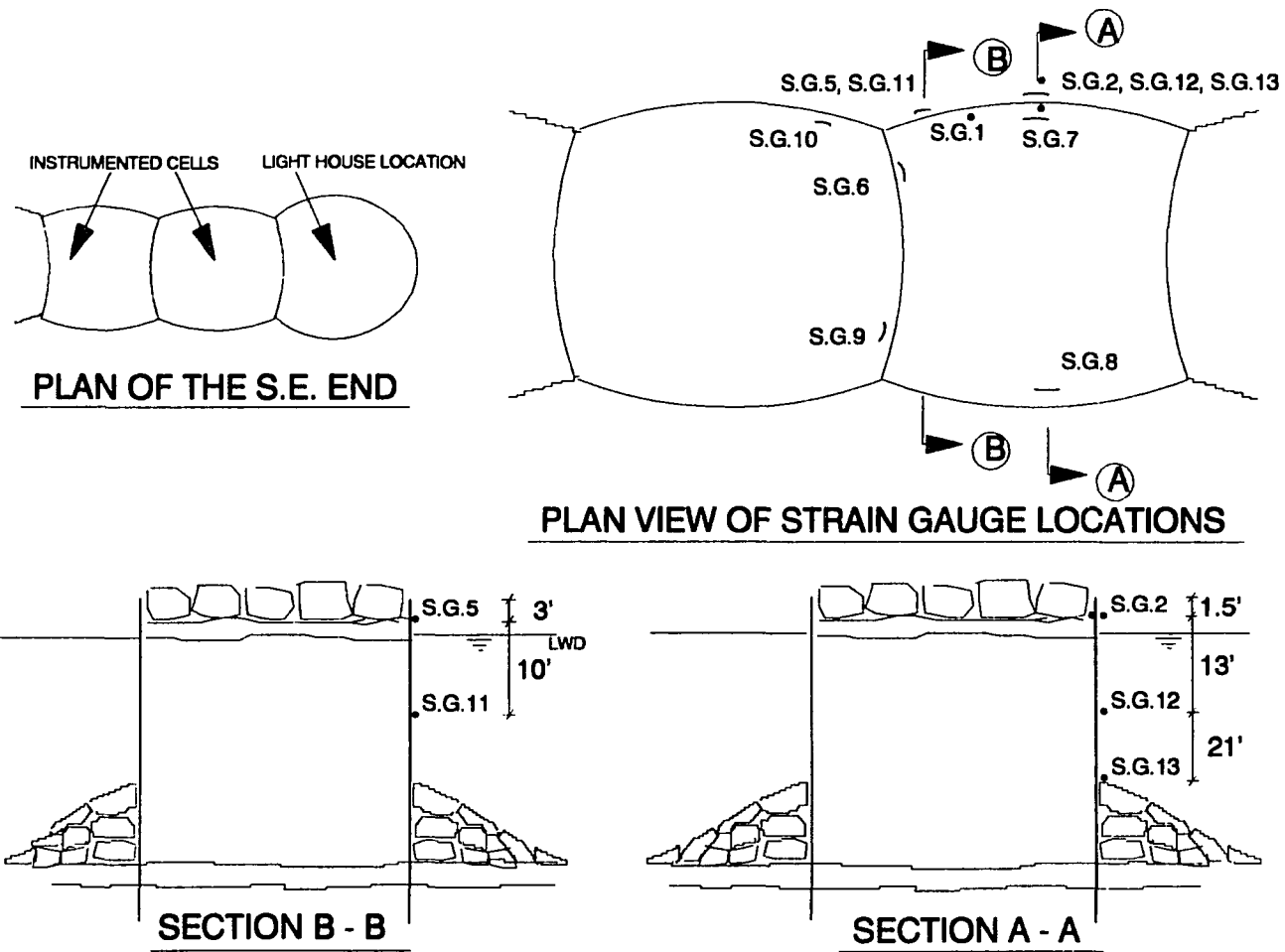
Figure 2.2   Location of strain gauges on the instrumented cells.

the cells. The strain gauges were installed on two cells immediately to the west of the cell at the eastern end of the breakwater. The location and orientation of the structure was shown in Figure 1.4. The lighthouse at the eastern end was used to station the system and the communications equipment. This arrangement formed the field station offshore. The Coast Guard station onshore served as a substation. The control station at I.S.U. is considered the base station.

The strain gauge installation scheme was designed to obtain data to be used as reference for validation of the finite element models of the breakwater structure. The strain gauges consisted of three gauges oriented to measure flexural strain and ten gauges to measure hoop strain. Three of the ten hoop gauges are installed under water (see Figure 2.2). Two surface hoop strain gauges were installed on the diaphragm of the cells (gauge 6 and gauge 9). Three surface hoop strain gauges were installed on the central portion of the cells, two on the harbor side (gauge 2 and gauge 7), and one on the lake side (gauge 8). Two hoop strain gauges were located near the diaphragm of the cells (gauge 6 and gauge 9). Of the three under water strain gauges, one was installed near the diaphragm (gauge 11) and two were installed at different elevations at the central portion of the cell toward the lake side (gauges 12 and 13).

Data were collected from December 1989 to early March 1990. Strain gauges 2 and 11 and the pressure transducer

ceased operation after the last week of December. The prime
indicator to prompt data collection was to be the presence of
the strong winds in the vicinity and corresponding significant
wave activity; the data collection procedure was to be
initiated by weather reports obtained from the National
Weather Service at Chicago, the Coast Guard personnel at
Calumet Harbor station and commercial weather reports.
However, during the monitoring period, there were no major
storms and data were collected on a regular basis.

The data collected by the installed data acquisition
system consisted of the pressure values in feet of water and
the strains in microstrains. The total data collection time
in any one attempt was restricted by memory to about 6.5
minutes. This recording period is called a data segment. The
data were collected at intervals of 0.3 second in a data
collection segment. Part of the data collected on January
12th is shown in Figure 2.3. This typical variation was part
of a larger data segment. Twenty-four data segments were
recorded during the data acquisition period.

Real-time wave data were collected by a wave gauge
installed in Lake Michigan near the breakwater reach C by the
Army Corps of Engineers, Chicago District. These data were
reduced at the Coastal Engineering Research Center at
Vicksburg (CERC) and communicated through the Chicago
District. The reduced data consisted of the time of
collection and corresponding significant wave height. The
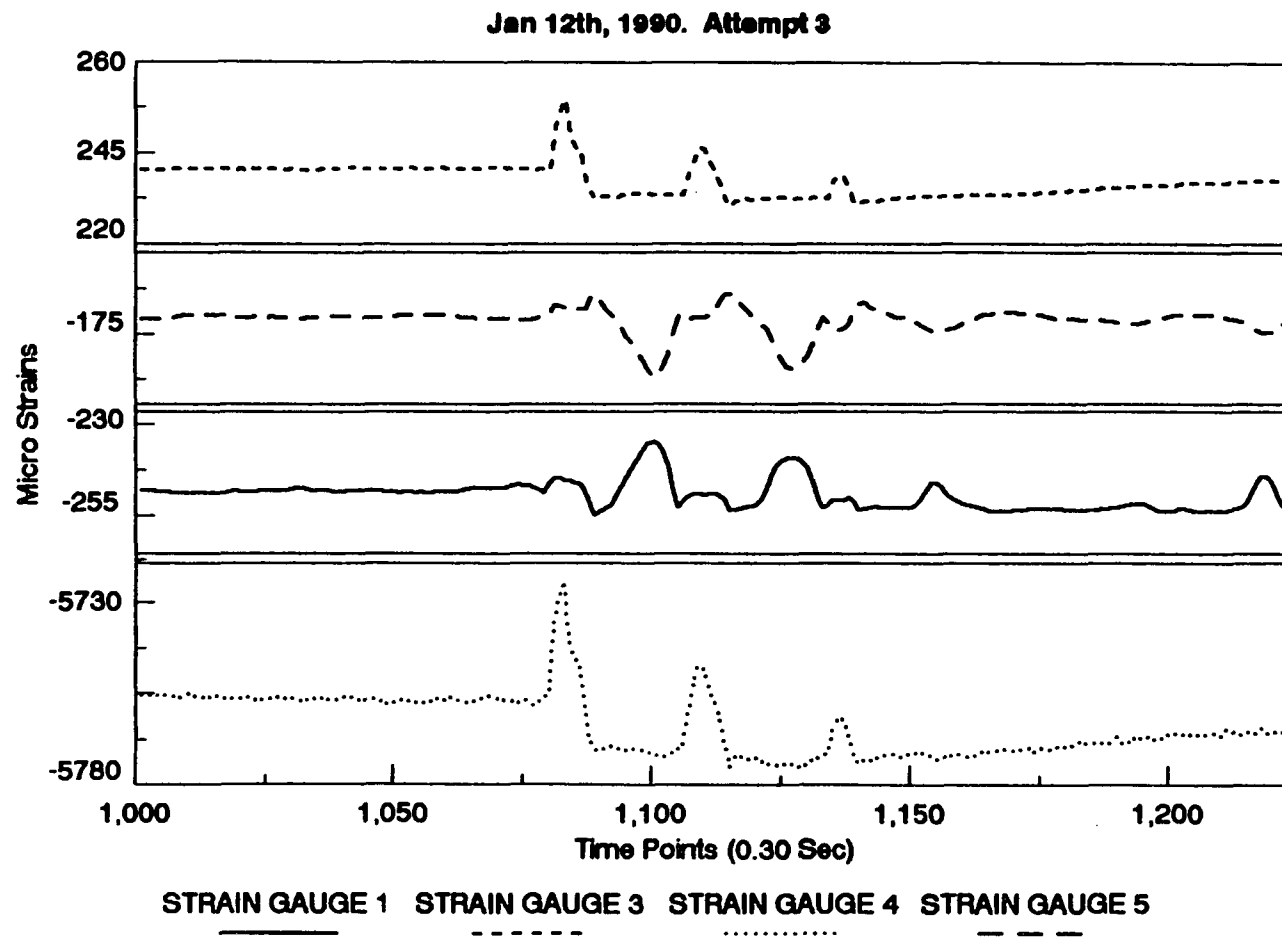
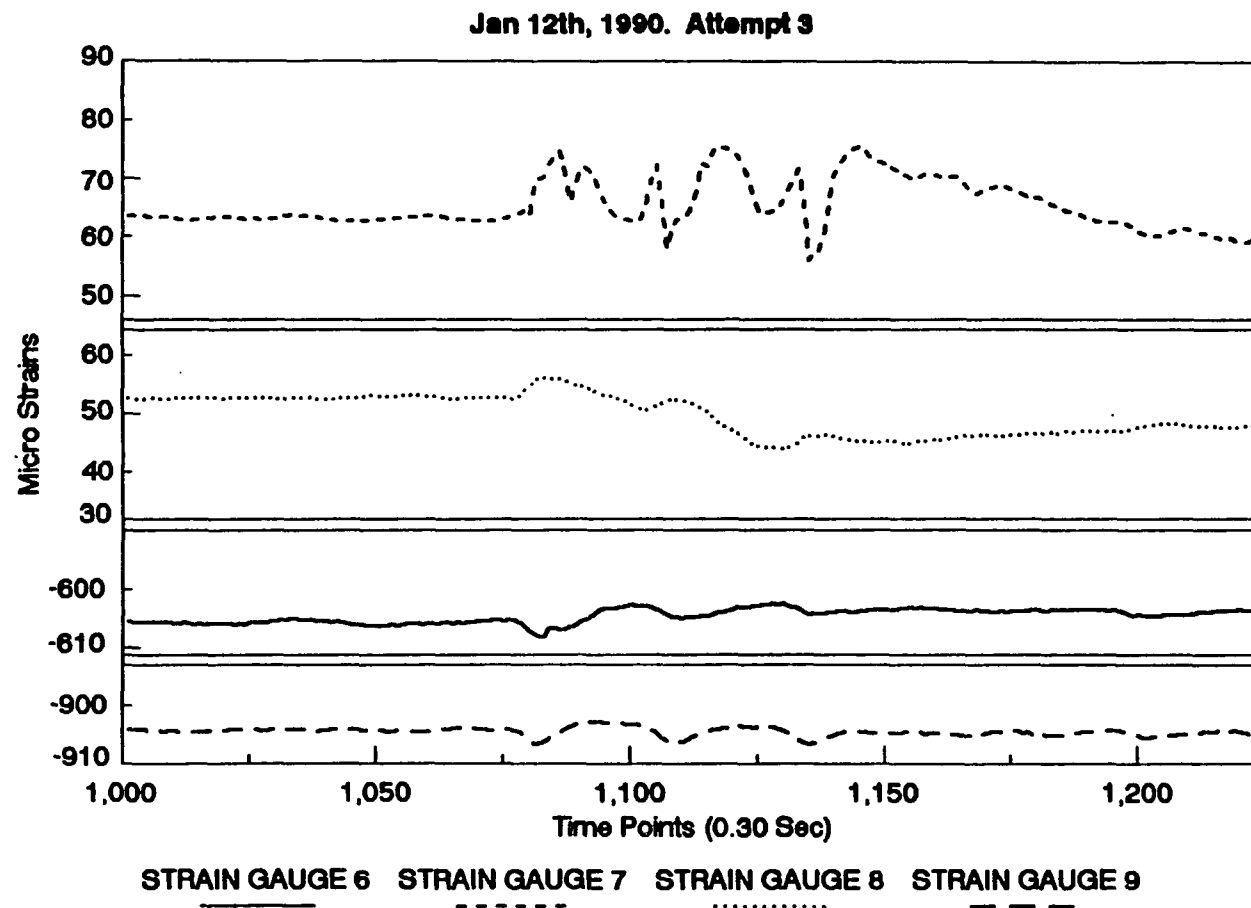Figure 2.3 Typical data segment - strain gauges 1,3,4 and 5.

Figure 2.3   (continued) strain gauges 6,7,8 and 9.

Figure 2.3 (continued) strain gauges 10, 12 and 13.

data collection time spanned December 1989 to April 1990.

Table 2.1. illustrates the dates, recording time, and the maximum wave height for the different dates. Table 2.2 indicates the corresponding recorded maximum hoop-force ranges at three of the strain gauges. On the basis of the reduced CERC data, of the 24 recorded segments, only 19 were significant. The other periods for which no reduced data were available probably referred to quiescent lake conditions. The diagnostic tests detailed in the final report [2] were used to transform the recorded strain ranges into the hoop force ranges on the structure.

The data regarding the weather conditions, the wind direction and speed, and other climatological data were obtained from the National Climatic Data Center, Ashville, North Carolina. The data were from the marine coastal weather log maintained at the Calumet Harbor.

Table 2.1 Time, date, max. wave height in the record and corresponding wind and wave directions.

Date	Time of Record	Maximum Wave Height H_{max} (ft)	Wind Dir. Marine Log	Wave Dir. Real Time Statistics
Dec 3rd	20:46 hrs	4.01	SW	NNW
Dec 10th	22:30 hrs	6.41	N	NW
Dec 12th	21:07 hrs	3.13	NW	NW
Dec 21st	13:15 hrs	3.01	NW	NW
Jan 12th	11:46 hrs	9.40	NW	WNW
Jan 12th	14:57 hrs	9.40	NW	NNW
Feb 4th	14:35 hrs	3.03	NE	NNW
Feb 24th	11:17 hrs	13.90	NW	NW
Mar 5th	16:47 hrs	6.21	NE	N

Table 2.2   Recorded hoop-force ranges.

Date	H_{max} (ft)	S.G. 12 (lb/in)	S.G. 13 (lb/in)	S.G. 7 (lb/in)
Dec 3rd	4.01	164.32	165.31	5.38
Dec 10th	6.41	373.97	299.20	141.32
Dec 12th	3.13	23.92	35.40	1.70
Dec 21st	3.03	39.74	50.05	6.18
Jan 12th	9.40	62.47	78.00	11.76
Jan 12th	11.40	121.47	332.61	68.47
Feb 4th	3.03	34.96	50.92	3.47
Feb 24th	13.90	130.91	382.54	134.54
Mar 5th	6.21	44.71	60.24	6.68

3. VERIFICATIONS AND PARAMETRIC STUDIES WITH ANSYS FINITE ELEMENT PACKAGE

The finite element package ANSYS was used for the structural analysis of the Calumet Harbor Breakwater structure. In this chapter, the capabilities of this software are verified by comparisons with soil tests and classical earth pressure theories. The Drucker-Prager plastic constitutive model, which is suitable for granular materials, is an option in the ANSYS package. This model, which is typically used for geomaterials in finite element modelling, is described along with the general plasticity formulation and is verified with triaxial test results from literature. Also the effect of a number of model parameters on the results are studied with an axisymmetric sheetpile cofferdam model.

3.1. ANSYS Finite Element Package

ANSYS is the trademark of a self contained general purpose commercial finite element package developed and maintained by Swanson Analysis Systems [28]. It is written in FORTRAN code and has its own command language. The package contains numerous routines, all interrelated and all for the main purpose of achieving a solution to an engineering problem by the finite element techniques.

The package currently contains over 80 elements suitable for applications in various areas, including structures, hydraulics, heat transfer and electromagnetics. Several

material models that account for nonlinearity and plasticity
are implemented in ANSYS. It provides capable pre- and post-
processor routines and plotting capabilities and is well
documented.

3.2. Drucker - Prager Elastic - Perfectly Plastic Model
for Geomaterials

3.2.1. Background

In general, stress-strain characteristics of soil
materials are nonlinear and complex. There exist several
factors such as state of stress, residual or initial stress,
volume changes under shear, stress history or stress paths,
inherent and induced anisotrophy, change in the physical state
and fluid in the pores which influence the nonlinear behavior
of this class of materials.

Constitutive models that reasonably represent the
material behavior play a significant role in providing
reliable results in engineering practice. Their importance
has been enhanced significantly with the great increase in the
development and application of many modern computer based
techniques such as the finite element, finite difference and
boundary integral methods.

Since the foundation of classical plasticity theory were
laid in the 1950s [29,30,31,32], soil mechanics specialists
have been preoccupied with extending these concepts to model
the complex problems of soil behavior. The search for more
representative constitutive models for soils is still one of

the major fields of study in soil mechanics. Numerous models with various capabilities for specific soil types have been developed [33]. However, most of these models include parameters which require sophisticated laboratory methods and devices to determine and, thus, are not fit for many practical uses. There are two major aspects that constitute the theory of plasticity: (a) the yield criterion and (b) post yield behavior.

The yield criterion can be defined as the limit of elastic deformations expressed by a combination of states of stress. For triaxial states of stress, it is convenient to define a scalar function, f, as the yield criterion. That is:

$$f = f(\sigma_{11}, \sigma_{22}, \sigma_{33}, \sigma_{12}, \sigma_{23}, \sigma_{13}) \tag{3.1}$$

in which σ_{ij} represents the components of the stress tensor. For the case of an isotropic material in terms of principal stresses, the above equation becomes:

$$f = f(\sigma_1, \sigma_2, \sigma_3) \tag{3.2}$$

This can be expressed more conveniently in terms of the invariants of the stress tensor J_1, J_2, J_3 as follows:

$$f = f(J_1, J_2, J_3) \tag{3.3}$$

where,

$$J_1 = \sigma_{ii} = \sigma_{11} + \sigma_{22} + \sigma_{33} = tr(\sigma) \tag{3.4}$$

$$J_2 = \frac{1}{2}\sigma_{ij}\sigma_{ji} = \frac{1}{2}tr(\sigma)^2 \qquad (3.5)$$

$$J_3 = \frac{1}{3}\sigma_{ik}\sigma_{km}\sigma_{mi} = \frac{1}{3}tr(\sigma)^3 \qquad (3.6)$$

Here "tr" denotes the trace.

The presence of the first invariant, J_1, of the stress tensor in the yield function implies the dependence of the yield criterion on the mean pressure. A physical model involving a mass resting on a frictional surface can be considered to explain this effect. Here, the frictional force will be proportional to the normal load acting on the surface. For many metals the influence of hydrostatic stress on the plastic deformation has been found to be negligible [34]. This type of materials are called frictionless. The behavior of geologic media, however, is dependent on hydrostatic stress with certain exceptions. Under fully or partially drained conditions, the strength of soil increases with mean pressure. Post yield behavior is controlled by two major factors: the flow rule and the hardening rule.

In the theory of plasticity [29,35] the direction of the plastic strain vectors is defined through a flow rule. The incremental strain vectors are assumed to be orthogonal to a plastic potential function. The increments of the plastic strain can be expressed by the normality rule as:

$$de_{ij}^{p} = \lambda \frac{\partial Q}{\partial \sigma_{ij}} \qquad (3.7)$$

where,

Q = plastic potential function, and

λ = a positive scalar factor of proportionality.

For some materials, the plastic potential function, Q, and the yield function, f, can be assumed to be the same. Such materials are considered to follow the associative rule of plasticity. For geological materials these two functions are often different. These materials are considered to follow the nonassociative flow rules of plasticity.

Due to plastic flow, certain materials display hardening behavior. Two hypotheses have been proposed to define the degree of hardening: (1) the work hardening, and (2) the stress hardening hypothesis. The work hardening hypothesis, proposed by Hill [29], assumes that hardening depends only on the plastic work and is independent of the strain path. According to this hypothesis, the yield criterion can be written as:

$$f = f(\sigma_{ij}, W^{p}) \qquad (3.8)$$

Drucker [30] and Prager [31] later presented and discussed the conditions and postulates on which the formulation of work hardening is based.

The second hypothesis assumes that plastic strain, ϵ^{p}, is a measure of hardening. According to this hypothesis, the

yield function can be written as:

$$f - f(\sigma_{ij}, e^P) \qquad (3.9)$$

The Drucker-Prager model uses the outer cone approximation to the Mohr-Coulomb failure condition and is applicable to granular (frictional) materials such as soils and rocks. In its original form, the model is associated and the post yield deformations are independent of time. But the associated behavior contradicted observation and gave excessive dilation [36]. It became necessary, therefore, to extend the formulation to a non-associated form in which the plastic potential and yield surfaces are defined separately [37].

The ANSYS version of the model provides control over dilation during plastic flow but does not have the options for strain hardening or softening behavior. In other words, the yield surface does not change with progressive yielding so the behavior is elastic-perfectly plastic. This behavior, although rather idealized, is globally in good agreement with the observed granular soil response. Plastic deformations take place in real soils for even small strains and generally there is a display of strain hardening behavior between the presumably elastic and plastic stages (fig.3.1)

Considering the numerical analysis, it is not practical to use a very sophisticated constitutive law, because it needs much computing time as well as substantial effort to determine

the various parameters required. The Drucker-Prager model is one of the simplest models and is quite widely used in practical applications. The input for the ANSYS version of the model consists of only three constants (1) the cohesion value, (2) the angle of internal friction, and (3) the dilatancy control parameter.

3.2.2. Drucker-Prager model formulation

The yield criterion for the Drucker-Prager model [38] accounts for the effects of all principal stresses and has the form:

$$f = \sqrt{J_{2D}} - \alpha J_1 - k \qquad (3.10)$$

where,

α and k = positive material parameters,

J_1 = the first invariant of the stress tensor, and

J_{2D} = the second invariant of the deviatoric stress

tensor expressed in the form

$$J_{2D} = J_2 - \frac{J_1^2}{6} \qquad (3.11)$$

Equation 10 represents a straight line on a J_1 versus J_2 plot (Figure 3.2). For cases of triaxial states of stress, the function above can be represented in a three dimensional stress space where the principal directions have been selected as the coordinate axes (Figure 3.3). This is known as the Haigh-Westergard stress space [33]. The plane passing through the origin normal to the space diagonal is known as the Π-

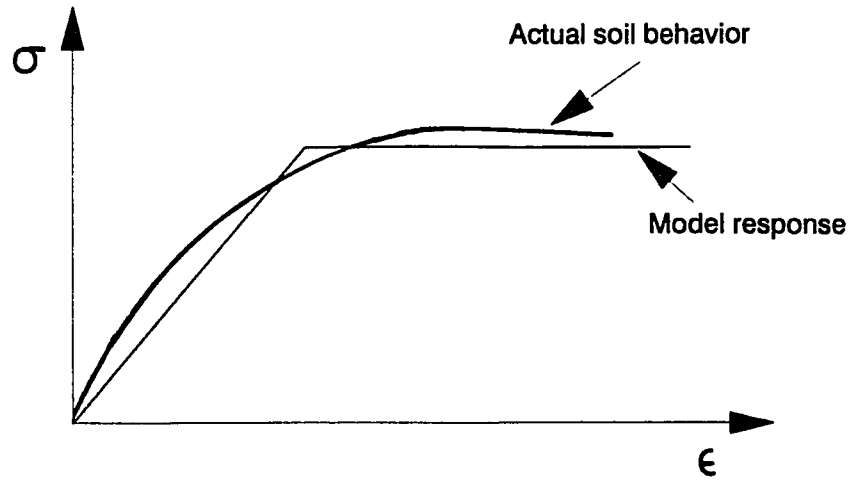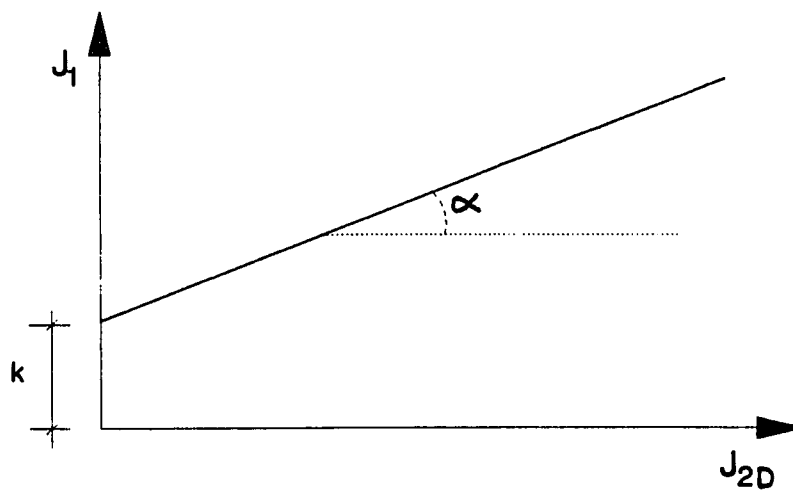**Figure 3.1   Drucker-Prager model response.**

Figure 3.2   Drucker-Prager model parameters.

plane, and is frequently used in depicting the yield function. In the three dimensional stress space, the criterion plots as a right circular cone and the projection on the Π-plane is a circle as shown in Figure 3.3. When the state of stress reaches the failure surface (Equation 3.10), the material undergoes plastic deformations. According to the criterion, a state of stress outside the surface is not stable and the material undergoes plastic deformations while the stress point moves on the failure surface.

The two parameters α and k in the yield criterion equation can be determined from the slope and intercept of the failure envelope plotted in the J_1-J_{2D} space (Figure 3.2). The failure envelope for a specific material can be established by performing laboratory tests up to the ultimate or failure conditions. Conventional triaxial testing devices are well suited for this purpose.

The ultimate condition is usually defined as the asymptotic value of stress in the final range of a stress-strain curve. Failure may also be defined as a state corresponding to a chosen strain condition. The failure state may coincide with the ultimate state or correspond to a lower state of stress.

The values of α and k can be expressed in terms of angle of the internal friction angle, ϕ, and cohesion, c, as follows [39]:
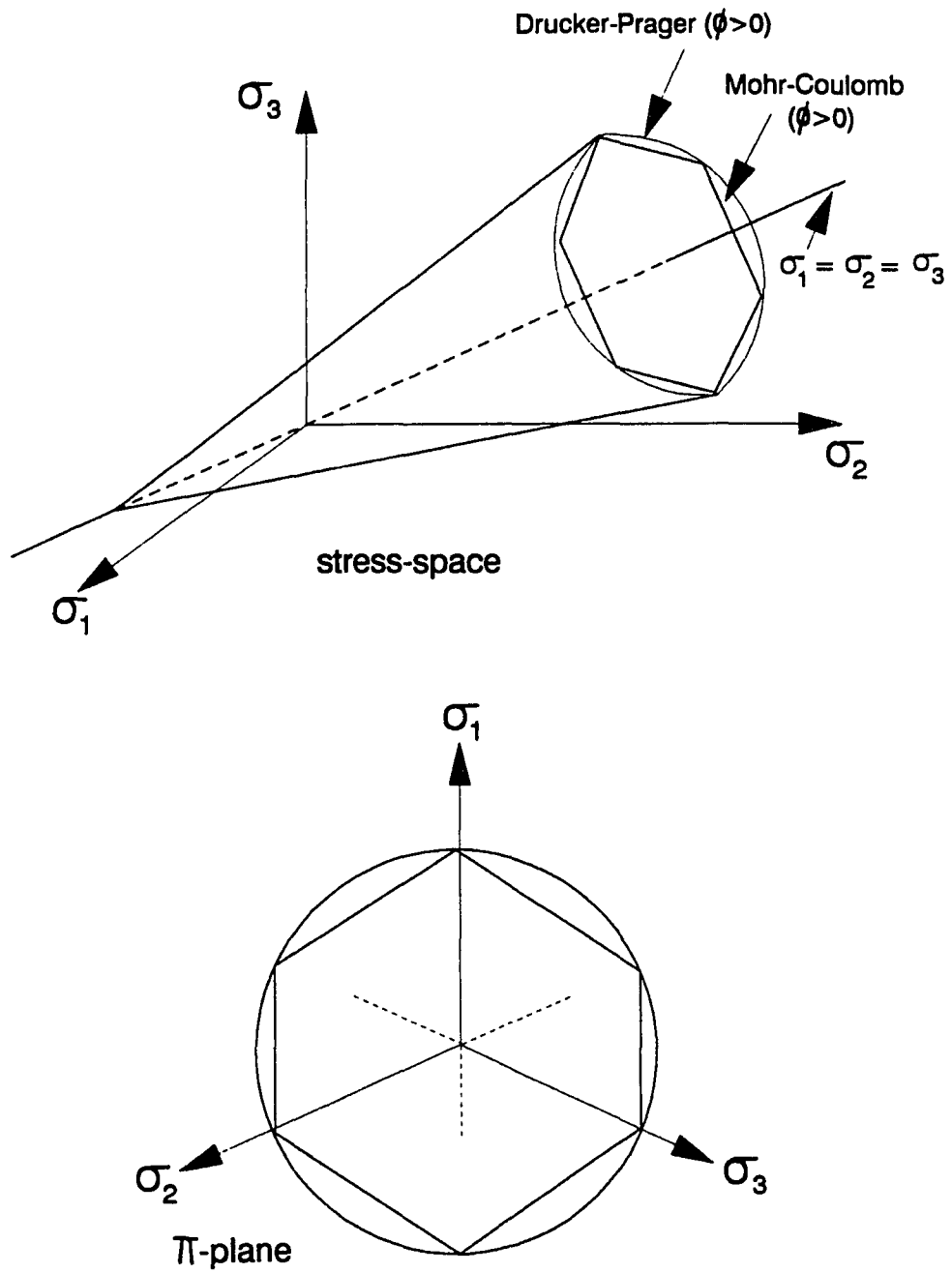
Figure 3.3   Expression of Drucker-Prager model in   Plane.

$$\alpha = \frac{2\sin\phi}{\sqrt{3}\,(3-\sin\phi)} \qquad\qquad (3.12)$$

$$k = \frac{6\,c\cos\phi}{\sqrt{3}\,(3-\sin\phi)} \qquad\qquad (3.13)$$

The expression for plastic potential, Q, is similar to the expression for yield condition, f, but is evaluated using a parameter which is called the dilatancy constant (ϕ_r). When the dilatancy constant is equal to the internal friction angle, the flow rule is associated, plastic straining occurs normal to the yield surface, and there will be a volumetric expansion of the material with plastic straining. If the dilatancy constant is less than the internal friction angle, there will be less volumetric expansion.

3.2.3. Solution method

ANSYS uses the initial stress method to solve the nonlinear equations involved in a plasticity analysis. The stiffness matrix remains unchanged (as the elastic stiffness matrix) since the nonlinearity is accounted for by a load vector term, so the stiffness matrix needs to be triangularized only once during an analysis [28]. The static equilibrium equation is:

$$[K]\,(u) = (F^{nd}) + (F^{pl}) \qquad\qquad (3.14)$$

where,

$[K]$ = total elastic stiffness matrix

(u) = nodal displacement vector

(F^{nd}) = applied load vector

(F^{pl}) = $\Sigma(F^{pl})$

(F^{pl}) = $\int [B]^{T}[D](\epsilon^{pl})$ d(vol)

where,

N = number of elements

$[B]$ = strain - displacement matrix

(ϵ^{pl}) = plastic strain vector

$[D]$ = elastic stress - strain matrix

Equation 3.14 is solved iteratively, in which the plastic strain vector is updated after each iteration. Convergence is obtained when the plastic strains have changed very little from iteration to iteration. The overall flow chart is given in Figure 3.4.

The algorithm used to compute the plastic strain increment assumes that the total strain is relatively small (i.e. the components of $(d\epsilon)$ are small compared to the size of the yield surface) and that the strain increment is linear over the iteration. The differential increments $(d\epsilon)$ and $(d\epsilon^{pl})$ are replaced by finite increments $(\Delta\epsilon)$ and $(\Delta\epsilon^{pl})$. For the details of the algorithm to calculate the plastic strain increments, the ANSYS theoretical manual [38] should be referred.
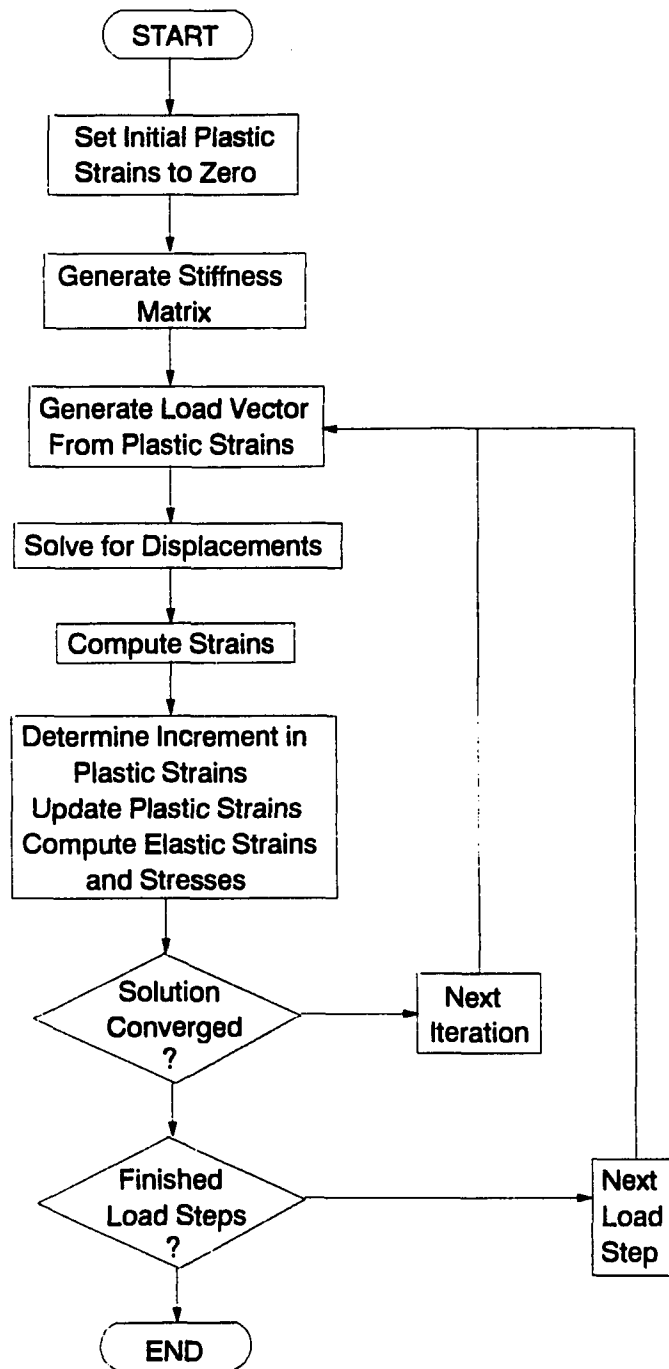
Figure 3.4 Solution procedure - plasticity with stepped loading and convergence checking.

3.2.4. Tests for Drucker-Prager model performance

The prediction capability of the Drucker-Prager elastic-perfectly plastic model as it is implemented in the ANSYS package was tested by comparison to the results of triaxial tests. The soil subject to test was classified as sandy clay with a cohesion value of 20 kPa and an internal friction angle of 26° as determined from the results of drained triaxial test results [40] under three different cell pressures.

A simple finite element model consisting of a single three dimensional isoparametric solid element with eight nodes (coded as STIF45 in ANSYS) was considered to be appropriate for this case. The element was modeled as a cube with assumed frictionless boundaries on the surfaces. Proper boundary conditions were imposed so that the element can freely deform without free body motion under deviatoric loads.

To simulate the drained triaxial test conditions, the model was loaded in two successive steps. In the first step the cell pressure alone was applied to the model to simulate the sample consolidation. Then, in the second step the sample is loaded with an increasing axial deviatoric force until failure was reached. The model responses for the three cases are plotted in Figure 3.5. As is clearly observed, following a linear elastic stage, the failure is sudden with no strain hardening and the model deforms without limits once the failure load is reached. The failure loads obtained from the model study are tabulated in Table 3.1. along with the
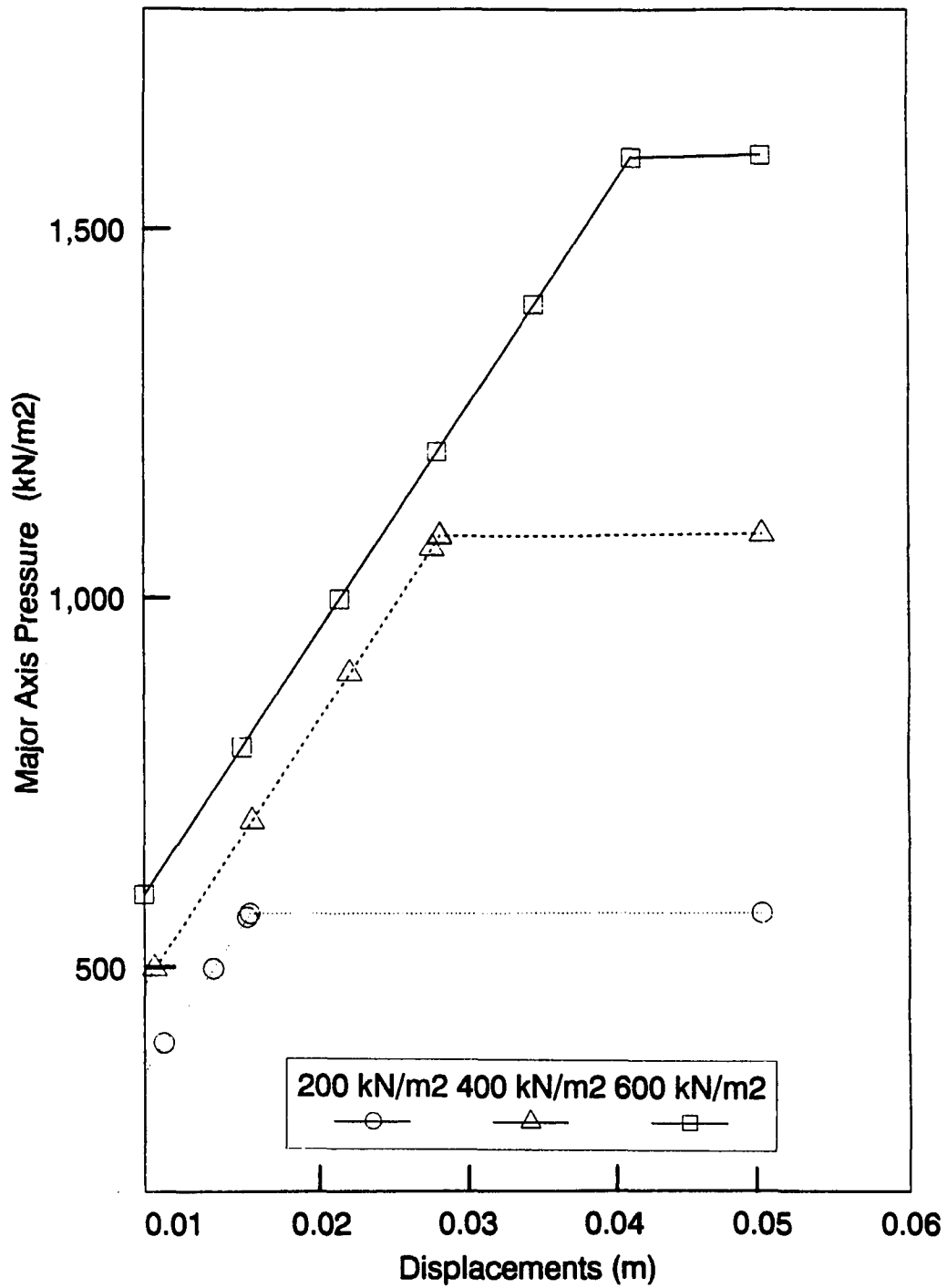
Figure 3.5 Triaxial test simulation using Drucker-Prager model.

Table 3.1 Failure loads for the test and model study results.

Cell Pressure (σ_3)	Triaxial Test Failure Load (σ_1)	Drucker-Prager Model Failure Load (σ_1)
200	582	577
400	1091	1089
600	1620	1602

* Values are in kN/m3

triaxial test results. The failure loads for the test and model study were also plotted in Figure 3.6. in the form of stress paths for a direct visual comparison. Overall results indicate that the failure loads predicted by Drucker-Prager model as implemented in ANSYS package are in good agreement with these simple test results. The values predicted by the model are slightly lower than those of the triaxial test results in all three cases. However this is partially caused by the idealized boundary conditions in the model. In actual triaxial test conditions, frictional and/or cohesive forces are developed at the edges of the sample and the porous plates bounding the sample on the top and bottom. These forces together with the support of the rubber membrane surrounding the sample cause somewhat higher failure loads during testing. Although it may be possible to model these effects with a more elaborate finite element model, such an attempt is beyond the scope of this study.

3.3. Verifications and Parametric Studies with ANSYS Finite Element Package

In this section a series of parametric studies were conducted to evaluate the effects of several factors that are involved in the finite element modelling of a sheetpile structure. These studies also serve the purpose of verification of the performance of the ANSYS package for the specific modelling application. Individual element and routine performance are illustrated in detail and verified
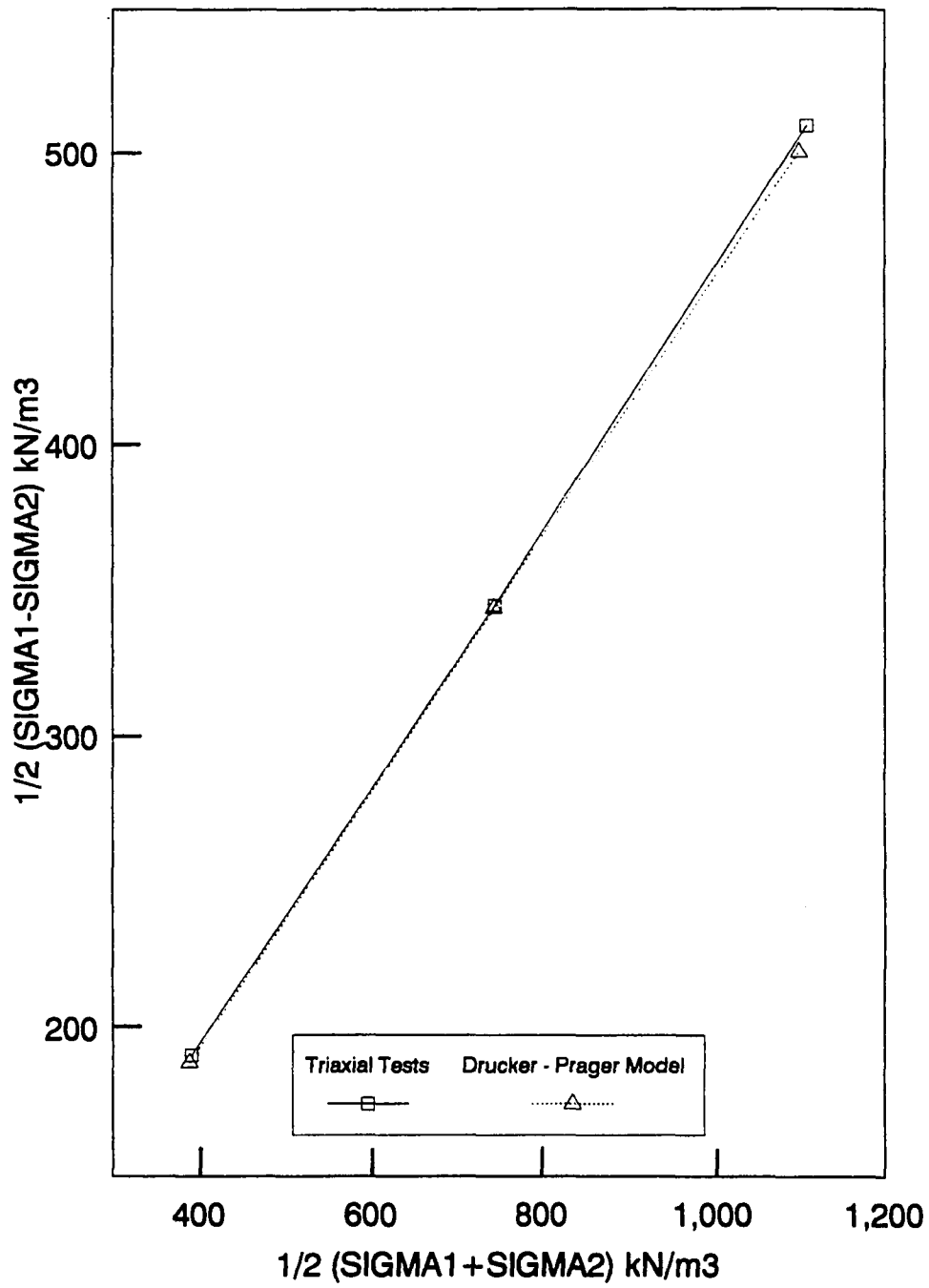
Figure 3.6 Stress path representation of model response and test results.

with theoretical solutions in the ANSYS manuals [28].
Therefore, the focus here is on the collective performance of
the elements together with the Drucker - Prager model. Earth
pressure profiles are presented for each parameter.

A wedge model with the approximate dimensions and
material properties of a typical cell in the Calumet Harbor
Breakwater structure was used for the analyses. The model
represents an isolated cell with a cell diameter of 22.5 ft.
and a cell height of 42 ft. as shown in Figure 3.7. The cell
fill has a saturated unit weight of 130 pcf and a friction
angle of 30°. The elastic modulus and Poisson's ratio are
assumed to be 1800 ksf and 0.4, respectively. The water level
is assumed to be at the top of the cell. This condition
corresponds approximately to the calm lake condition with the
actual water level located at 2 ft. below the still water
level.

To consider the softening effect of the sheetpile cross
sectional geometry, the elastic modulus of the cell has to be
reduced in the circumferential direction with respect to the
elastic modulus of the sheetpile material. However, as the
structure becomes less stiff, the number of iterations
required for the solution increase impractically. In Section
3.3.1. a parametric study was presented with four different
values of the circumferential modulus. In the rest of this
chapter the circumferential modulus is assumed to be 1/10 of
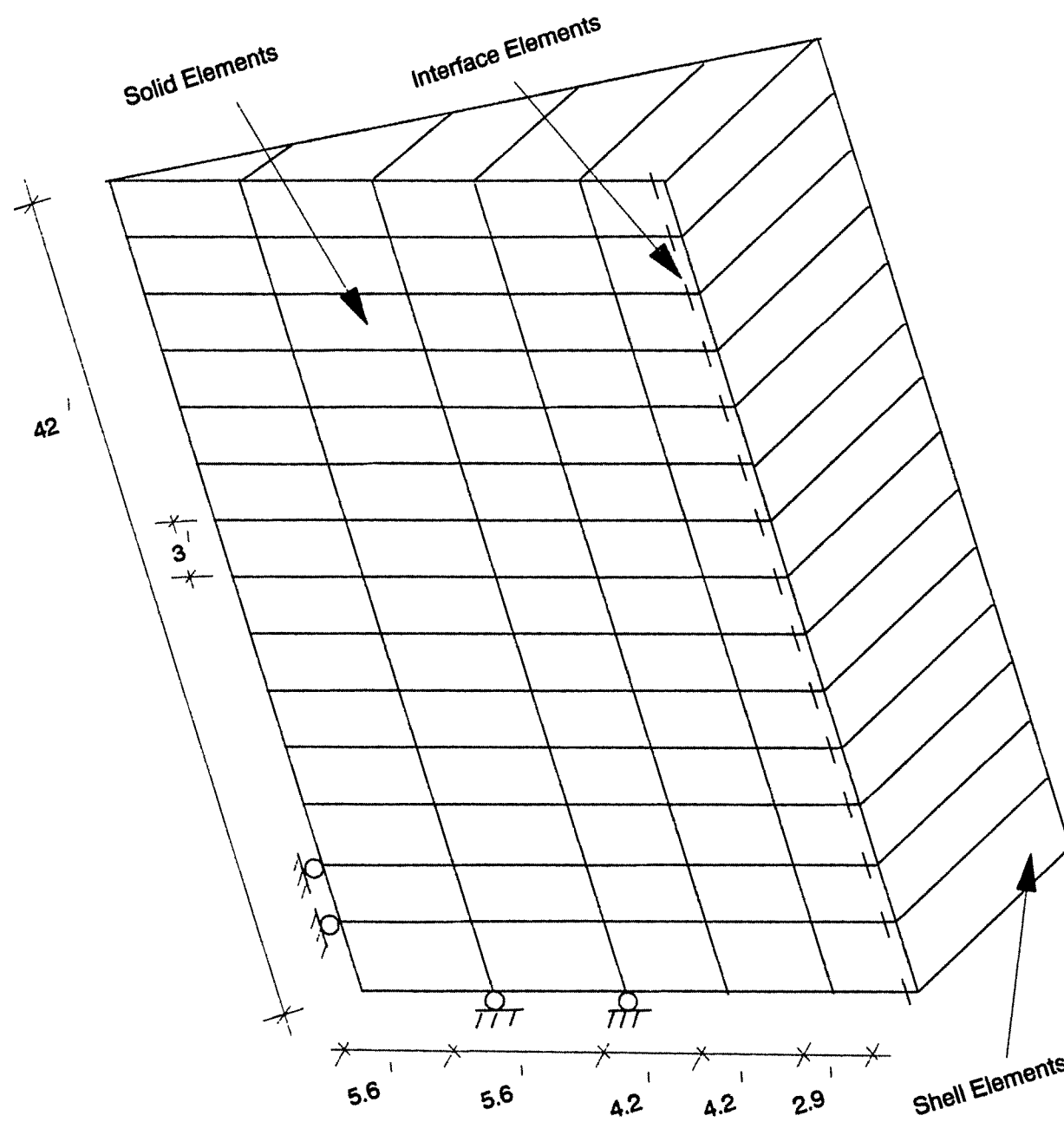the elastic modulus of steel for the cell.

Figure 3.7 Finite element model used in the parametric studies.

Three different element types are used in the model from the ANSYS element library. These include the 8-node three dimensional solid element for the fill, 4-node shell element for the sheetpile and 3-dimensional frictional interface element for the fill/sheetpile interface which are coded as STIF45, STIF63 and STIF52, respectively.

3.3.1. Sheetpile lateral stiffness

Dependence of the lateral earth pressures on the circumferential modulus of the sheetpile wall was investigated. Normally, as the circumferential stiffness of the sheetpiles is reduced, a decrease in the lateral soil pressures would be expected since the soil strength would be further mobilized due to the additional deformations. Furthermore, these pressures would be either bounded by or comparable to the active and at rest earth pressure distributions as defined in the classical soil mechanics. Five different circumferential modulus values for the sheetpile were tested on the model. These values with respect to the elastic modulus of the steel were 1/50, 1/10, 1, 10 and 50.

Profiles of the earth pressures resulting from each case are shown in Figure 3.8. A consistent increase in lateral earth pressure profiles was observed with the increasing lateral sheetpile stiffness. The resulting earth pressure profiles were bounded by the active and at rest earth pressure profiles of the Rankine's lateral earth pressure theory with
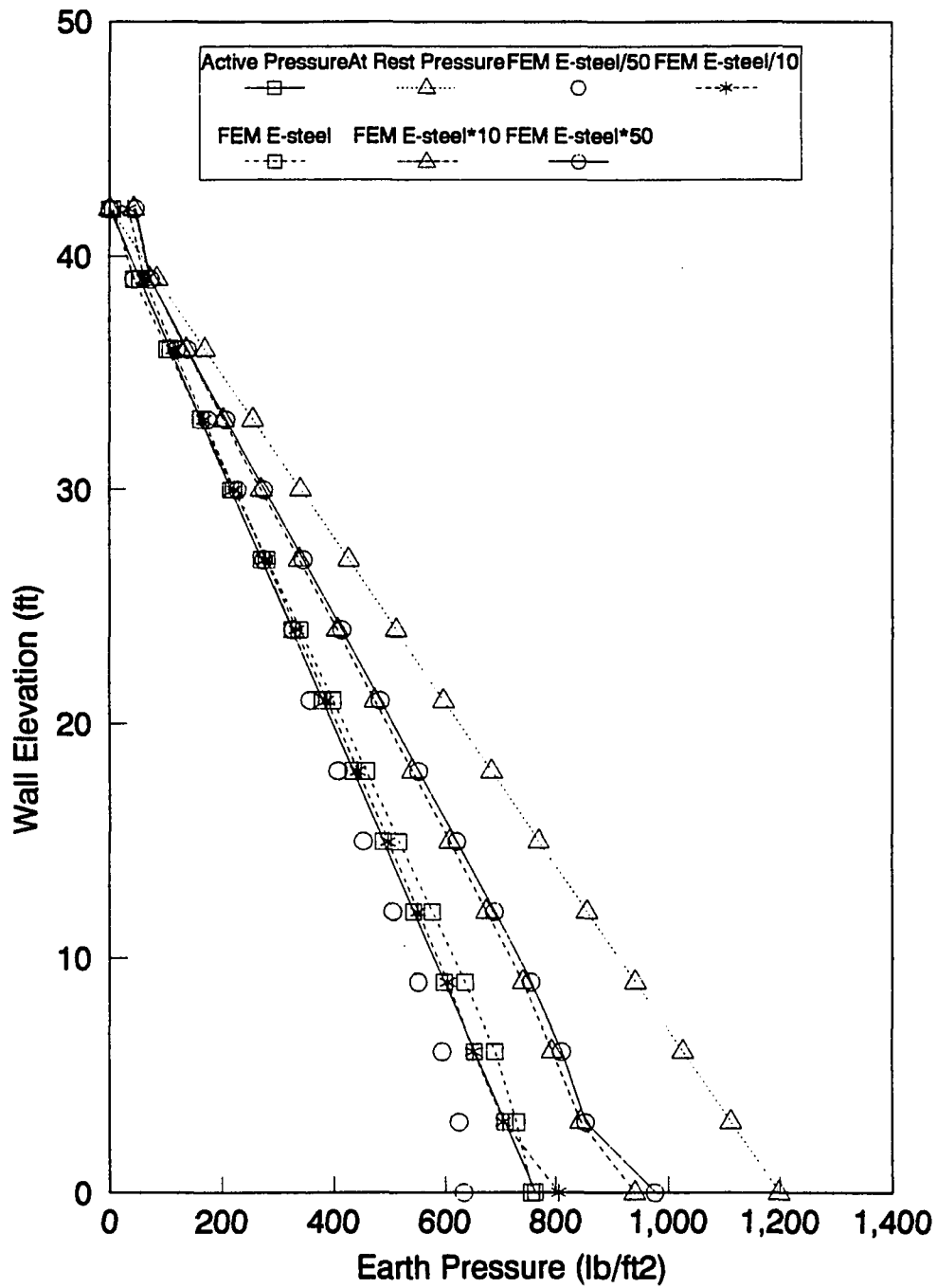
Figure 3.8   Effect of lateral sheetpile stiffness on lateral
earth pressures.

the exception of the case for 1/50 which fell slightly below

the active profile.

3.3.2. Associativity

As previously discussed in this chapter, the

associativity parameter describes the volumetric changes

during plasticity under shear stresses. Lateral earth

pressures calculated from the associated and nonassociated

cases are presented in Figure 3.9. The differences in

pressure profiles between the two cases are small. Although

this may seem surprising, the results of previous studies [36]

on the effects of associativity indicate that such effects are

largely dependent on the nature of the problem and the loading

conditions.

3.3.3. Wall-soil friction

The sensitivity of the pressure profiles to the

frictional coefficient of the interface elements is

investigated. A value of 0.3 was commonly used for the

frictional coefficient of the interface elements throughout

the parametric analyses in this chapter. Values of 0.0 and

0.7 were used to investigate the sensitivity of the pressure

profiles to the frictional coefficient. These two values

constitute the limits for possible range of the frictional

coefficient since 0.7 corresponds to the internal friction

angle of the fill (tan 35·). The resulting earth pressure

profiles are presented in Figure 3.10. A small increase in

the pressure profile was observed at the bottom 2/3 of the
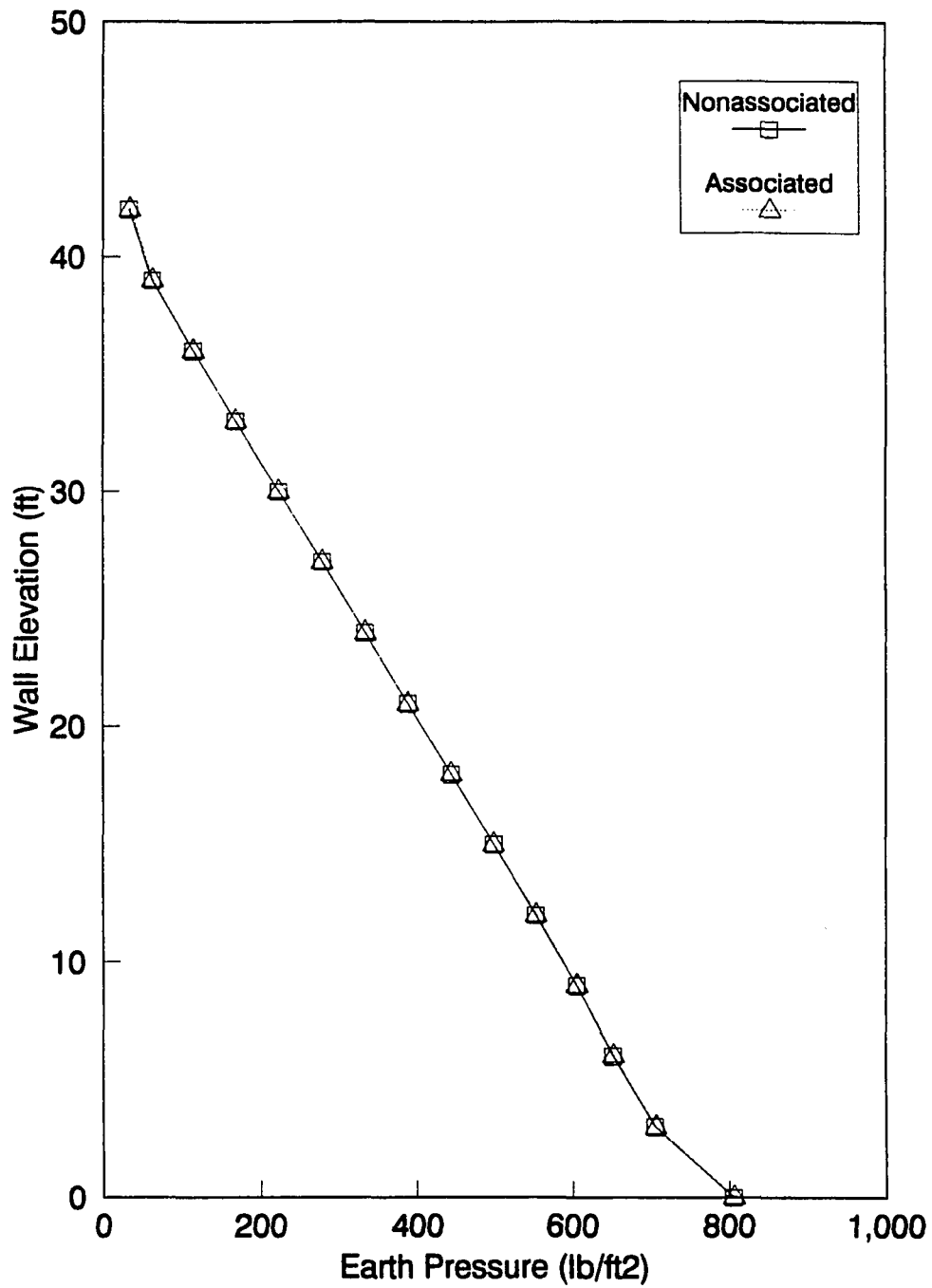
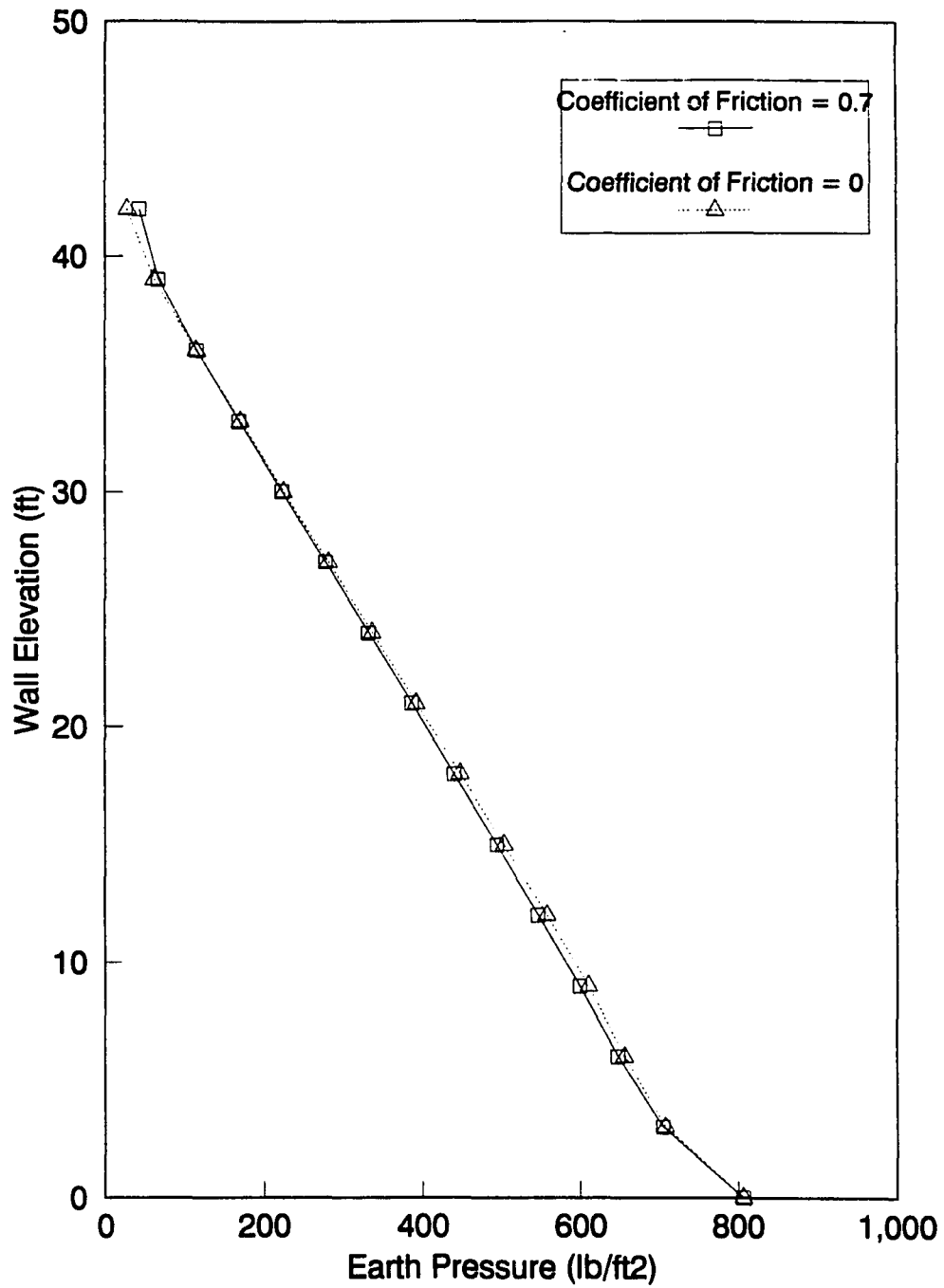Figure 3.9   Effect of associativity on lateral earth
             pressures.

Figure 3.10   Effect of wall-soil friction on lateral earth
              pressures.

wall height in the frictionless case.

3.3.4. Mesh density sensitivity

A second finite element model having the same dimensions as the previous model but with 1/3 fewer elements was used to examine the mesh density effects on the earth pressures. The solid elements were reduced in the vertical direction only and the interface and shell elements were arranged accordingly.

Results indicated slight but consistent decrease in the prediction of earth pressures by the second model as shown in Figure 3.11.

3.3.5. Permanent effects of lateral loads

In Chapter 1 it was noted that the horizontal forces imposed on the structure by the waves could possibly have caused permanent changes in the lateral earth pressure levels and pressure profiles which may sharply contradict with the predictions by the conventional methods. Although this hypothesis will be investigated in greater detail in the following chapters with the more elaborate models, a preliminary attempt is made here to illustrate the existence of such effects.

The model is loaded in four steps to simulate the loading sequence. The pressures resulting on the sheetpile wall after each step are shown in Figure 3.12. The first step consisted of the solution for the self weight of the fill and sheetpiles. In the second step, a 480 psf pressure was applied on top of the fill to simulate the capstone placement.
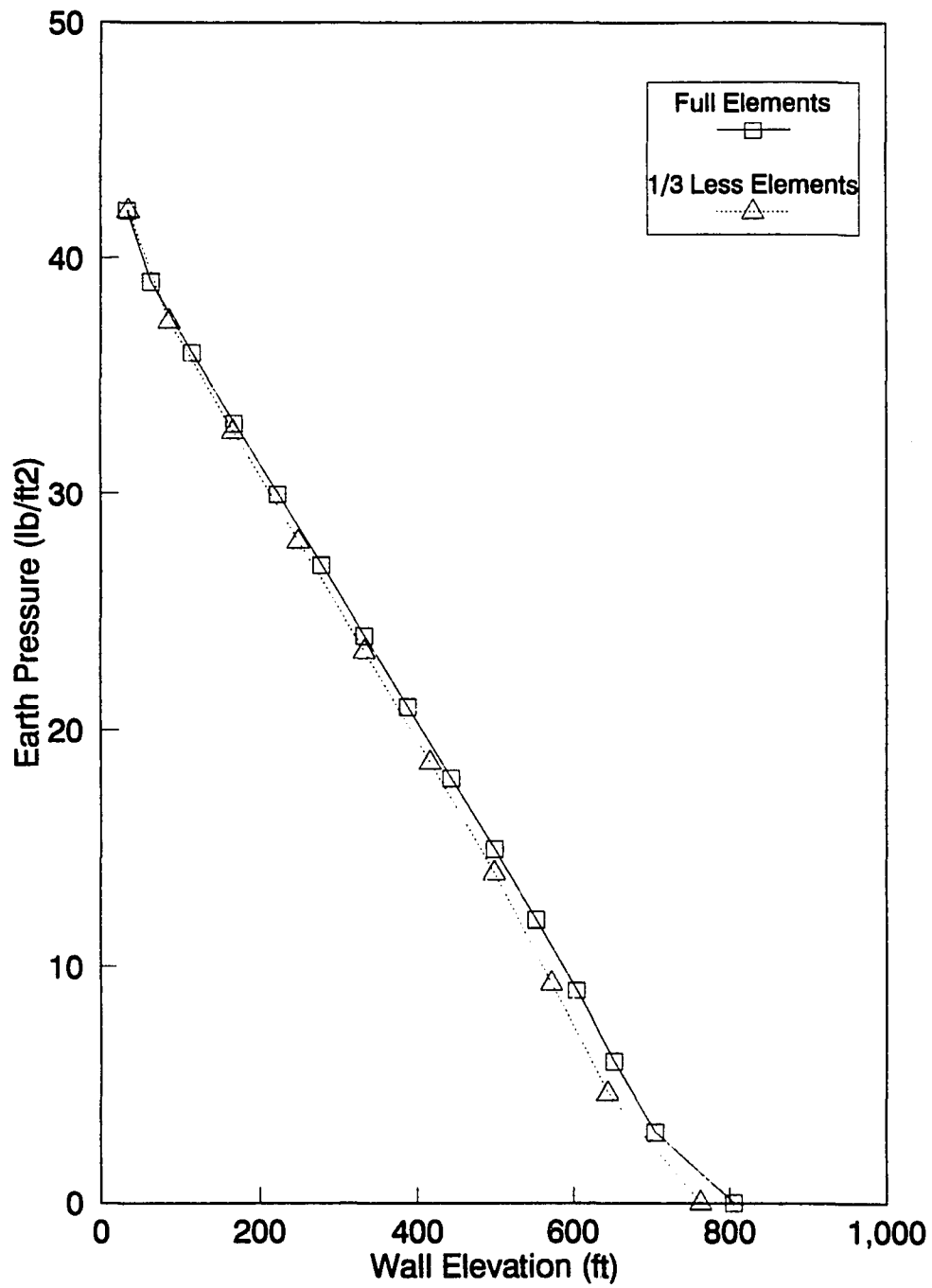
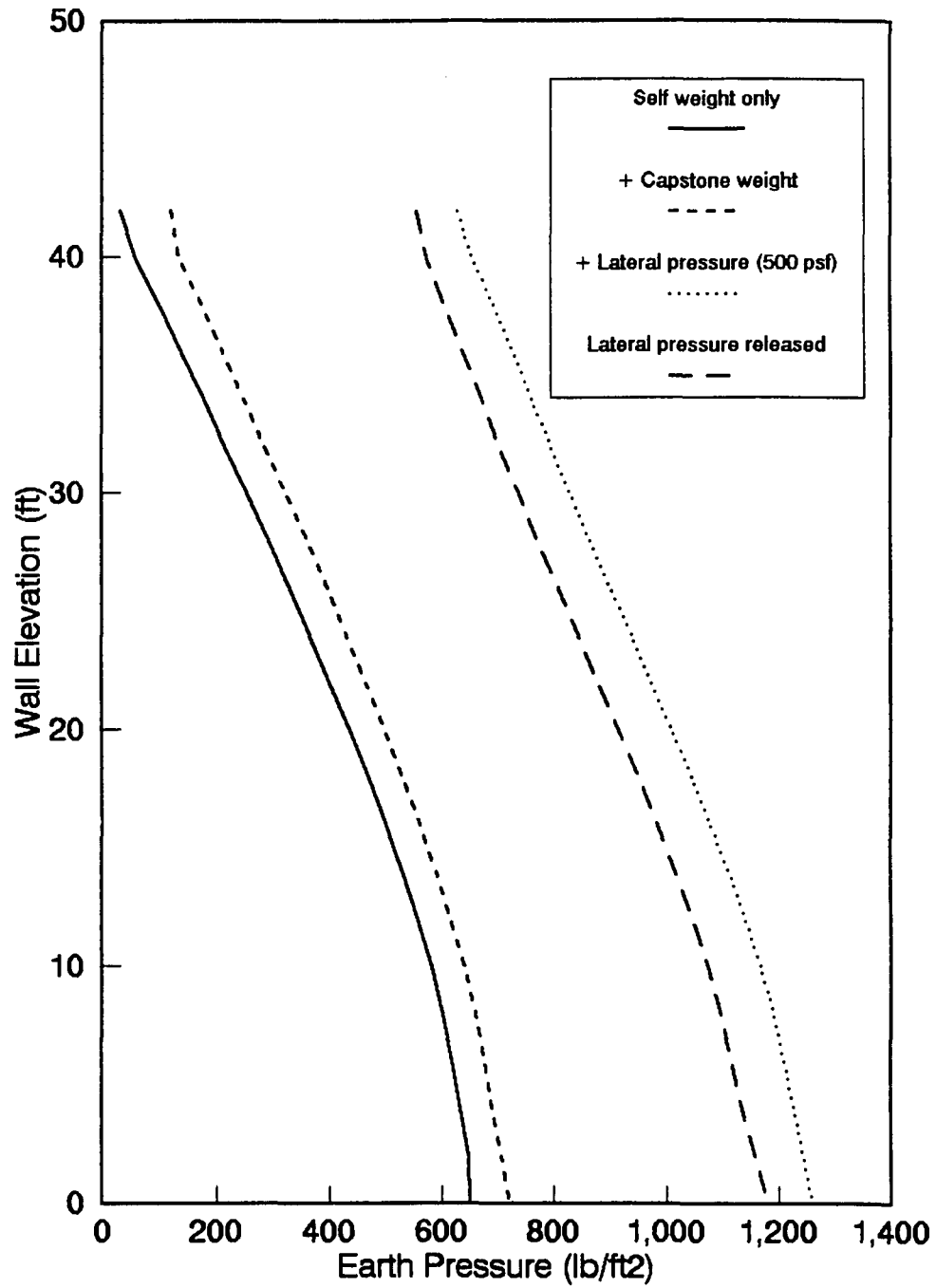Figure 3.11 Effect of mesh density on lateral earth
pressures.

Figure 3.12 Permanent effect of lateral loads on lateral earth pressures.

An overall increase in the lateral pressure profile of about 90 psf occurred at the top of the cell and about 50 psf at the bottom. This pressure profile corresponds to the condition after construction with no storm wave effects on the structure having acted yet. In the third step, a hypothetical horizontal pressure of 500 psf was applied on the sheetpile surface in the outward direction of the cell. In the final step, the loading condition in the second step is resumed with the release of the hypothetical pressure.

The final pressure profile has a significantly different pressure magnitude even though it has a similar trend to the initial two profiles. Approximately 450 psf additional pressure remains on the sheetpiles throughout the wall height after the release of the hypothetical pressure.

4. FINITE ELEMENT ANALYSES OF THE CALUMET HARBOR BREAKWATER

4.1. Introduction

In this chapter, structural analyses of the Calumet

Harbor Breakwater using two- and three-dimensional finite

element models are introduced. A vertical slice model was

utilized for the two dimensional analysis since, as discussed

in Chapter 1, it is the only available two-dimensional finite

element technique which allows application of nonsymmetrical

lateral loads on the structure. In the finite element

analyses, the loads generated by cell filling, capstone

placing and waves are applied in a series of increments which

are designed to model the actual loading sequence.

Since one of the goals of this study was to compare the

applicability of the two- and three-dimensional approaches in

modeling, inherent advantages of each model were utilized.

Consequently, while the three-dimensional model formation is

relatively sparse, it represents the true geometry of the

structure. The two models were intended to be compatible with

one another and the meshes were developed according to the

location of the strain gauges (Figure 2.2) to provide a

reliable basis for comparison of analytical and recorded data.

4.2. Analysis Methodology and Assumptions

The methodology described in this section was applied for

two and three dimensional models during the analyses. The

analysis consists of three sequential stages which represent

the realistic load history on the breakwater. These stages
are: (1) simulation of the breakwater construction sequence,
(2) simulation of the cumulative wave effects on the
breakwater, and (3) wave load analyses. The loads were
applied in incremental steps wherever necessary and the
iterations were performed using the modified Newton-Raphson
method until convergence conditions were reached for each load
step. These conditions constitute the stabilization of the
interface elements and the reduction of the displacement
increment and the ratio of plastic to elastic displacements
(termed "plasticity ratio" in ANSYS) to a specified magnitude
(1.E-4 and 1 respectively) for elements representing the
geomaterials in the models. The Drucker-Prager model, which
is the plastic model used for the geomaterials, is described
in detail in Chapter 3.

The loading sequence for the construction simulation
stage is shown in Figure 4.1. The first step consists of the
placement of cell fill in four layers (Figure 4.1.(b)). The
foundation soils prior to this step were assumed to be at the
at rest condition and no stresses due to the pile driving were
assumed to exist in the sheetpiles and the surrounding soils.
Buoyant unit weight values were used throughout the analyses
for the materials in sections of the model falling below the
still water level of the lake.

In the second step of the construction stage, placement
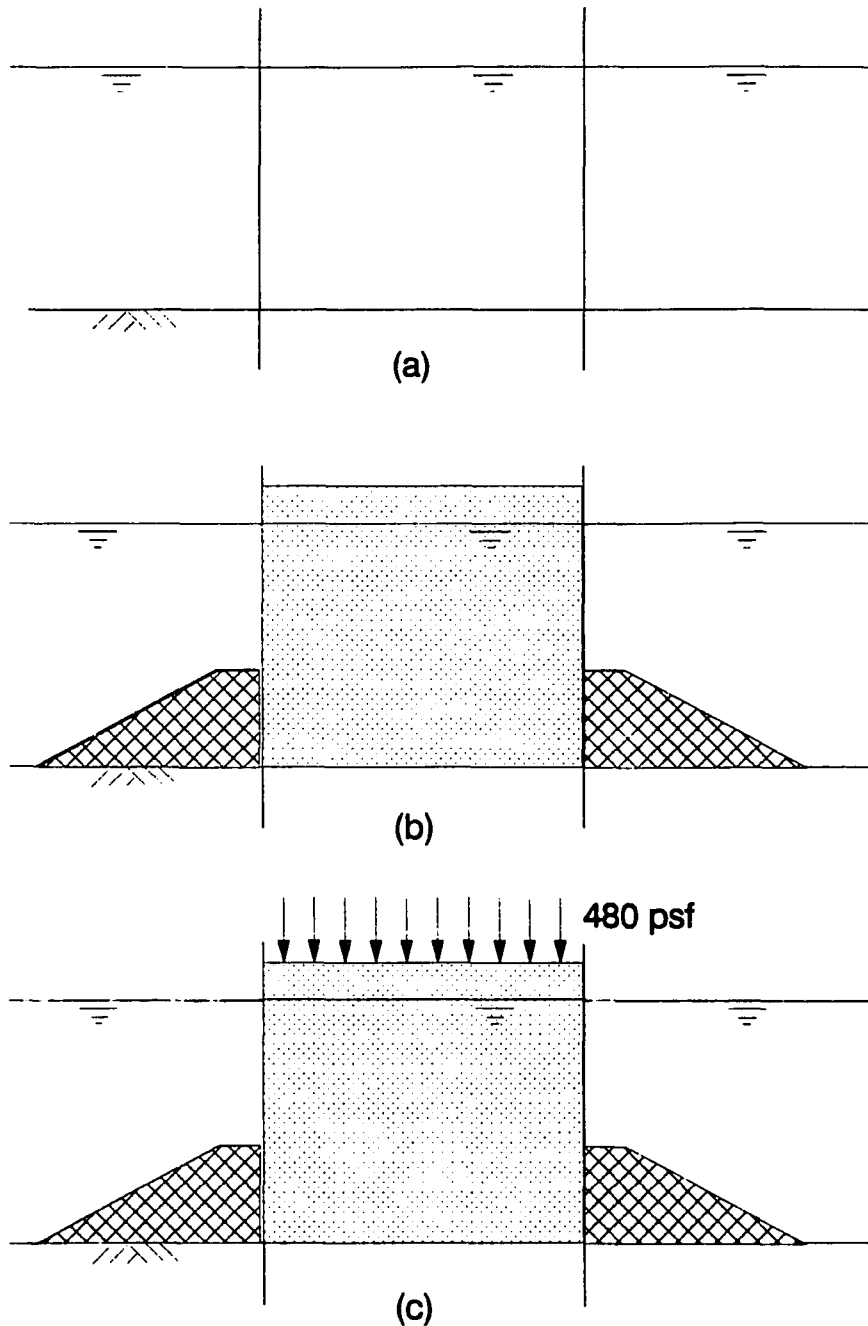of the capstones over the cell fill was simulated by applying

Figure 4.1 Construction simulation loading sequence: (a)
piles assumed to be placed prior to the loading,
(b) self weight imposed with fill and berm
placement, (c) capstone loading is applied on top
of the fill.

a surcharge load of 480 psf (Figure 4.1.(c)) on top of the bedding stone layer. The capstones are large concrete stones ranging from 7 to 20 tons each. The site observations indicated that the original configuration of the capstones were often disturbed and they appeared to be in contact with the sheet piles at several locations in a cell. However, these contacts were omitted in the model since they occurred infrequently and randomly and are difficult to model properly.

The results of the analysis at the end of the first stage correspond to the conditions that existed in the structure just after the completion of the construction and before any wave effects, herein after referred to as the "post-construction state". In Chapter 1 it has been hypothesized that the wave action over the decades could have caused considerable deviation from the post-construction state. In Chapter 3, using an axisymmetric model it has been verified that for a single cell temporary unbalanced lateral loads imposed permanent changes from the post-construction condition. This latter condition of the structure will be referred to as the "present state".

The objective of the second analysis stage is the determination of the present structural state of the breakwater structure. Behavior of the structure under wave action has already been discussed in detail in Section 1.3.3. The interlock forces in sheetpiles are increased due to the higher hydrostatic differential and the changing direction of

the hydrodynamic component of the wave as the wave peak

recedes to a wave trough at the lake side wall of the cell.

As a result, the sheetpiles stretch, and the fill can settle

under the effect of gravity. This process would realistically

be irreversible. A reasonably practical method to simulate

such complex cumulative effects in the finite element models

was necessary.

To determine an approximation of the present state, the

wave pressure profiles generated using statistical hindcasting

techniques for the Calumet Harbor were scanned for the wave

pressure values [2]. Two pressure profiles which

approximately envelope the maximum and minimum pressure values

in the direction normal to the longitudional axis of the

structure along the height of the cell wall above the lake bed

were considered (Figure 4.2.(b) and (c), respectively).

Cycles of these two pressure profiles were successively

applied to the models starting with the initial condition and

assuming the cell is full with water at all times during the

analysis (Figure 4.2.(a)). Cycling continued until the

displacements and interlock forces stabilized in a load cycle.

That is, the loads were changed from Figure 4.2. (a) to (b) to

(a) to (c) to (a) and so forth to simulate a large wave cycle.

The result of the analyses after the application of the

pressure profiles (end of second stage of analysis) and the

removal of the internal 6 ft water pressure correspond to the

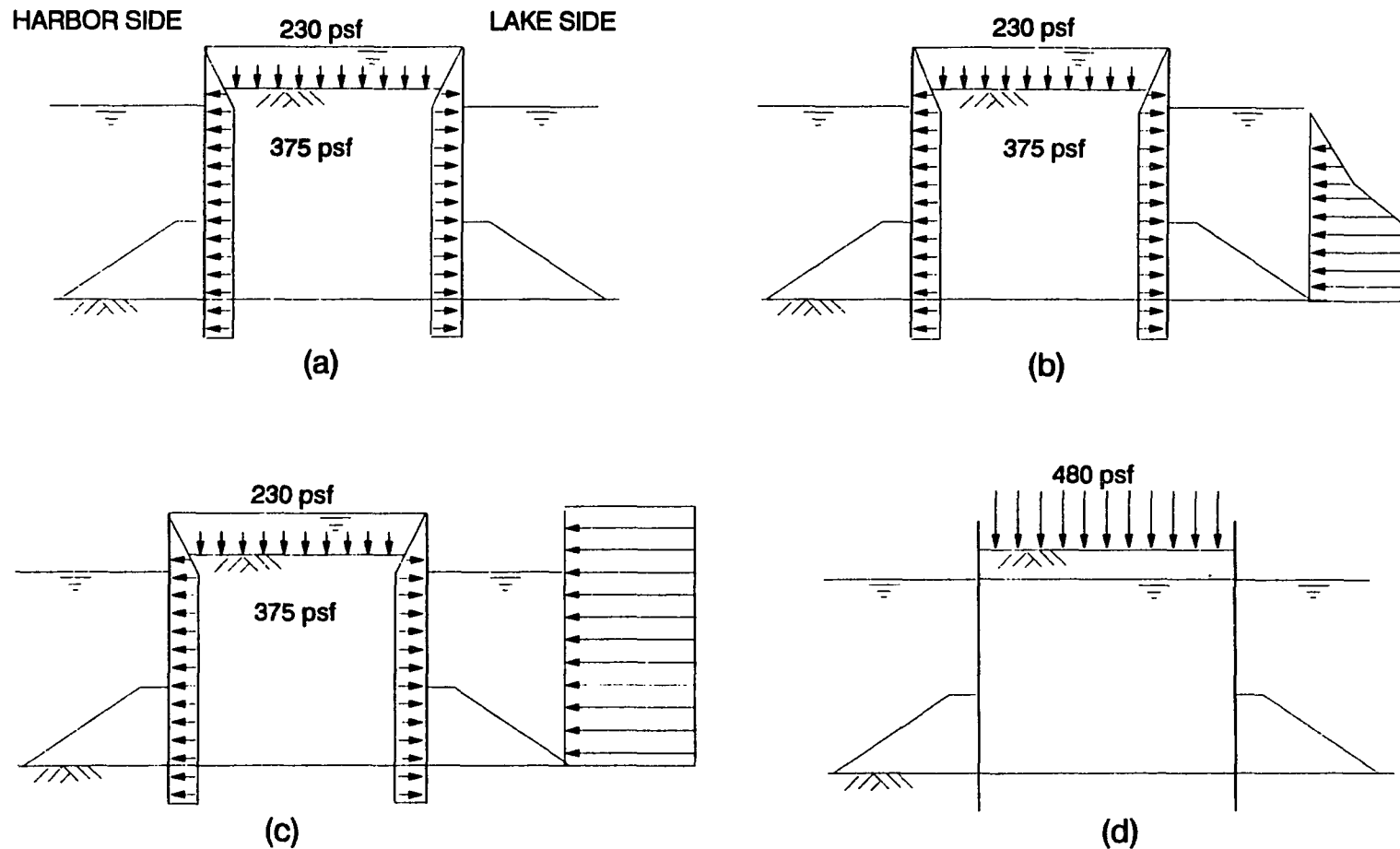"present state" of the structure for a calm lake condition

Figure 4.2 Simulation of the structure's present condition:
(a) cell full with water, (b) wave trough acts
over the cell, (c) wave crest acts over the cell,
(d) back to calm water condition.

(Figure 4.2.d). In the analyses, any further wave loading on
the structure was initiated from this state.

In the third stage, the structure was loaded with a
number of wave pressure profiles to simulate the fluctuating
force levels due to actual wave action. The wave pressures
were multiplied by contributory areas from the cell wall and
concentrated forces were applied to the nodes of the finite
element model. The total pressure profile of a wave is
composed of hydrostatic and dynamic components. The profile
of the hydrostatic component increases linearly along the
depth, whereas the dynamic component profile is variable
depending on the wave and the phase angle. Surface and
pressure profiles (static and dynamic) for a typical wave
acting on the breakwater are shown in Figure 4.3. The dynamic
pressure component, depending on the wave phase, has positive
and negative values for the crest and trough positions,
respectively [41]. Accordingly, to determine the total wave
pressure, the dynamic pressure component is added to the
hydrostatic pressure. Thus, the combination of hydrostatic
and dynamic pressure components at the crest and trough
positions of a wave form upper and lower limits of the total
pressure exerted on the structure.

Following the above argument, for a given wave acting on
the breakwater, the range of the force fluctuations in the
sheetpiles can be assumed to be contained within the two
stress states of the structure corresponding to the trough and

WAVE PROFILE

BREAKWATER

PRESSURE
PROFILE
FOR
PEAK WAVE

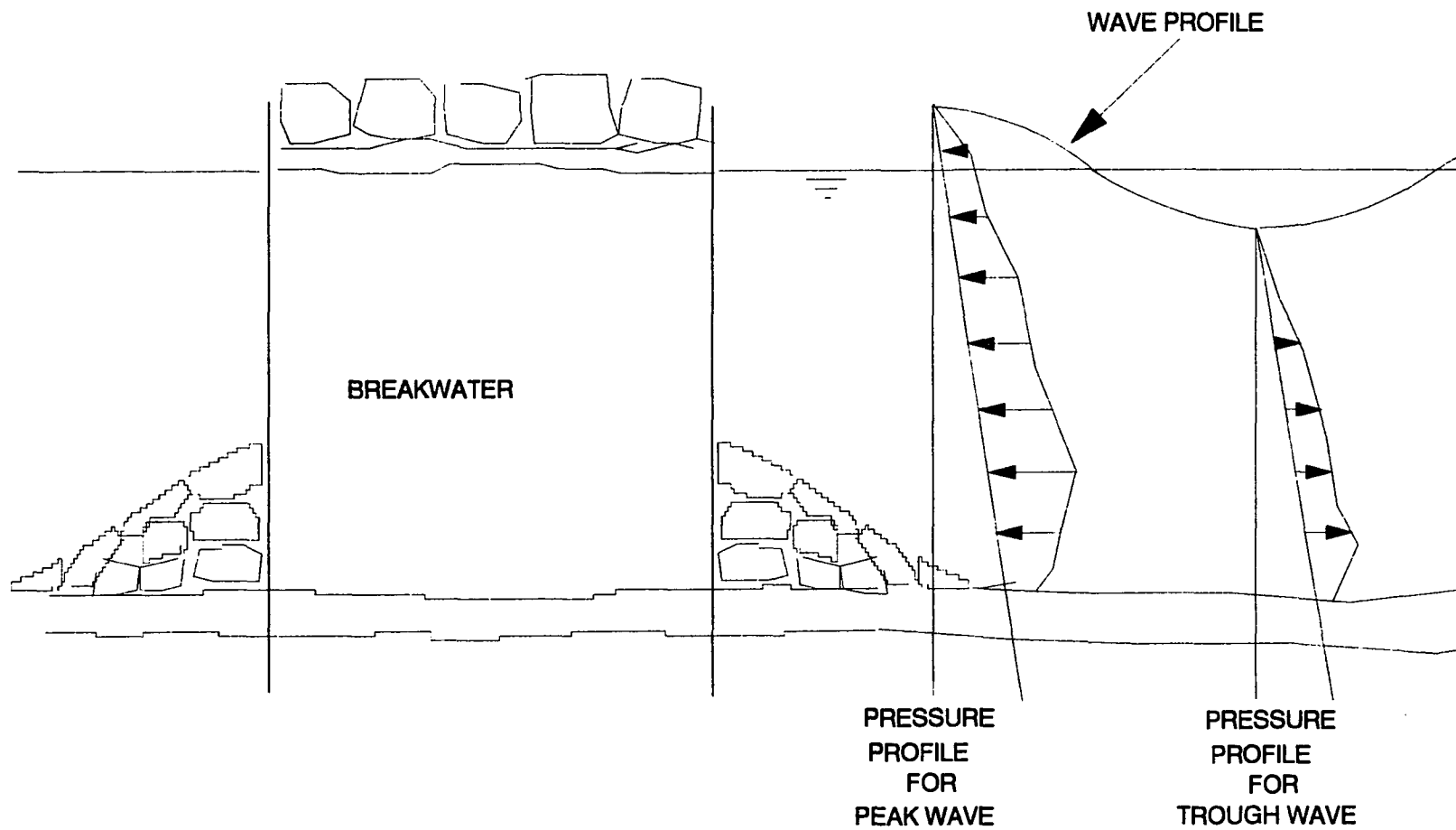PRESSURE
PROFILE
FOR
TROUGH WAVE

Figure 4.3   Schematic view of the forces acting on the
              breakwater.

crest loads of the wave. During the analysis, the interlock
force levels corresponding to the crest and trough positions
of a specific wave were obtained from the finite element model
solutions. The differences between the two conditions
indicate the range of force fluctuations in the sheetpile
system along the height of the structure.

The following assumptions apply to the analyses involving
the determination of the present state and the fluctuating
force levels due to the wave action (stages two and three,
respectively):

1. Wave pressures act over the portion of the sheetpiles
   extending above the lake bed.

2. The lake surface on the harbor side remains at calm
   water level at all times.

3. The cell is filled with water at all times during the
   wave action.

4. Downward pressures due to wave overtopping, and the
   fluctuating seepage forces in the fill and foundation
   soils due the unbalanced internal and external
   hydrostatic pressures were assumed to be negligible.

5. The fundamental periods of the breakwater structure in
   hoop and flexural directions were calculated for an
   isolated cell as 0.10 sec. and 0.18 sec.,
   respectively. Since these values are very low
   compared to the range of the periods of the Calumet
   Harbor Breakwater waves (the smallest periods are 1 to

2 sec. for 2 to 3 ft waves), the dynamic effects on the structural response were omitted.

4.3. Fill and Foundation Soil Parameters

As described in Section 1.3.1., four different types of soil materials occur in the finite element models. These are; 1) fill in the cell, 2) toe stone at the harbor and lake sides, 3) a sand layer at the lake surface, and 4) a clay layer at the cell foundation. It was mentioned in Chapter 3 that the Drucker-Prager model as implemented in ANSYS requires three constants (two strength parameters and a dilatancy parameter) for the analysis. In addition, elastic material parameters and unit weights of fill and foundation materials are required for the finite element analysis.

The failure analysis study of the Calumet Harbor Breakwater did not include an exploration and/or testing program for the fill and foundation soils. However, such a program was previously undertaken in 1987, in relation to the rehabilitation study of timber crib reaches A and B of the same harbor. The field investigation consisted of a total of eight site borings on the lake and harbor sides within a mile distance of reach C of the harbor. Disturbed and undisturbed soil samples were obtained by means of split barrel and Shelby tube sampling procedures. A complete laboratory testing program was performed with the samples. For further information regarding this study, Major Rehabilitation General Design Memorandum [42], a report submitted to Corps of

Engineers, should be referred to.

In the absence of field and laboratory data at the specific locality of the Reach C of the breakwater, the data provided in the above mentioned report were used as a basis in selecting the strength parameters and unit weights of the foundation soils for the finite element analysis. The properties of the cell fill material were obtained from the Reconnaissance Report [1].

The elastic parameters, Poisson's ratio and elastic modulus for fill and foundation soils were selected from listed values in literature [43,44] considering the conditions of the site. A summary of all soil parameters used for the finite element analyses is presented on Table 4.1.

4.4. Circumferential Sheetpile Stiffness

Sheetpiles in cofferdam structures behave like orthotropic shells (Section 3.3.) because the stiffness of an assemblage of sheetpiles in the direction normal to the interlock axis is considerably lower than in the interlock axis direction. When loaded in the horizontal direction, the general load deformation response of a sheetpile assemblage is nonlinear. Depending on the pile type, the stiffness of the assemblage characteristically increases under increasing load. This behavior is caused by the initial elimination of slack in the interlock joints, gradual seating of the bearing surfaces, and the deformations in the cross-sectional geometry of the pile due to interlock rotation and dishing of the web. After

Table 4.1 Material properties as used in the finite element
models.

Material Type	Bouyant Unit Weight $_b$ (lb/ft³)	Internal Friction Angle ϕ (deg.)	Cohesion Intercept c (lb/ft²)	Elastic Modulus E (lb/ft²)	Poisson Ratio μ
Cell Fill	67.0	35.0	0.0	3.E6	0.25
Clay	66.0	15.0	200.0	0.8E6	0.35
Sand	60.0	30.0	0.0	0.6E6	0.25
Toestone	80.0	35.0	0.0	0.75E6	0.25

these initial effects occur, the response becomes practically linear. In contrast, a linear response with a stiffness equal to that of flat steel plate is displayed when a sheetpile is subjected to uniform loads in the vertical direction.

The Reconnaissance Report [1] contains data on pull tests performed on the PSA23 sheetpiles. The tests were conducted with three different samples, each being loaded in 1,000 lb/in steps up to 10,000 lb/in. The change of length, both elastic and permanent, the rotation of interlocks and the deflection of the web (dishing) were recorded for each load increment. In Figure 4.4 average changes in overall length are given for the three sheetpile samples. These data were used in assessing the lateral stiffness of the cofferdam sheetpile through selection of an elastic modulus value. Assuming the sheetpile specimens as members of uniform cross-sectional area and length, an effective elastic modulus value in the circumferential direction can be calculated for each load increment step using the pull test data in the following formulation:

$$E_i = \frac{P_i L}{A(\Delta L_i)} \qquad (4.1)$$

where,

E_i = effective elastic modulus for a specific load step

P_i = load increment per step

L = specimen length

A = specimen area

L_i = elastic elongation for a specific load step

The range of effective elastic modulus values varies between 0.023 and 0.1 times the modulus of steel.

The piecewise linear load-deformation and permanent set curves are plotted in Figure 4.4. The permanent set data indicate the permanent deflections in the sample corresponding to each load level. The load-deformation curve has consecutive constant modulus values from zero load to 3000 lb/in and between 3000 lb/in to 5000 lb/in which are 0.023 and 0.03 times the elastic modulus of steel, respectively. These two ranges are denoted as Section I and Section II, in Figure 4.4. Preliminary computations performed with the axisymmetric model indicated that force levels above 3000 lb/in can possibly exist in the interlocks during the wave load analysis. Therefore, it was considered suitable to assign the average of the elastic modulus values for sections I and II, or 0.0265 times the elastic modulus of steel. This value was used in both models throughout the analysis.

4.5. Two-Dimensional Finite Element Modeling

The mesh used to represent the breakwater and its foundation in the two-dimensional vertical slice analyses is shown in Figure 4.5. The mesh consists of 212 two-dimensional isotropic quadrilateral elements (STIF42 in ANSYS), 17 bar elements (STIF1 in ANSYS), 36 beam elements (STIF3 in ANSYS), and 34 one dimensional interface elements (STIF12 in ANSYS).
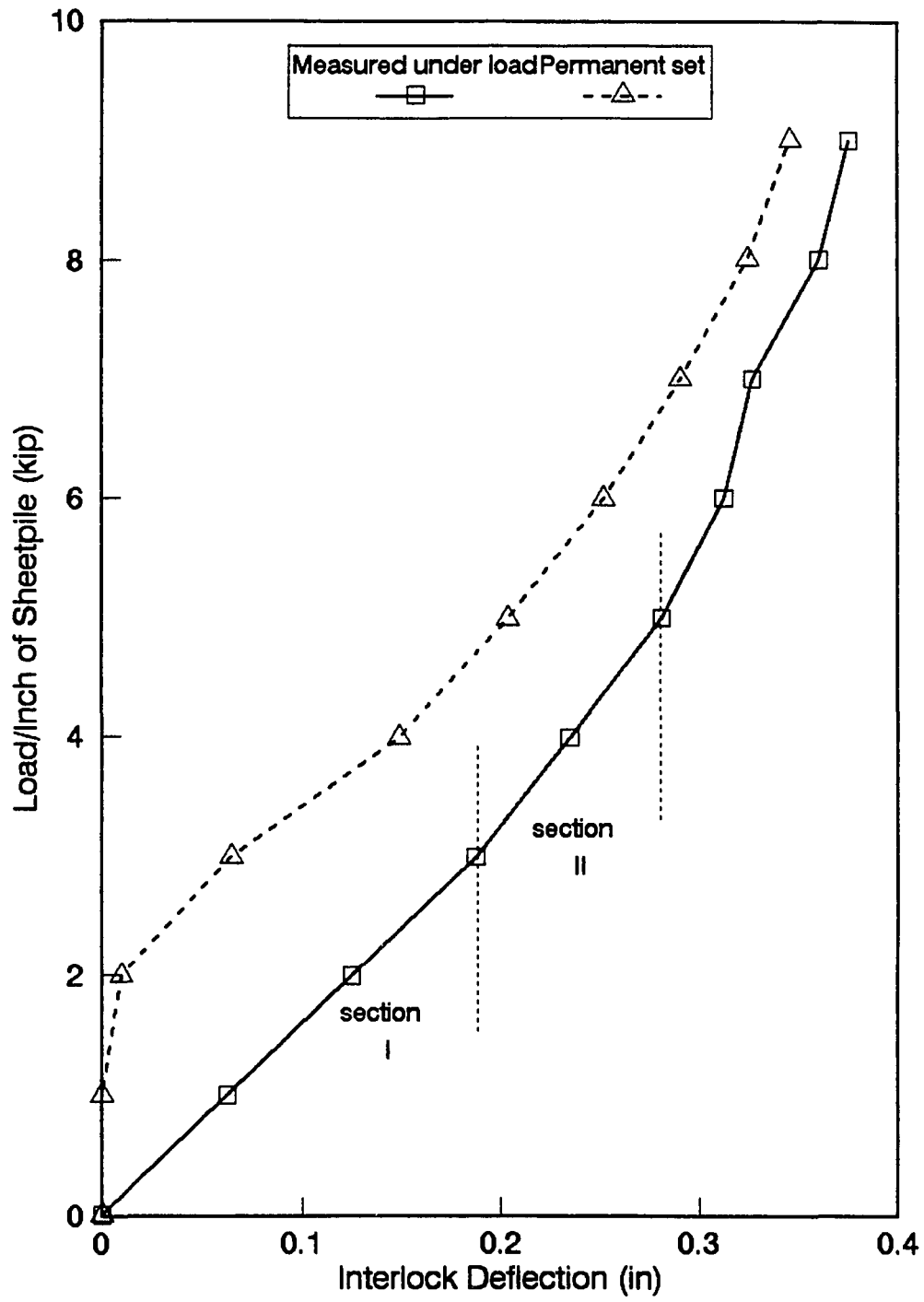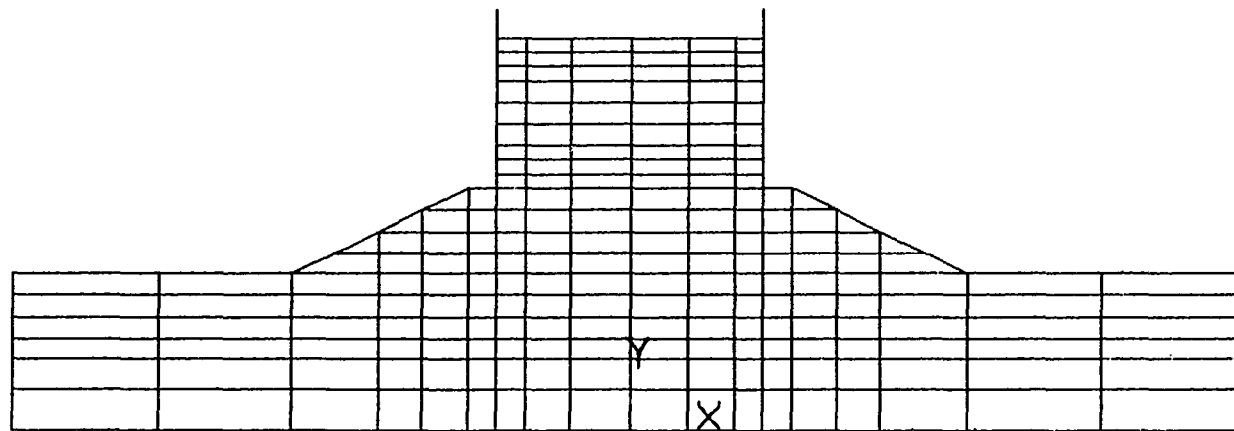
Figure 4.4 Interlock pull test results.

Figure 4.5 Finite element mesh used in the two-dimensional
analysis.

Information regarding the capabilities and application of these elements can be found in Ref. [28]. The rightmost and leftmost boundaries of foundation soils extend 55 feet from the outer wall of the cell on each side. The base of the foundation soil is 13 feet below the bottom of cell walls and assumed to be fixed.

As a common practice in design, a group of cells arranged along a straight line are represented by a row of equivalent fictitious rectangular cells [13]. The form and the cell geometry of the Calumet Harbor Breakwater is quite suitable for an idealization of this kind (see Figure 4.6). The idealization can be further extended to the form of an average vertical slice of unit thickness for a two-dimensional finite element model implementation. For this purpose the stiffness of the diaphragm wall and the flexural stiffness of the outer walls were scaled to a unit thickness of the structure. The stiffness of the diaphragm wall corresponding to the vertical slice was then distributed along the height of the cell using bar elements which act like stiff springs connecting the outer walls and transmit axial forces, thus exerting no restraint on the vertical movements of the fill inside the cell (Section 1.4.2). The details of this idealization process for the Calumet Harbor breakwater structure is also presented in Appendix A.

Beam elements (STIF3 in ANSYS) were used to model the two walls of the cofferdam cell in the planar system of the
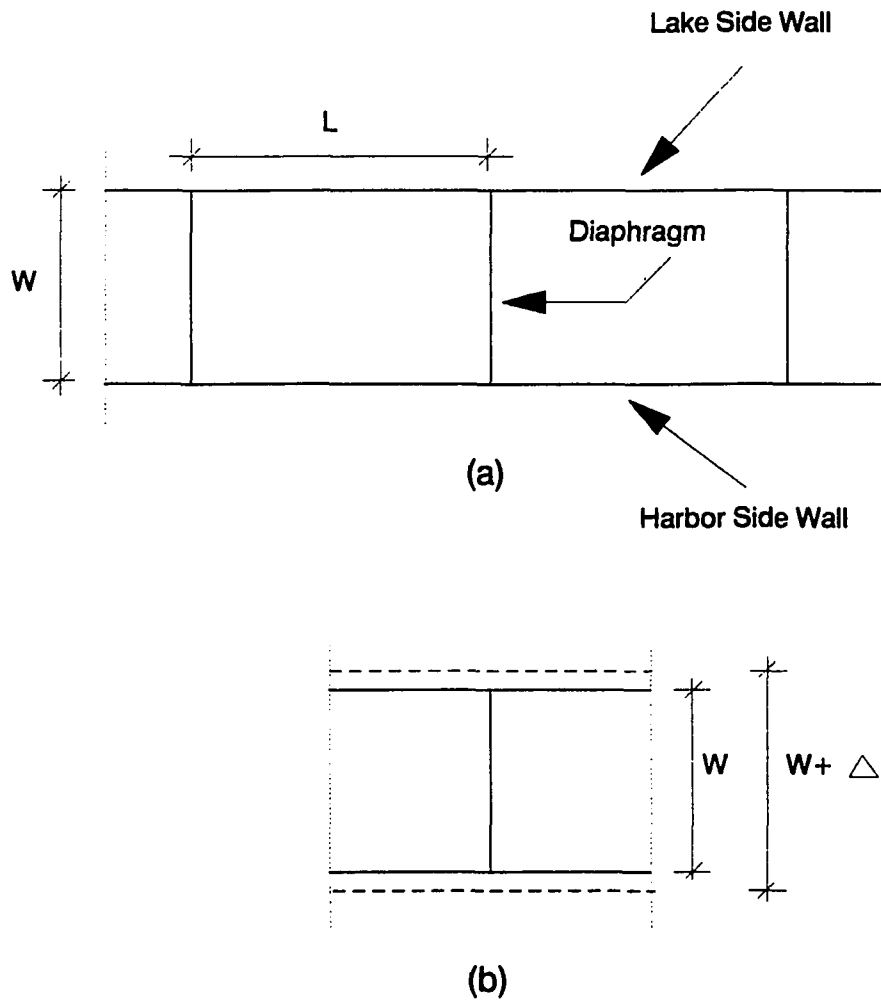
Figure 4.6.(a)   Top view of the equivalent straight-walled rectangular cofferdam, (b) the repetitive structural pattern used in the bar element stiffness assessment.

vertical slice model. The cell fill and the foundation soils

are represented by two dimensional quadrilateral elements

(STIF42 in ANSYS). The walls were connected with bar elements

(STIF1 in ANSYS). One dimensional interface elements (STIF12

in ANSYS) were located between the beam and the two-

dimensional isoparametric elements to allow relative movements

to occur between the sheetpiles and the adjacent soils in the

fill. The element connection detail between quadrilateral

soil elements, interface elements, beam elements and spring

elements are illustrated in Figure 4.7.

Figure 4.8 shows a free body diagram of the Y-joint where

the diaphragm and external wall piling are connected. The

spring forces that were generated from the two-dimensional

finite element model were resolved into forces in the

diaphragm wall and the external walls on the basis of geometry

and statics.

4.6. Three-Dimensional Finite Element Modeling

Only an isolated repetitive pattern of the breakwater as

shown in Figure 4.9 needs to be represented in three-

dimensions due to the existing symmetry conditions in the

longitudional direction (see Figure 4.8). In order to provide

a basis for comparison of interlock forces and displacements

between the models, the vertical mesh density in the two

dimensional model was used. However, a sparser mesh than used

in the two-dimensional model was used in the horizontal

direction in order to not exceed the wavefront and memory
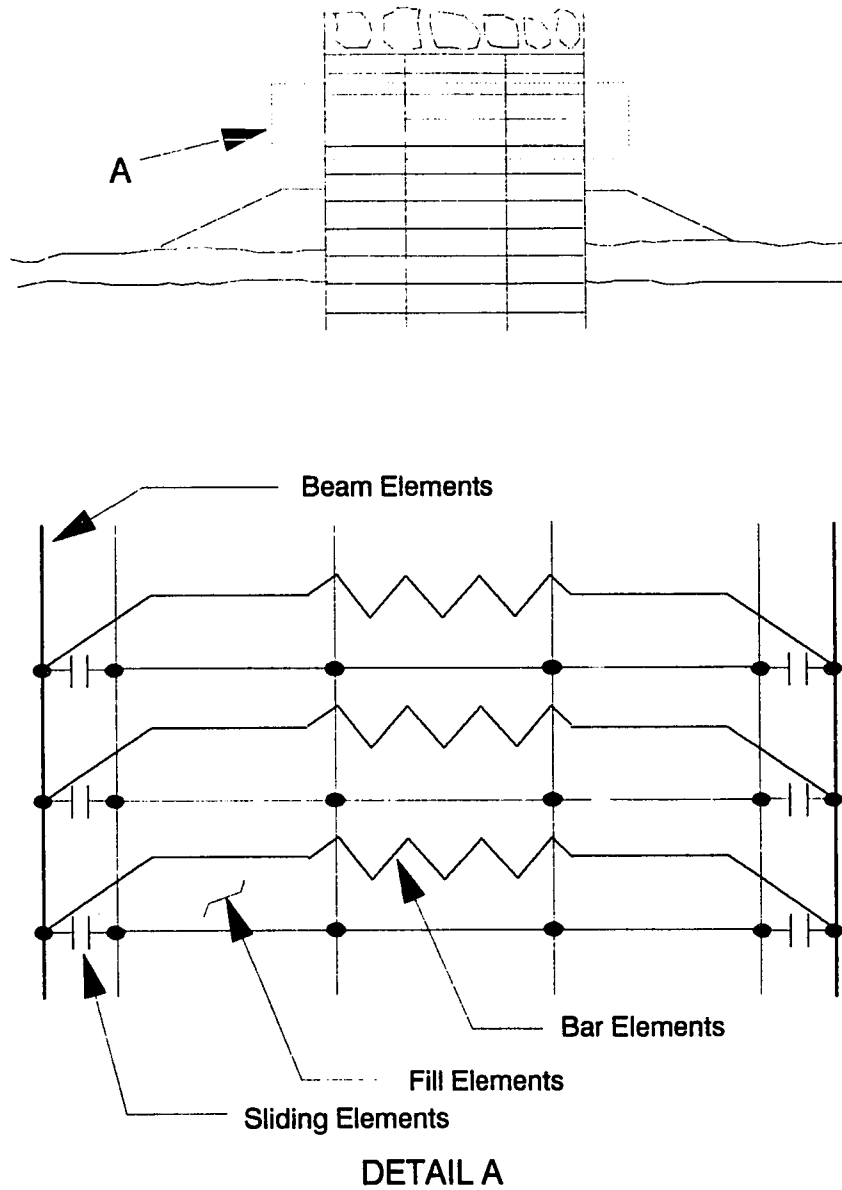
DETAIL A

Figure 4.7 Element connection detail of the finite element
mesh in the cell (expanded view indicates the
region inside the dotted line in the top figure).
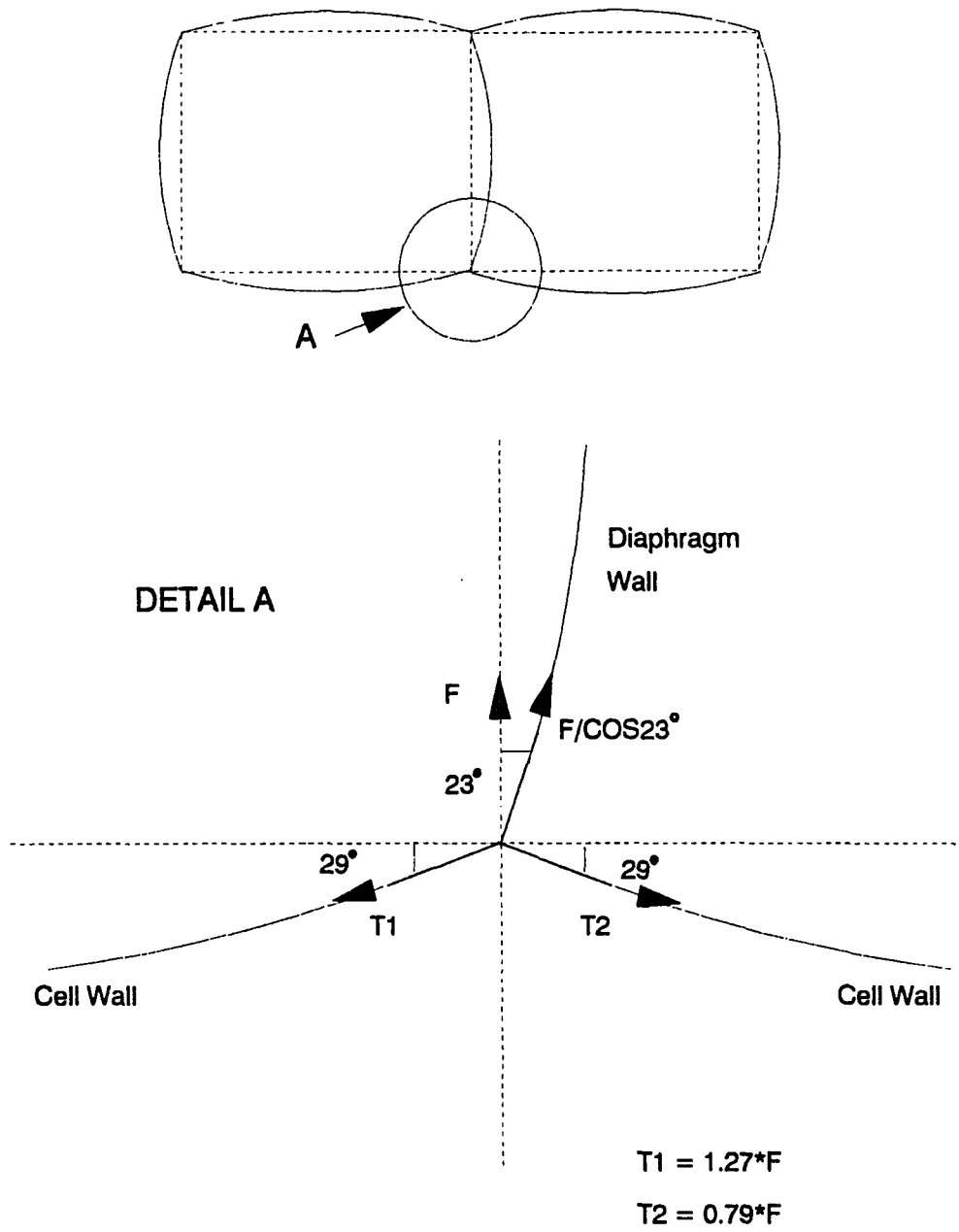
Figure 4.8   Free body diagram of Y-connection and relation between hoop and diaphragm forces and spring force, F.
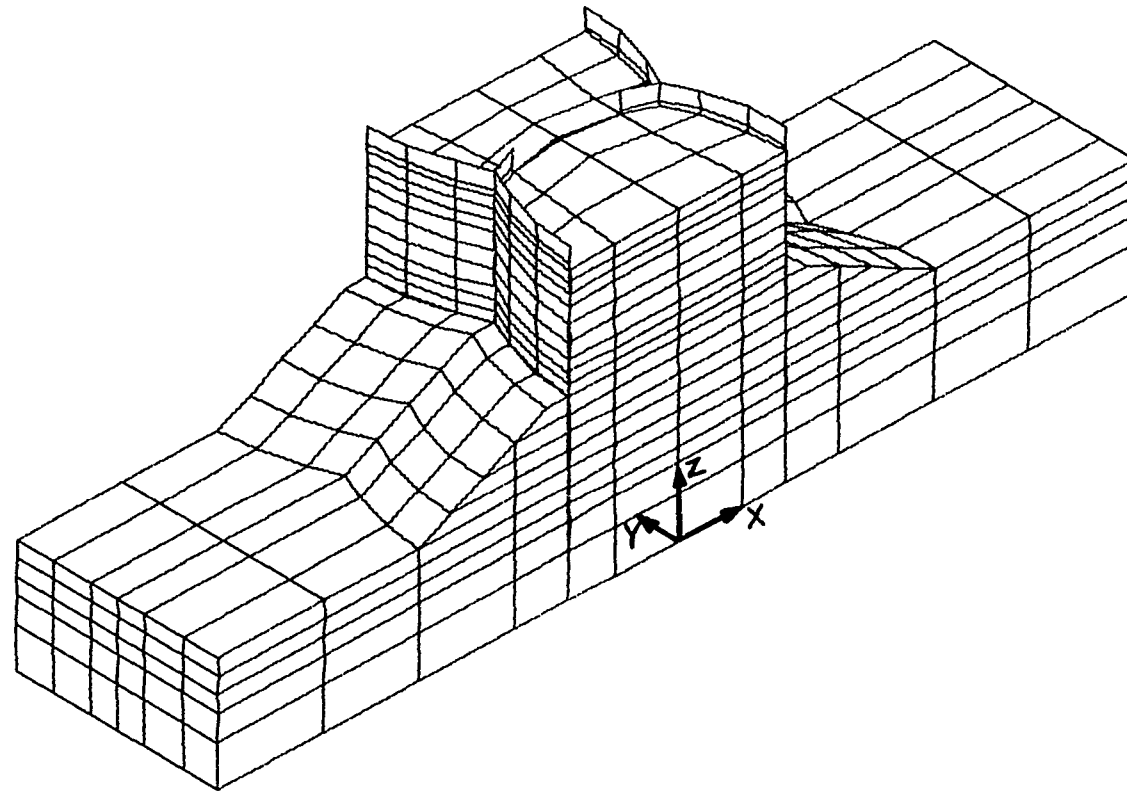
Figure 4.9   Isometric view of the three-dimensional finite
element model used in the analyses.

limitations imposed on the ANSYS package and to provide affordable run times. The mesh consists of 756 three-dimensional isoparametric solid elements (STIF45 in ANSYS), 428 quadrilateral shell elements (STIF63 in ANSYS) and 598 three-dimensional interface elements (STIF52 in ANSYS).

Solid elements were used to model the fill and foundation soils. To simulate the interlock rotation of the sheetpile system, shell elements were connected with nodes which are coupled in all degrees of freedom except the rotational degree of freedom along the connection axis. The Y-sections were represented by an assemblage of three shell elements. Sheetpiles on the external and diaphragm walls were represented by six and four shell elements, respectively, as shown in Figure 4.10. The interaction effects between the sheetpiles and the adjacent soils in the fill, foundation and berm were predicted by the three-dimensional interface elements located between the shell and solid elements.

4.7. Results and Discussion of Finite Element Analyses

To study the response of the breakwater structure, analyses were conducted with the two-dimensional vertical slice and the three-dimensional models in three stages in accordance with the methodology described in Section 4.2. The resulting interlock forces, cell deflections and earth pressures were investigated for both models through each of the three stages and the results are presented on a comparative basis in the following three sections.
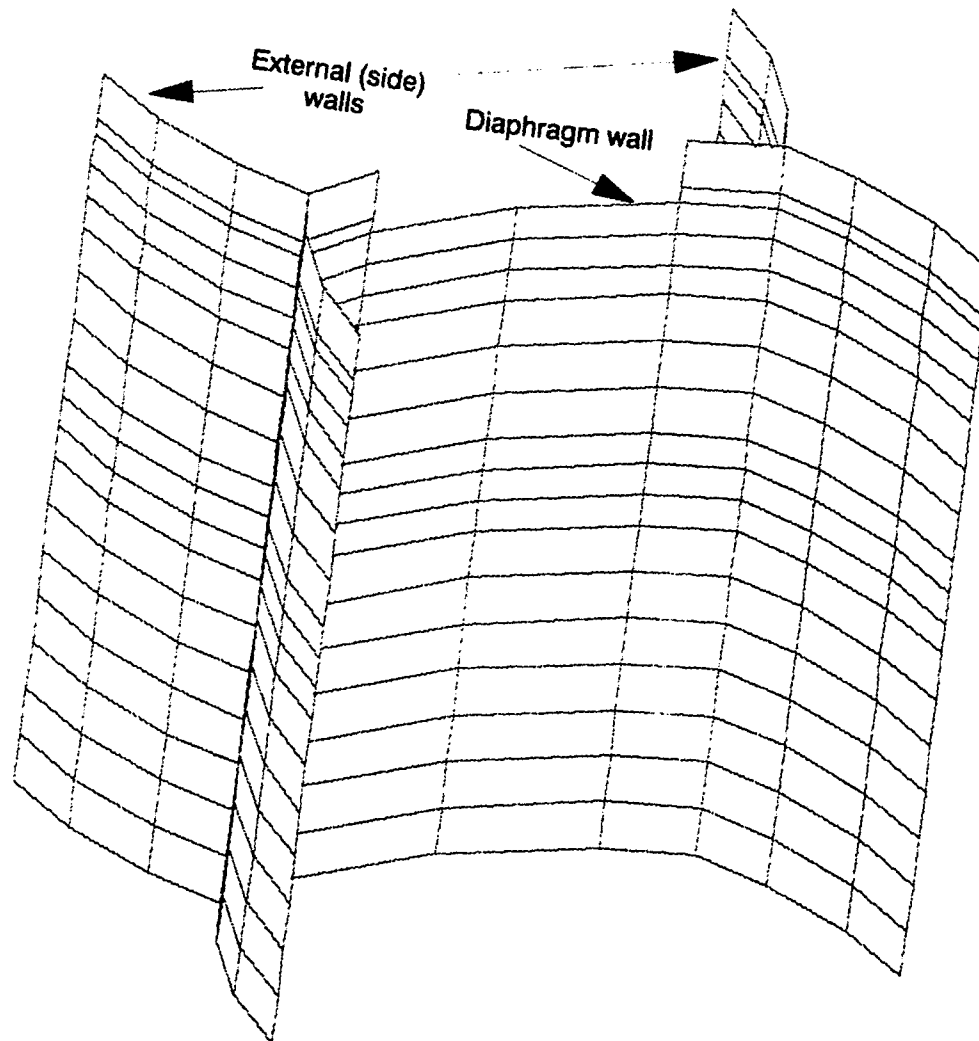
Figure 4.10   Isometric view of the sheetpile system as represented in the three-dimensional finite element model.

Due to the limitations inherent in the two-dimensional model, the interlock forces for the two models were compared at the diaphragm wall only. Similarly, since the two dimensional model can only provide in-plane deformations, deflections in the X-direction at the Y-joints (see Figures 4.5. and 4.9.) were the only possible means for comparison. The average earth pressure on an external wall was calculated from the three dimensional analysis to compare to the two dimensional results.

4.7.1. Stage I: Simulation of the breakwater construction sequence

The interlock forces resulting from the fill and berm placement are plotted in Figure 4.11. Notice that the two dimensional data for the interlock forces do not extend to the 46 ft level since sheetpiles are 4 ft shorter at part of the diaphragm wall (see Figure 4.10). Overall, very good agreement is observed between the predictions of the two models for this load step. The interlock forces from the three-dimensional analysis are in general slightly larger (up to 20 lb/in) at the bottom half of the diaphragm wall. Both maximum forces are close to 450 lb/in and occur near 27 ft level.

In the second step of the construction simulation stage, the capstone load (480 psf) was imposed on top of the cell fill. The resulting interlock forces are plotted in Figure 4.12. The agreement between the two- and three-dimensional
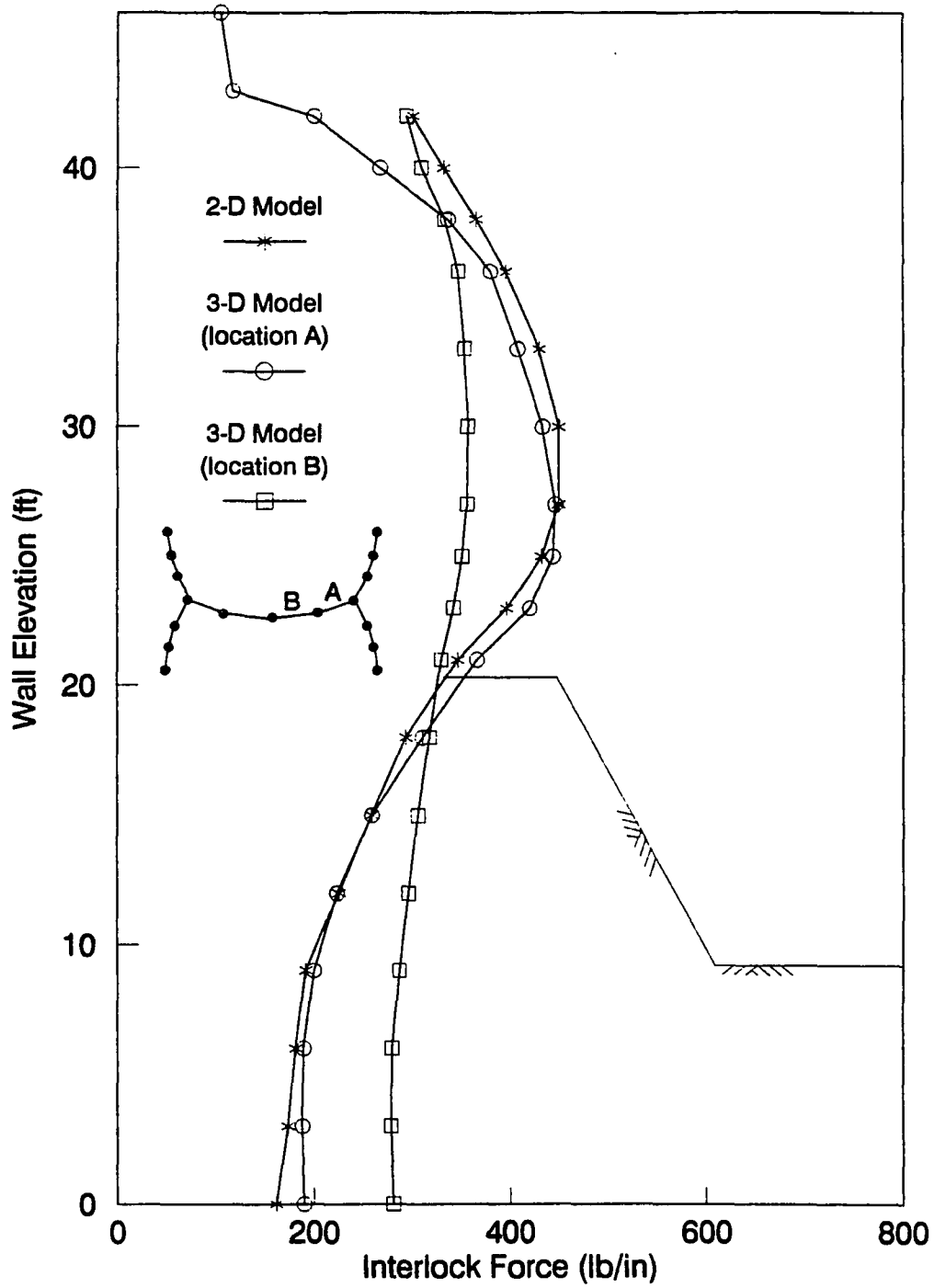
Figure 4.11   Interlock forces at the diaphragm wall after fill
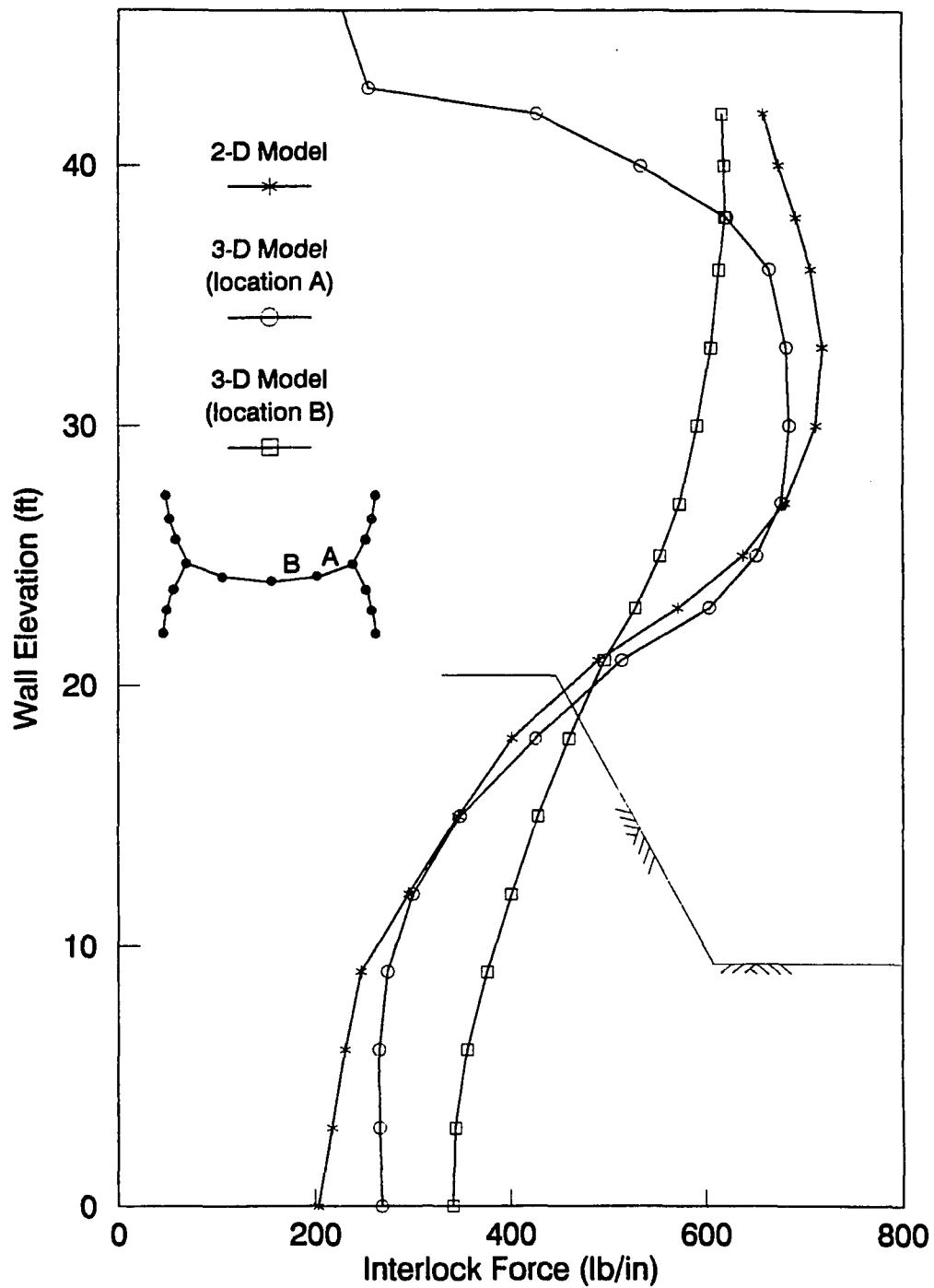and berm placement.

Figure 4.12   Interlock forces at the diaphragm wall after
placement of the capstones (initial structural
condition).

data sets is quite good between 12 ft to 30 ft levels.
However, the differences observed in the previous step became
more predominant with the increase in loading. The two-
dimensional model predicted interlock forces which are
consistently larger for the top fifteen feet of the structure.
The maximum interlock forces increased to 720 lb/in and 680
lb/in ,respectively, for the two- and three-dimensional
models. Additionally,the position of the maximum interlock
forces shifted upward by about 5 ft compared to the previous
step. The interlock force variation in the diaphragm wall
increased to 210 lb/in at the shorter level of the sheetpiles
in the diaphragm wall.

The results of the three-dimensional model analyses show
that the distribution of the interlock forces over the
diaphragm wall vary considerably along the height of the
sheetpiles. The differences become larger around 42 ft level,
indicating a local effect due to the shorter sheet piles of
the diaphragm wall (Figures 4.11 and 4.12).

Interlock force variation in the lakeward wall sheeting
of the cell, for which the diaphragm wall curvature is
concave, is given in Figure 4.13. The profiles are similar to
that of the diaphragm wall close to the Y-joint, except, a
sharp decrease takes place just above the diaphragm wall. The
force intensity increases through the central section of the
cell and reaches a maximum of 590 lb/in.

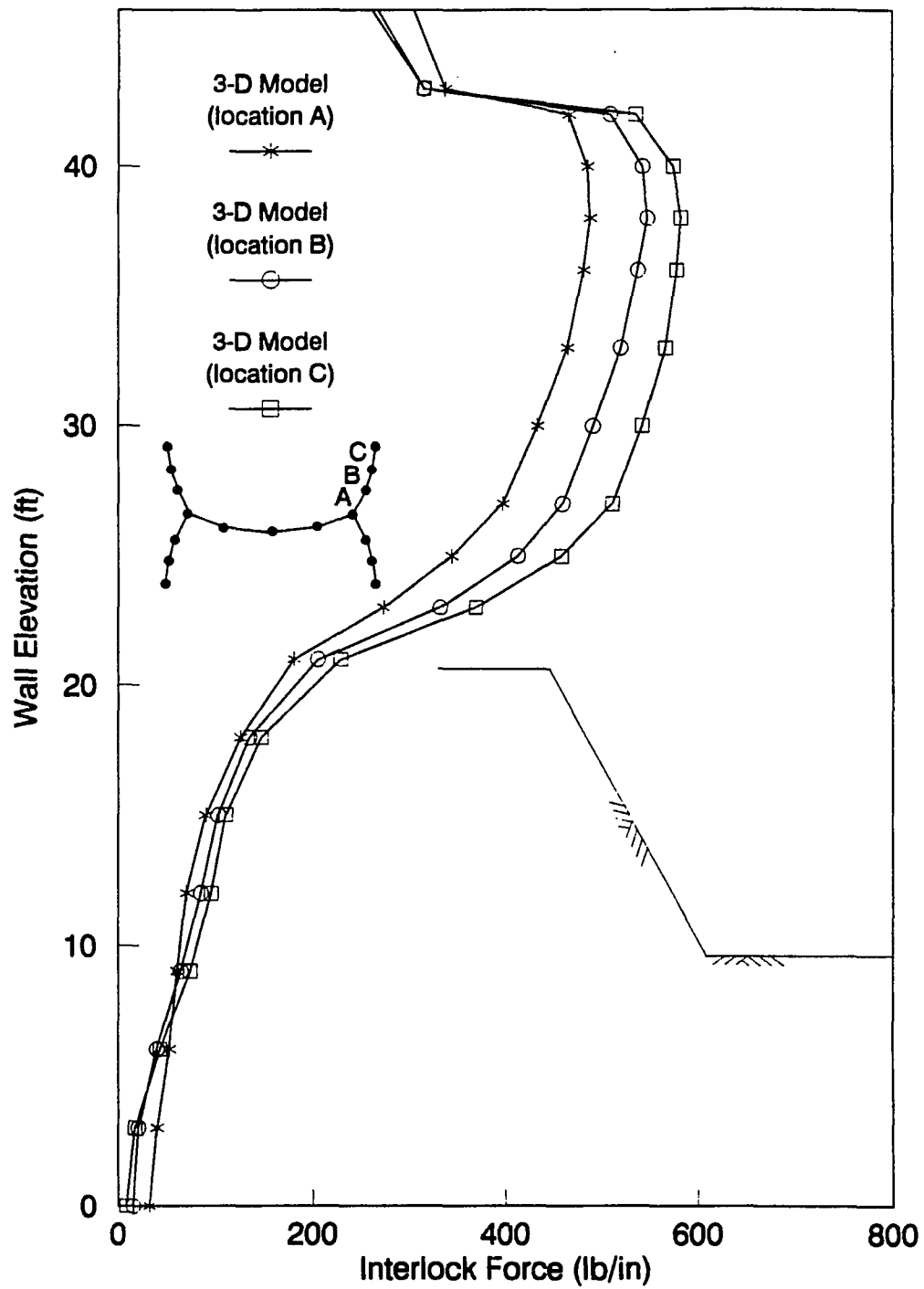Deflection plots for the two construction load steps are

Figure 4.13 Variation of the interlock forces at the lake
side wall sheeting.

given in Figures 4.14. and 4.15. The three dimensional model results in consistently larger deflections throughout the height of the structure. The difference between the two models increases through the upper one third of the structure and reaches 0.12 in. at the top of the sheetpiles after placement of the capstones. The outward deflections at the middle section of the cell reach peak values of 1 and 1.8 in., respectively, for the two load steps, are noticeably larger than the displacements at the Y-joint. Such behavior would be expected due to the stretching in the external wall sheeting and the decreased constraining effect of the diaphragm wall. Figure 4.16 shows a plan view of the relative magnitude of displacements in the sheeting for the 3-dimensional model at the top of the berm level (at the 21 ft level) after the placement of capstones.

Earth pressure distributions on the sheetpiles corresponding to the two load steps are shown in Figures 4.17. and 4.18., respectively. Pressures less than those of the active Rankine state that occur between 21 ft and 36 ft levels indicate active arching. Notice also that the largest outward sheetpile displacements take place in this region for both load steps. Differences between the two model predictions increase up to 150 psf in the vicinity of 27 ft level by the completion of the capstone loading.

A concurrent evaluation of the interlock force, deflection and earth pressure data presented above show that
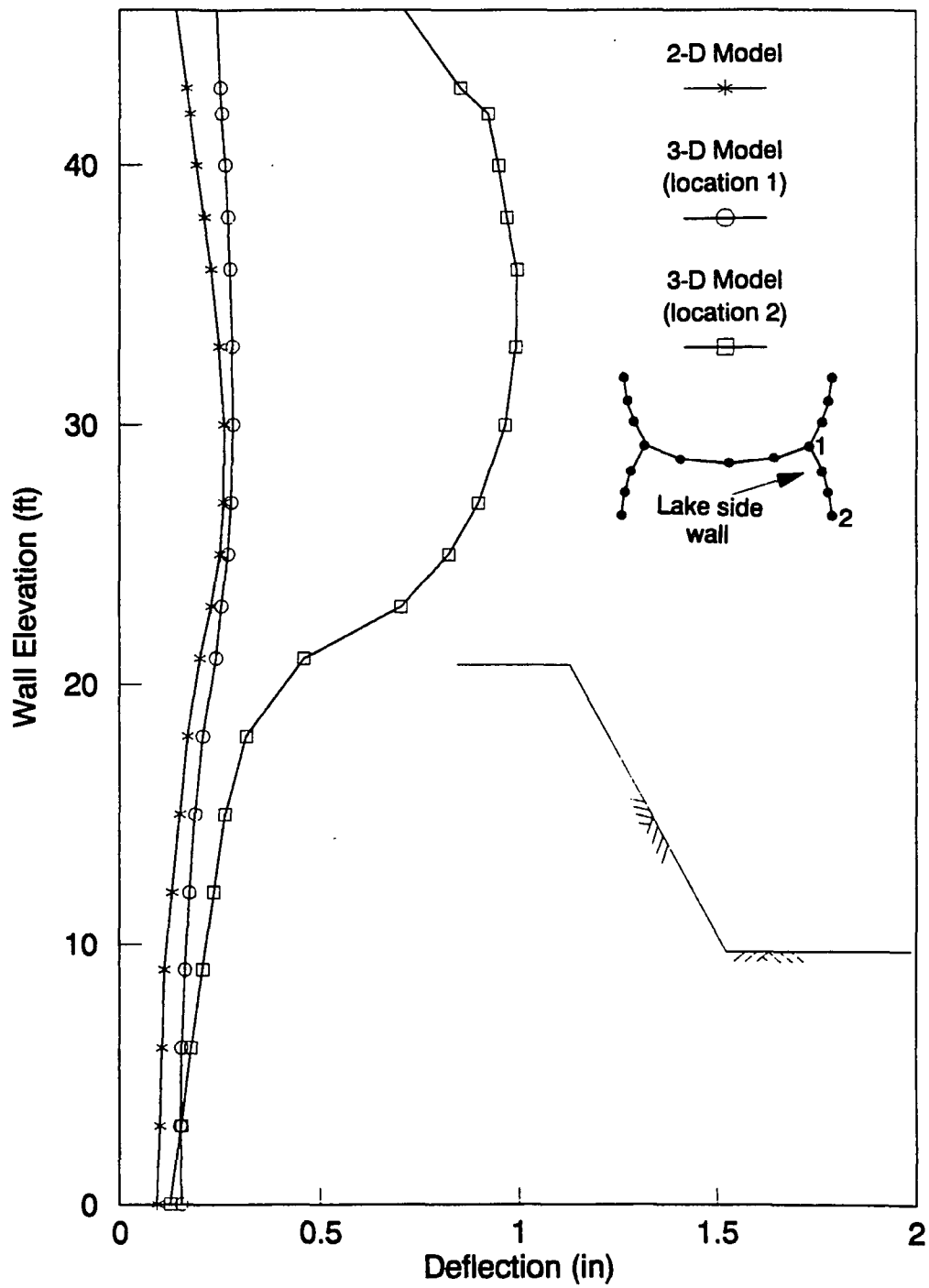
Figure 4.14 Deflections of the sheeting after fill and berm placement.
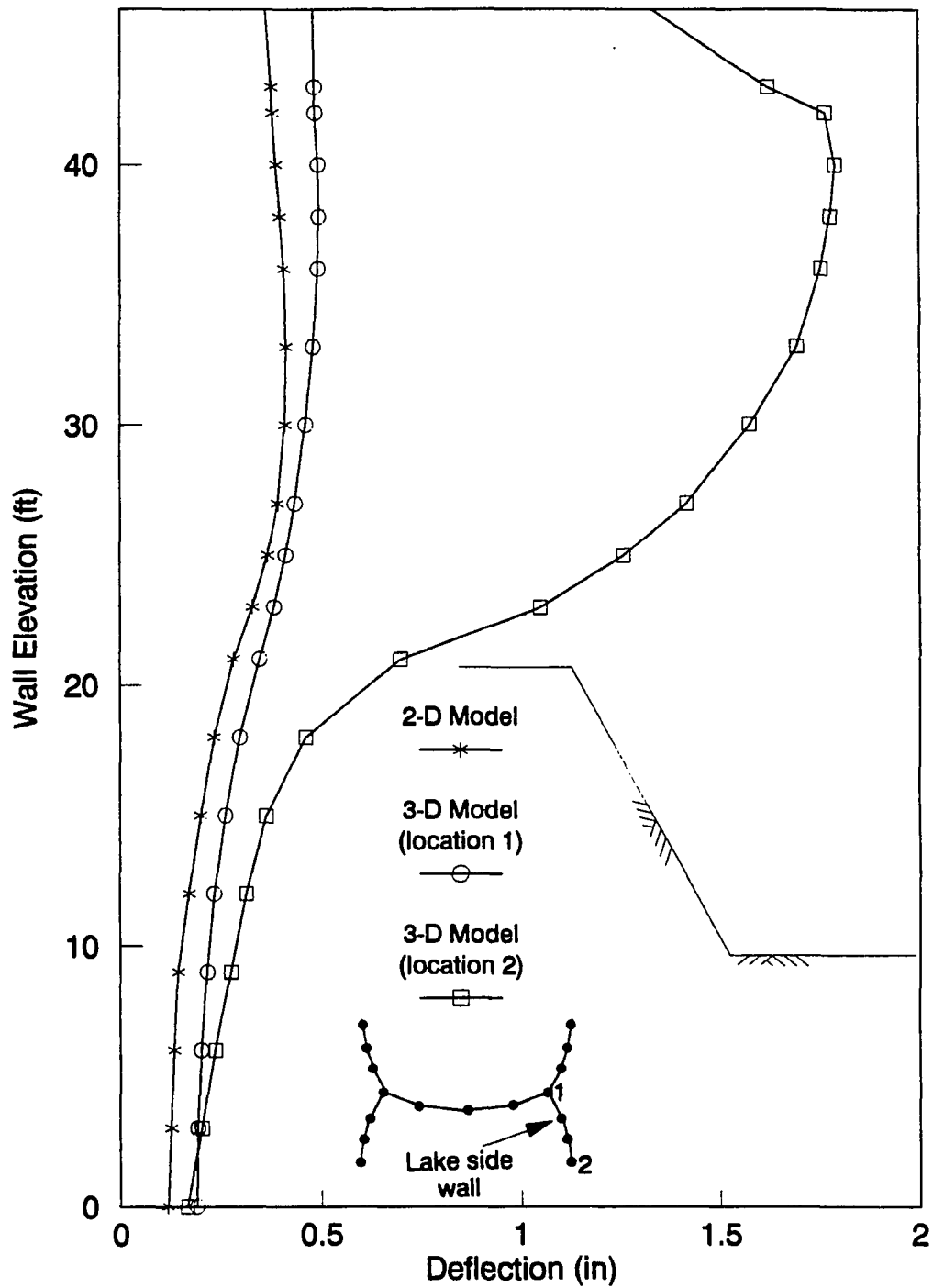
Figure 4.15   Deflections of the sheeting after capstone
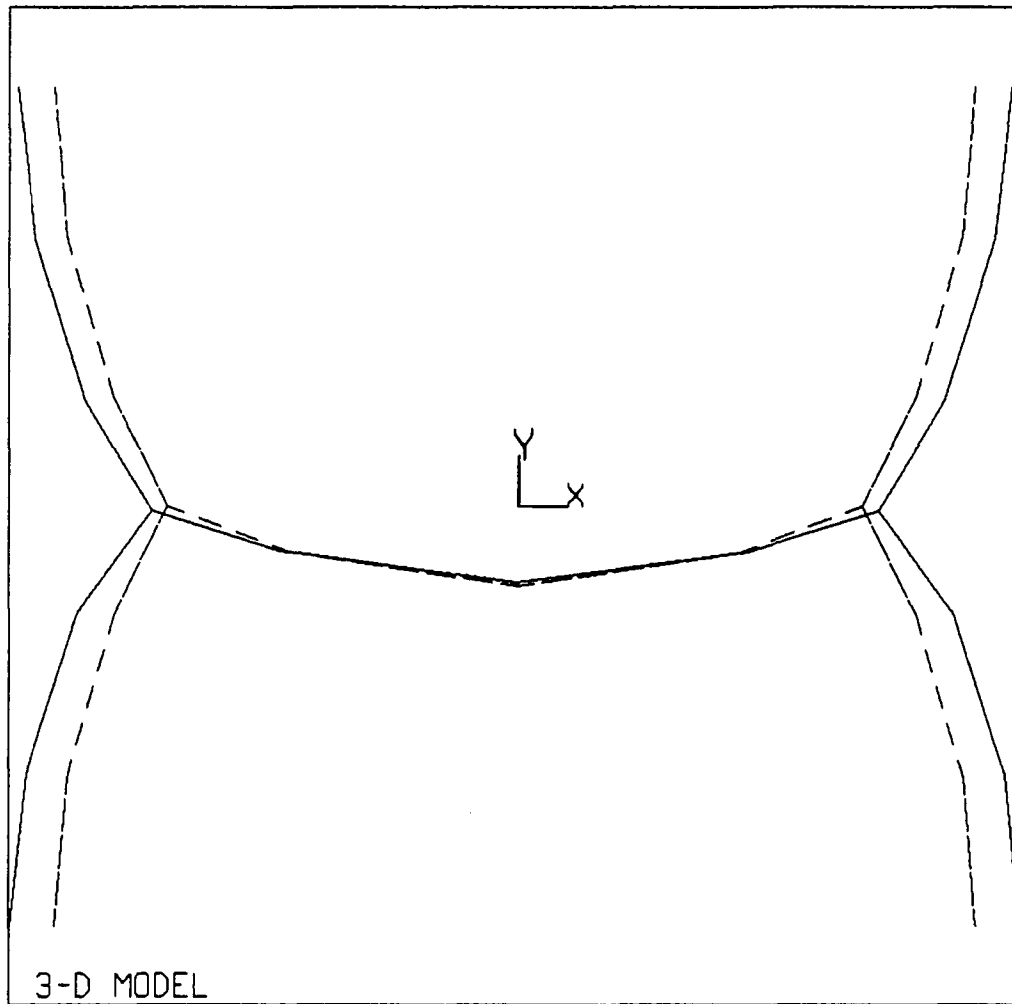placement (initial structural condition).

Figure 4.16   Deformed shape of the sheeting at the top of the
berm level after placement of the capstones
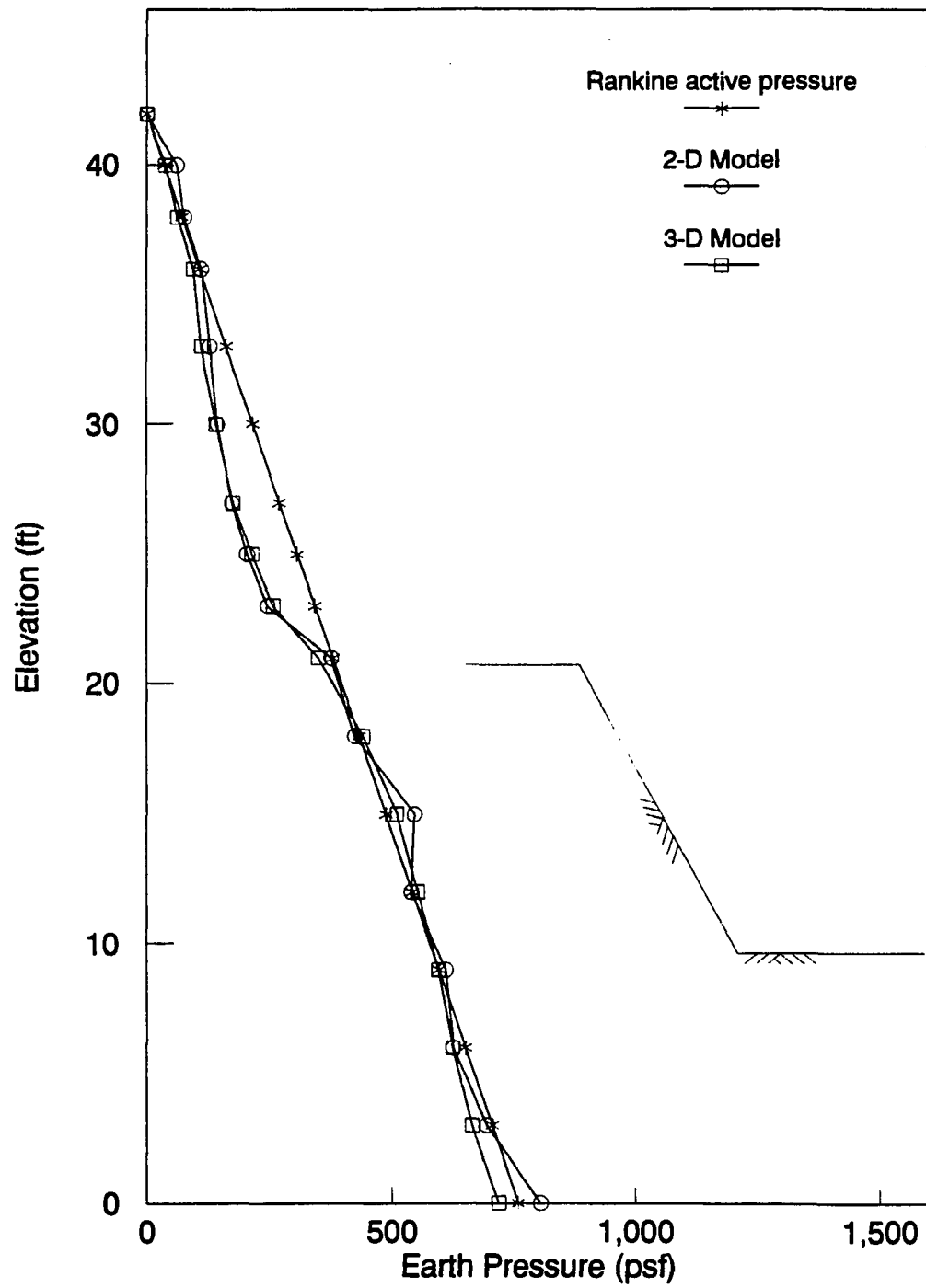(solid lines indicate the deformed shape).

Figure 4.17   Earth pressures against lake side sheeting after fill and berm placement.
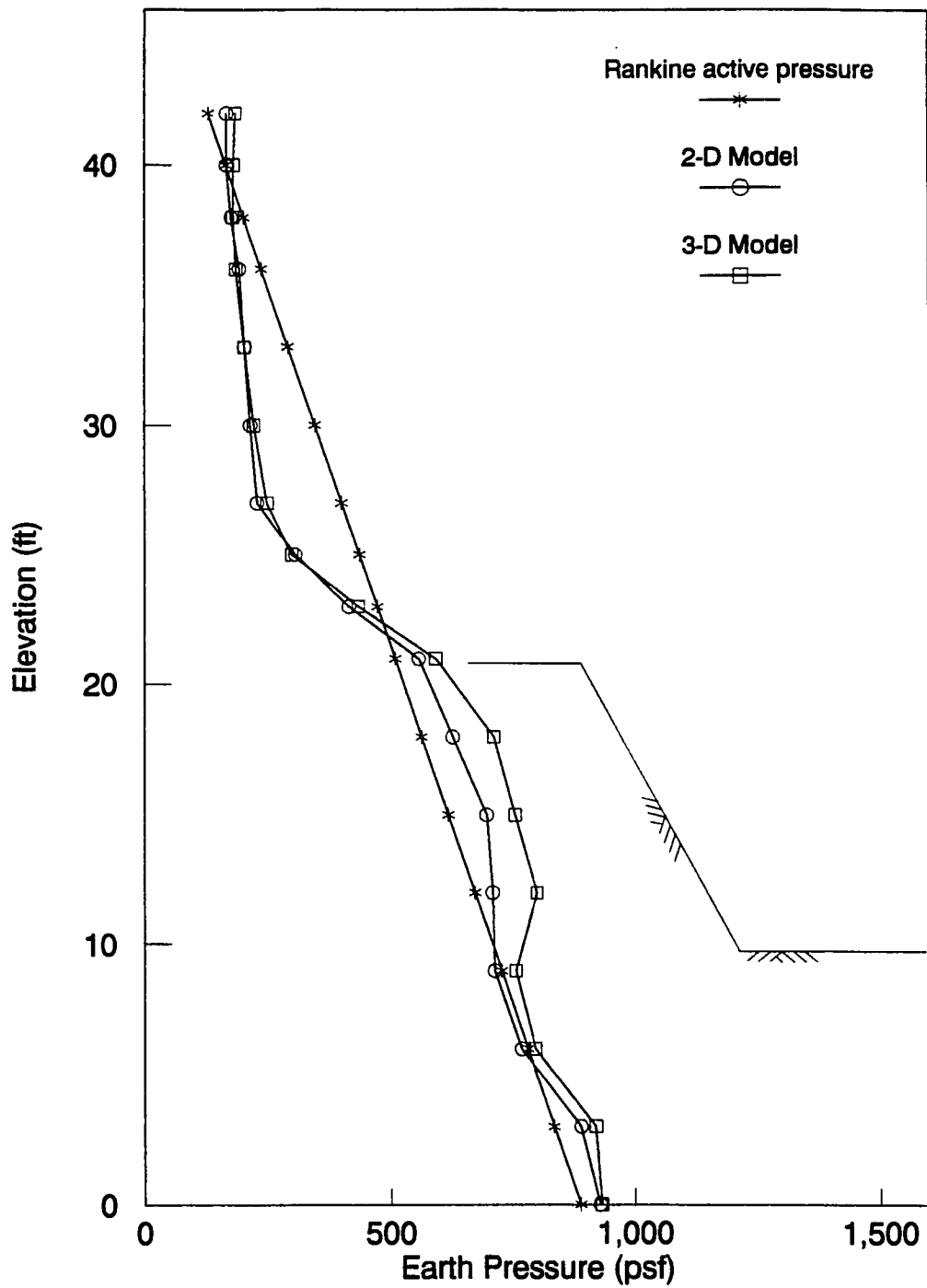
Figure 4.18 Earth pressures against lake side sheeting after capstone placement (initial structural state).

the three-dimensional model predicts smaller interlock forces at the diaphragm wall but larger outward deflections at the Y-joints with respect to the two-dimensional model. In addition, this behavior becomes more evident for higher interlock force intensities and in the upper one third of the structure. Two implications of these general observations are: (1) The two-dimensional model response is comparatively stiffer, and (2) In the three-dimensional model, a secondary lateral load bearing mechanism other than interlock tension becomes more active with the increased loading. In order to provide rational explanations to these implications, a closer examination of the inherent characteristics and the responses of the two models was necessary.

The first implication can be traced to the differences in the two approaches in modeling the diaphragm wall. In the two-dimensional model, the diaphragm wall, which is actually curved, was idealized as a series of linear springs. In the three-dimensional model, in which the true geometry is implemented, the diaphragm wall has the tendency to straighten during loading thus provide additional flexibility. Deflected shapes of the diaphragm wall corresponding to the end of the construction simulation stage are plotted in Figure 4.19 at three different elevations of the sheet piling. The geometric deformations are larger at the 42 ft level than at the 30 ft level where the interlock forces reach a peak. This would mean that the interlock force intensity is not the only factor
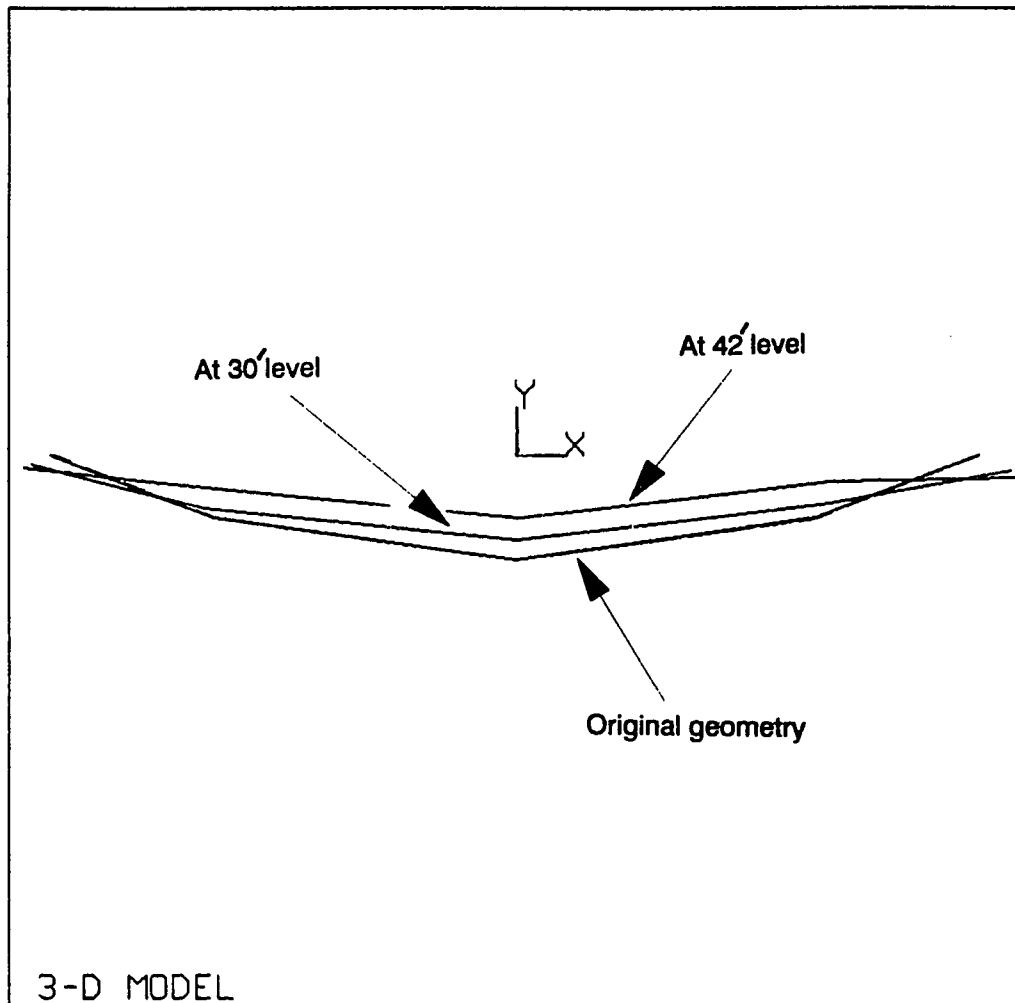
Figure 4.19 Plan view of the deflected shapes of the diaphragm wall at various elevations.

effecting the degree of geometric deformations. The other factor is the confinement effect on the sheetpiles due to the embedment and the berms. The diaphragm wall would be expected to be more flexible near the top because the confining effect of the soil is less and the pressures on the wall due to fill are reduced.

The second implication is a direct consequence of the vertical unit slice idealization concept. Since the diaphragm wall stiffness is normalized to a slice of unit thickness, the resulting outward deflection of the piles is equivalent to the deflections in the x-direction at the Y-joints in the three-dimensional model. However, the deflections predicted at the middle of the outer wall sheeting by the three-dimensional model are much larger than those at the Y-joints (refer to Figures 4.14 and 4.15). In the three-dimensional model, a greater part of the lateral load on the outer walls are carried by the bending action of the sheetpiles compared to the two-dimensional analysis, thereby reducing the hoop forces on the diaphragm wall.

4.7.2. Stage II: Simulation of the present condition

Hypothetical wave pressure profiles were applied cyclically to the lakeward wall of the breakwater to simulate the present condition of the structure as described in Section 4.2 and illustrated in Figure 4.2. Three successive cycles (each cycle consists four successive load steps containing trough and crest loads of the wave) were performed with the

models using the hypothetical wave.

The interlock force and displacement from the two models for one full load cycle is illustrated for the lakeward wall of the sheetpiles in Figures 4.20. through 4.23. An overview of the four figures indicates that the responses conform in general with the observations in the previous stage (stage I). However, by the end of the cycle, the maximum interlock force occurred at the 42 ft level (shorter level at the diaphragm wall) for the two-dimensional model (2450 lb/in); it was at the 30 ft level for the three-dimensional model (1840 lb/in). The maximum displacement responses of both models by the end of the cycle were at the top, and, 1.75 in. and 2.5 in., respectively, for the two and three-dimensional models. In Figure 4.22 it should be noted that the two-dimensional model displacement response for the wave crest load exceeds the three-dimensional model response considerably (see Figure 4.23). This may be due to the missing shear resistance of the diaphragm wall in the two-dimensional model idealization (Section 4.5). Accordingly, the differences between the displacement responses of the two models would be expected to increase under higher unbalanced lateral loads.

The interlock force responses of the two models at the end of each successive cycle are plotted in Figures 4.24 and 4.25. Corresponding displacement responses are plotted in Figures 4.26 and 4.27 respectively. A stabilization trend is noted in all of the plots as the incremental differences tend
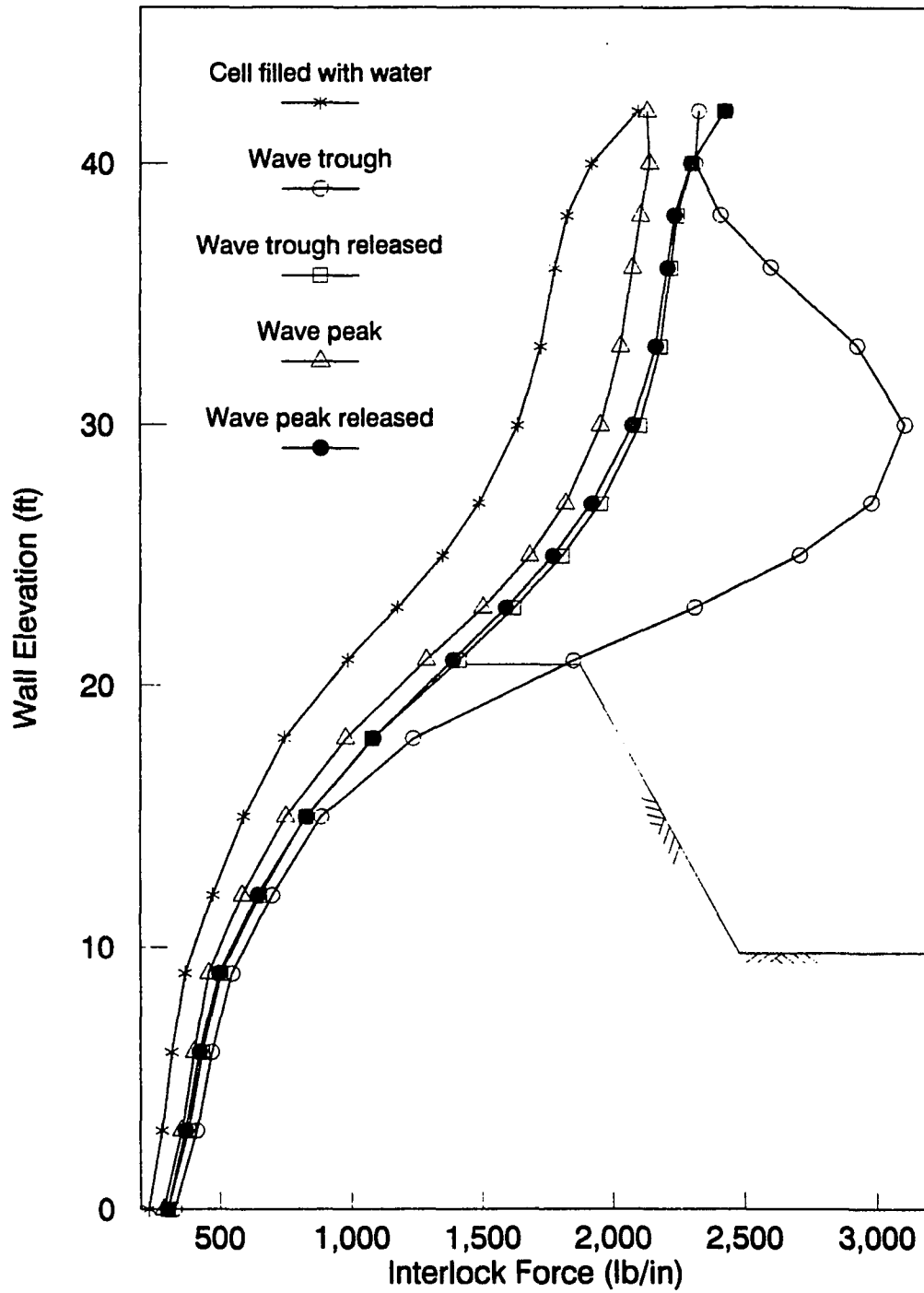
Figure 4.20 First cycle interlock force variations of the two-dimensional model.
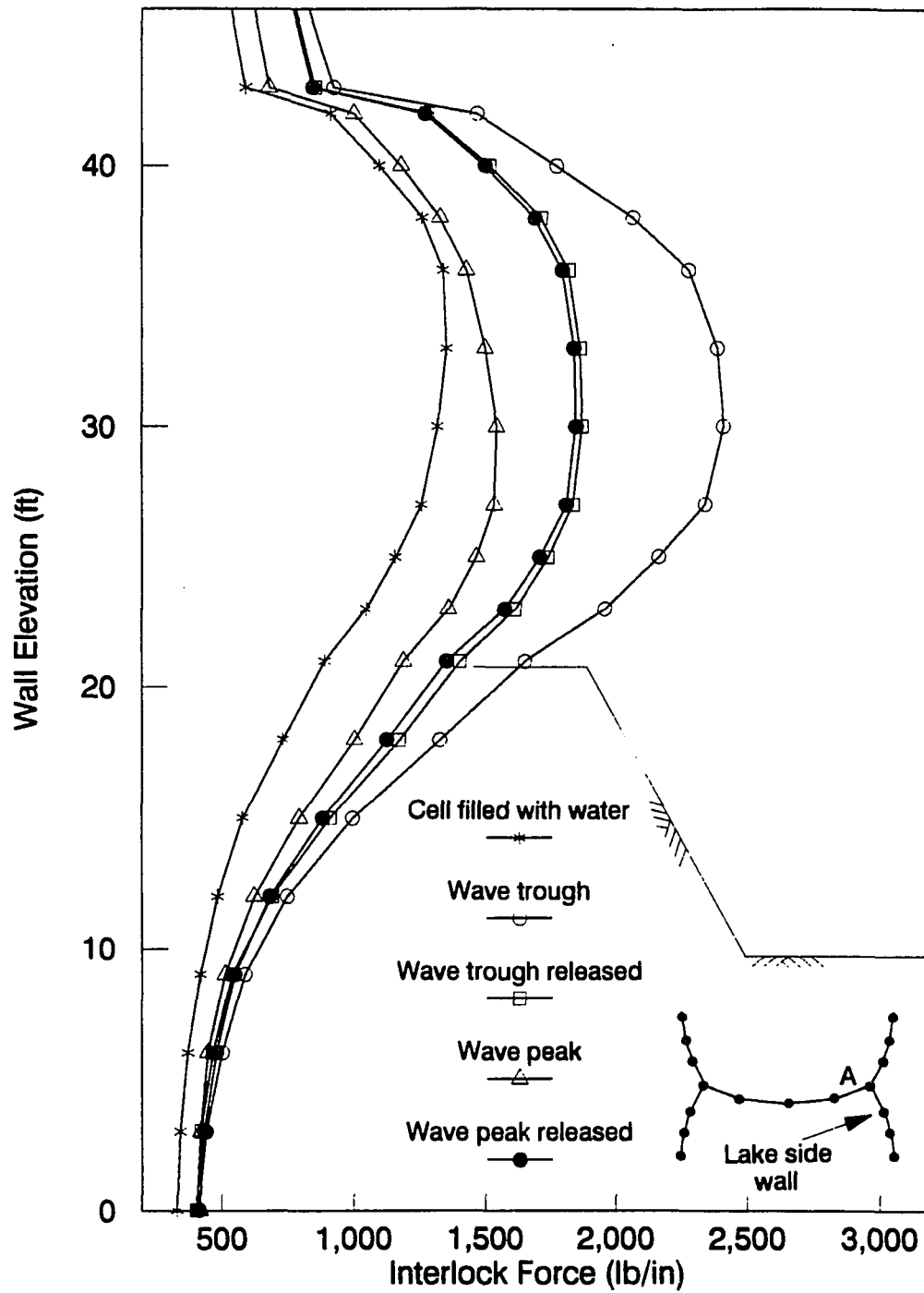
Figure 4.21 First cycle interlock force variations of the three-dimensional model.
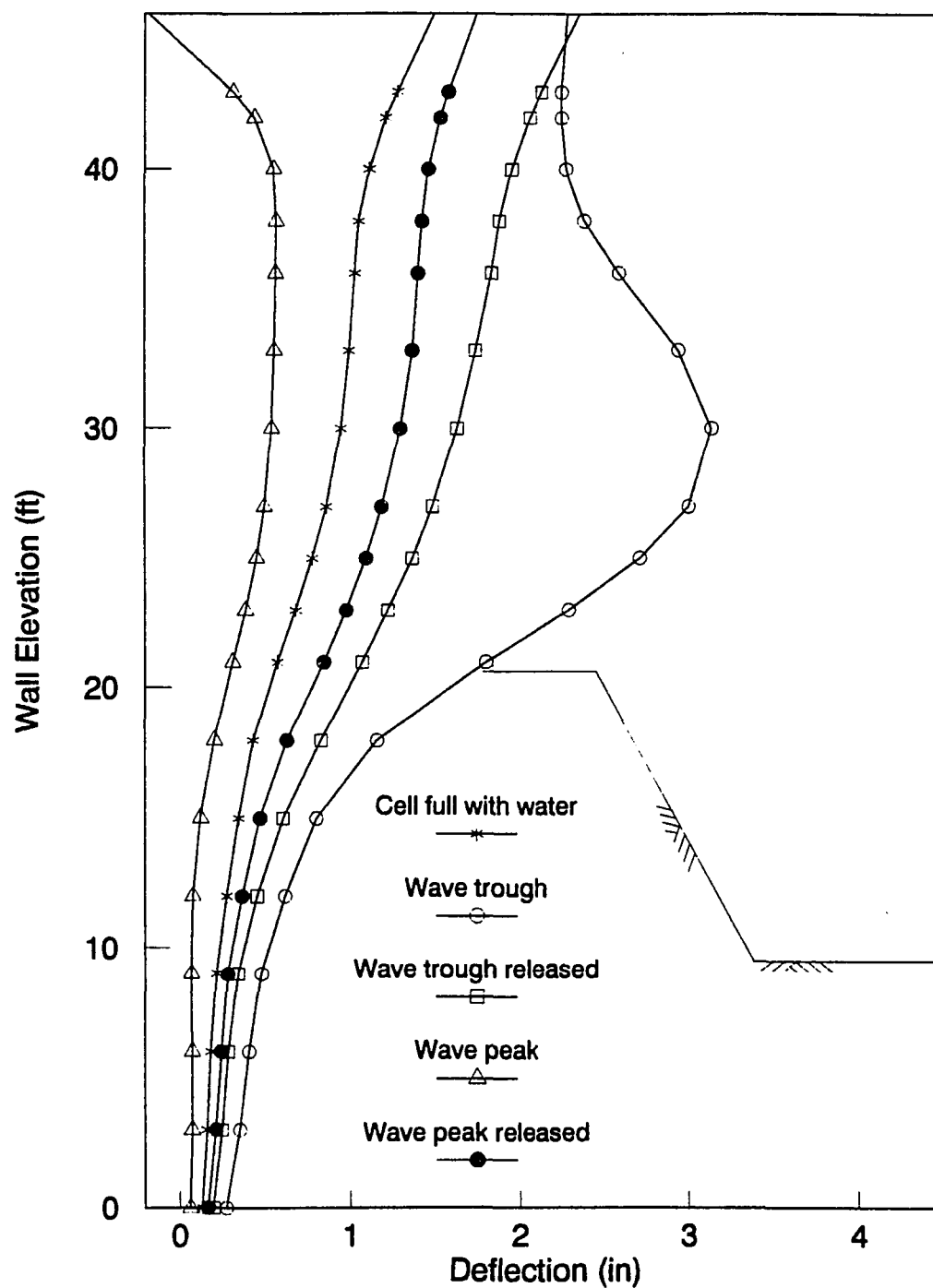
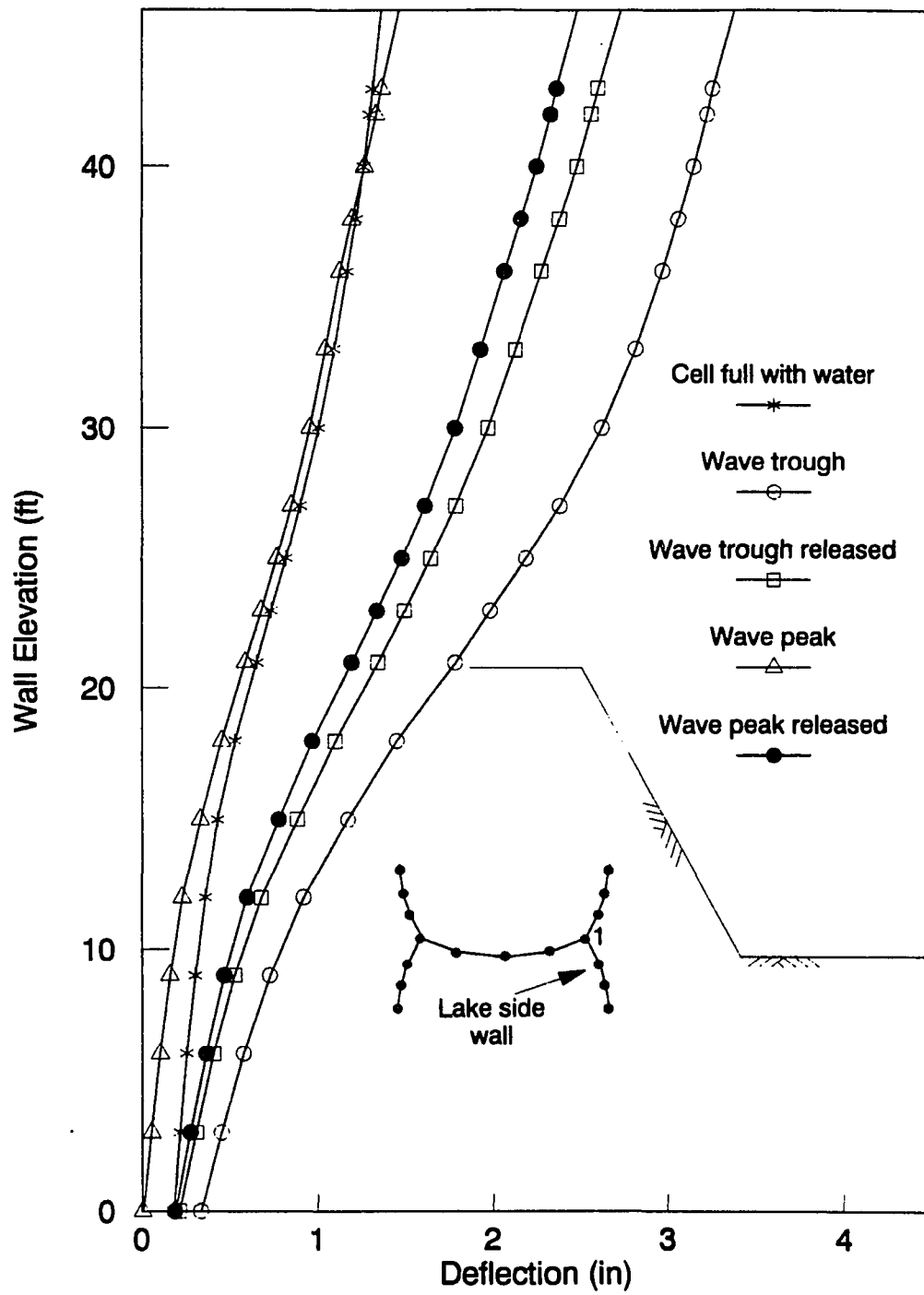Figure 4.22   First cycle displacements of the two-dimensional model lake side wall.

Figure 4.23   First cycle displacements of the three-dimensional model.
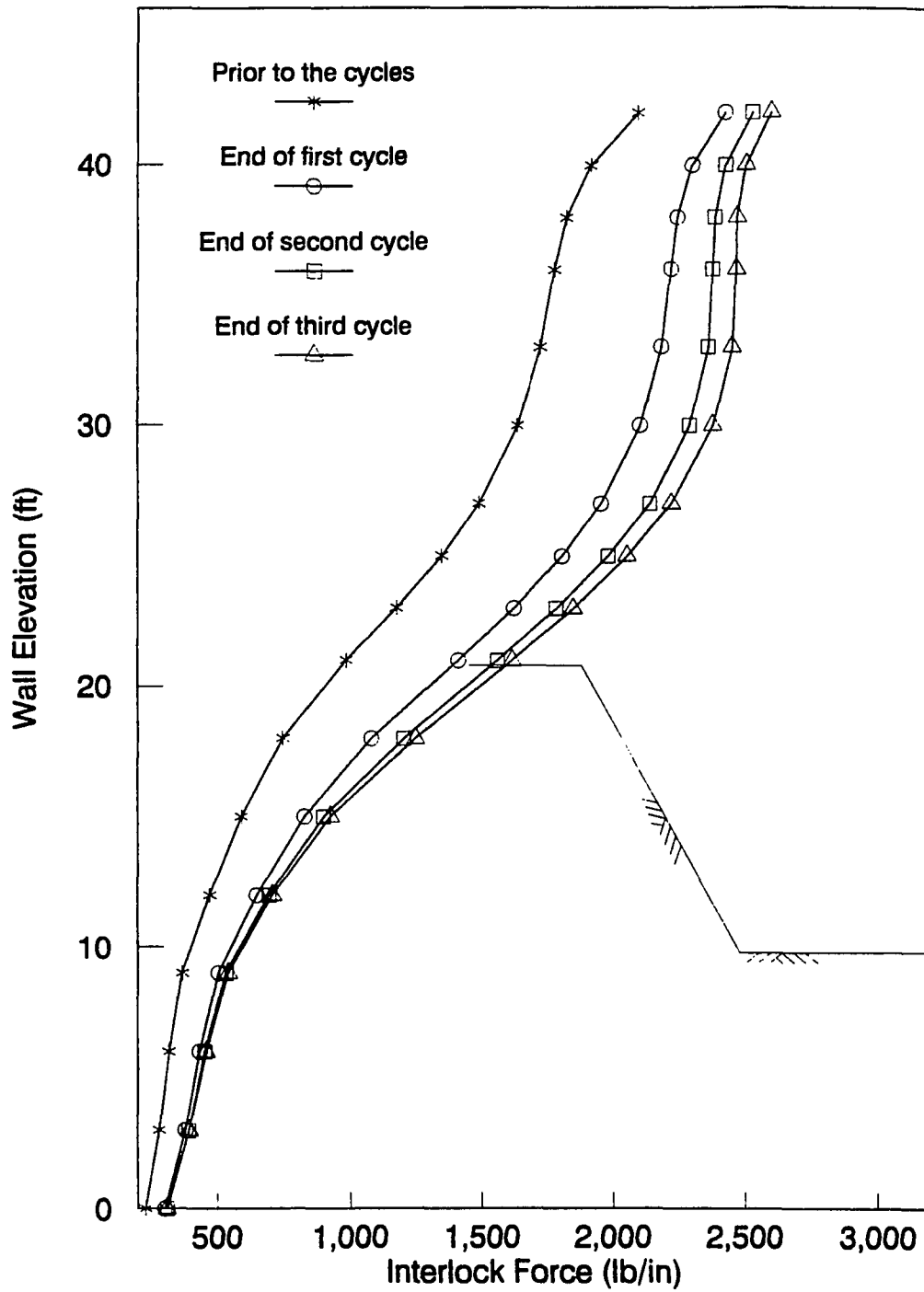
Figure 4.24   Interlock force variation of the two-dimensional
model at the end of each cycle.

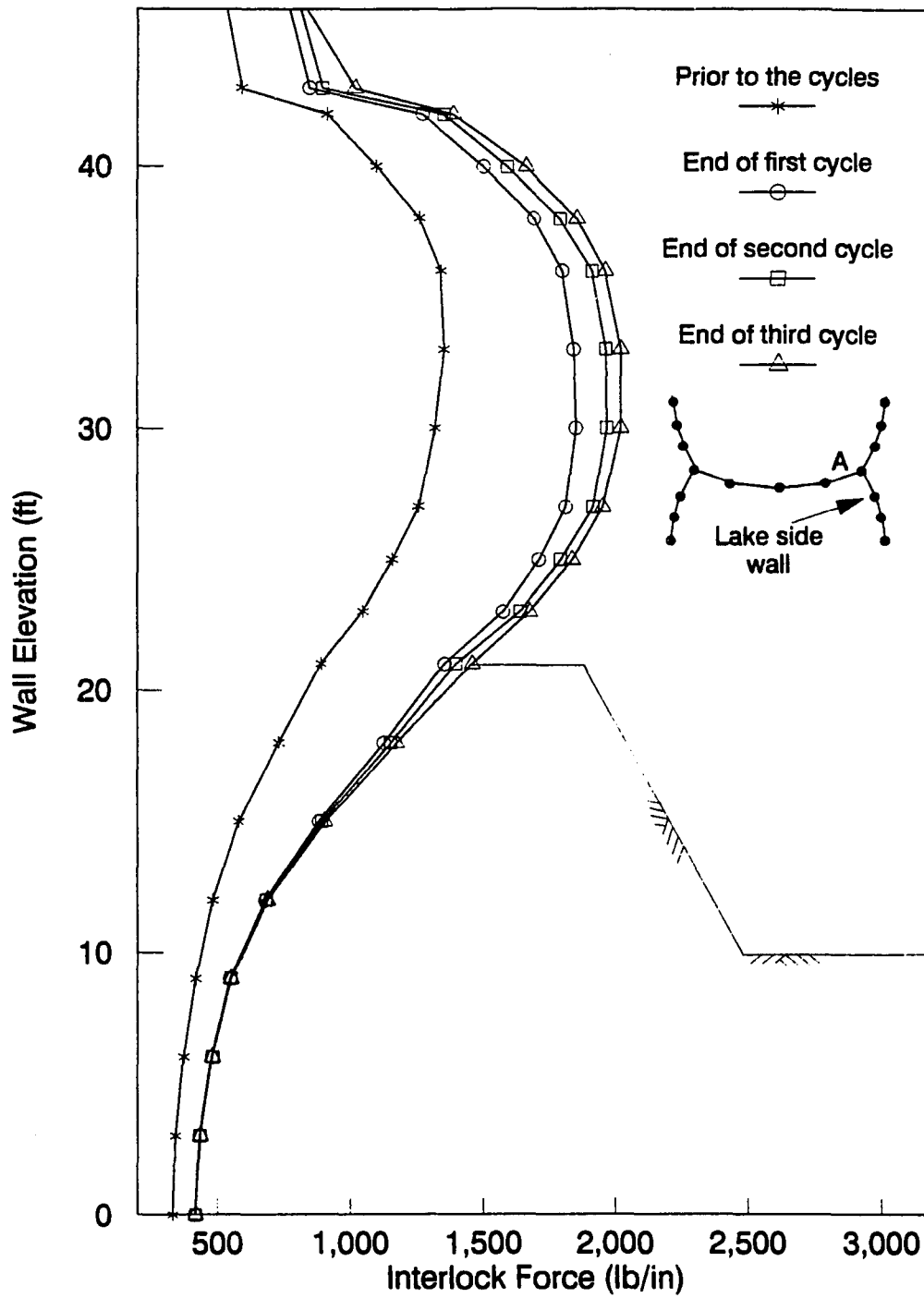Figure 4.25   Interlock force variation of the three-
               dimensional model at the end of each cycle.
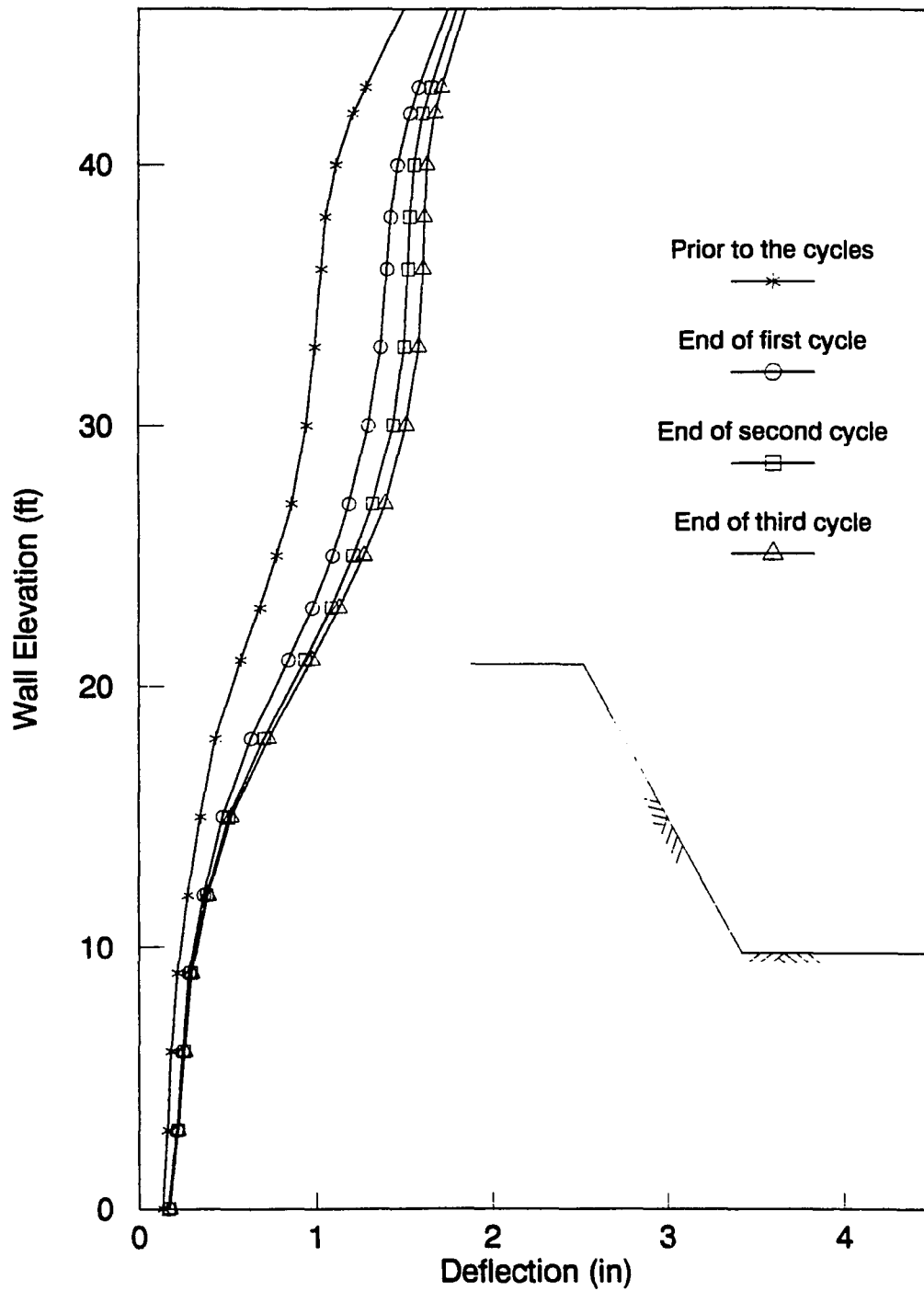
Figure 4.26   Lake side wall displacements of the two-
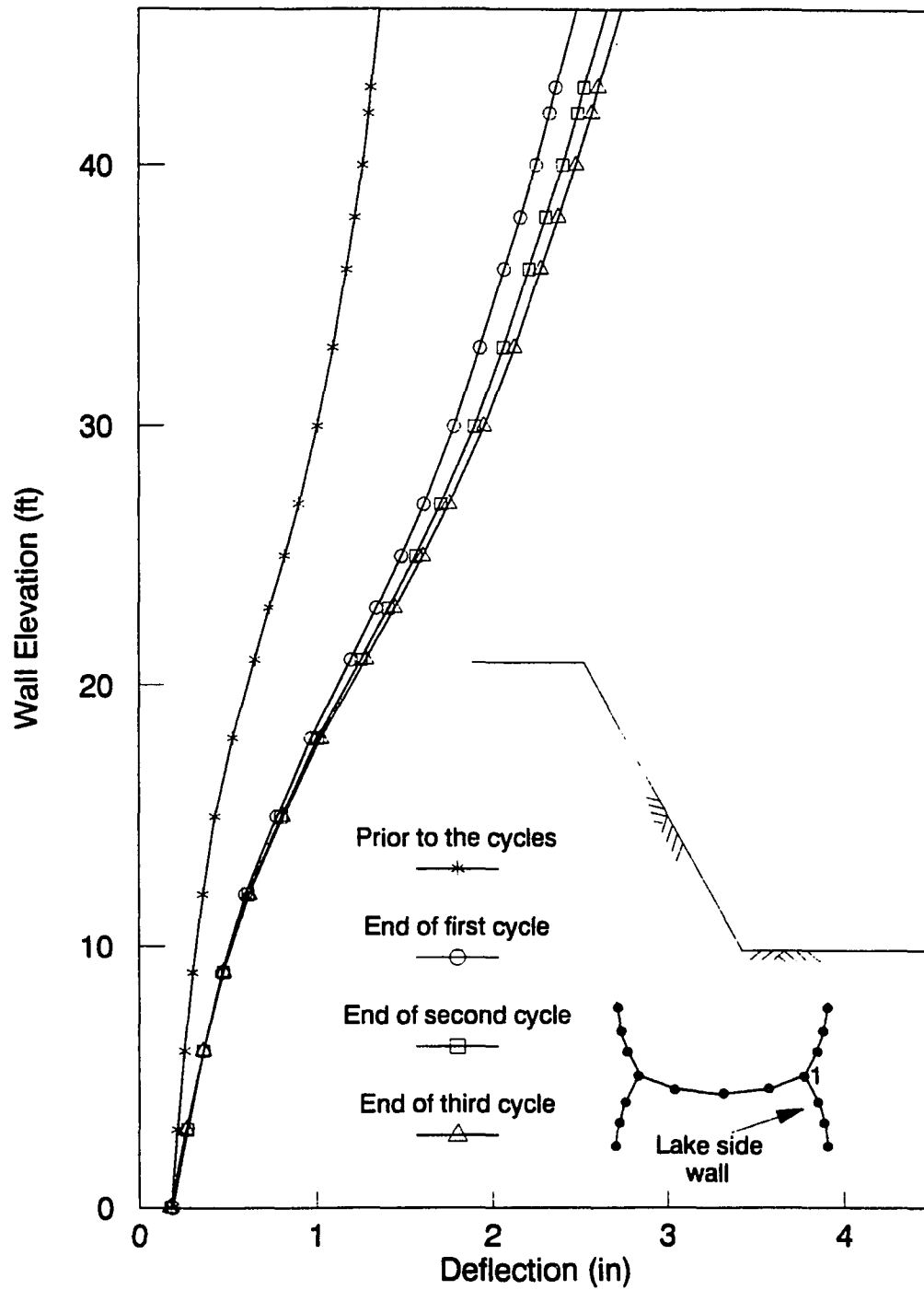   dimensional model at the end of each cycle.

Figure 4.27 Displacements of the three-dimensional model at the end of each cycle.

to reduce in the second and third iterations.

By the completion of the three consecutive cycles, interlock forces reach 2600 lb/in for the two dimensional model at the shorter level of the diaphragm wall with a total increase of 500 lb/in over the post-construction state. For the three-dimensional model, the maximum interlock force reached 2000 lb/in at a 30 ft level with a total increase of 680 lb/in. Two- and three- dimensional model results indicated maximum deflections of 1.85 in. (an increase of 0.35 in. total) and 2.74 in. (an increase of 1.35 in. total) respectively, at the top of the sheetpiles.

After completion of the hypothetical wave cycles and subsequent reduction of the water inside the cell to a calm lake water level, the present condition of the structure as described in Section 4.2 was assumed to have been reached. As seen in Figures 4.28 through 4.32, the structural state of the breakwater is considerably different compared to the post-construction state. Maximum interlock forces reached 2480 lb/in and 1900 lb/in, respectively, for the two- and three-dimensional models with increases exceeding 350% of the post-construction state (compare Figure 4.28 to 4.12 and 4.29 to 4.13). Displacements increased to 1.3 in. for the two-dimensional model and to 2.65 in. for the three-dimensional model at the harborside Y-joint (see Figures 4.30., 4.31. and 4.15.). The three-dimensional model resulted in a lateral deflection approaching 4.33 in. at the mid-cell. Lateral
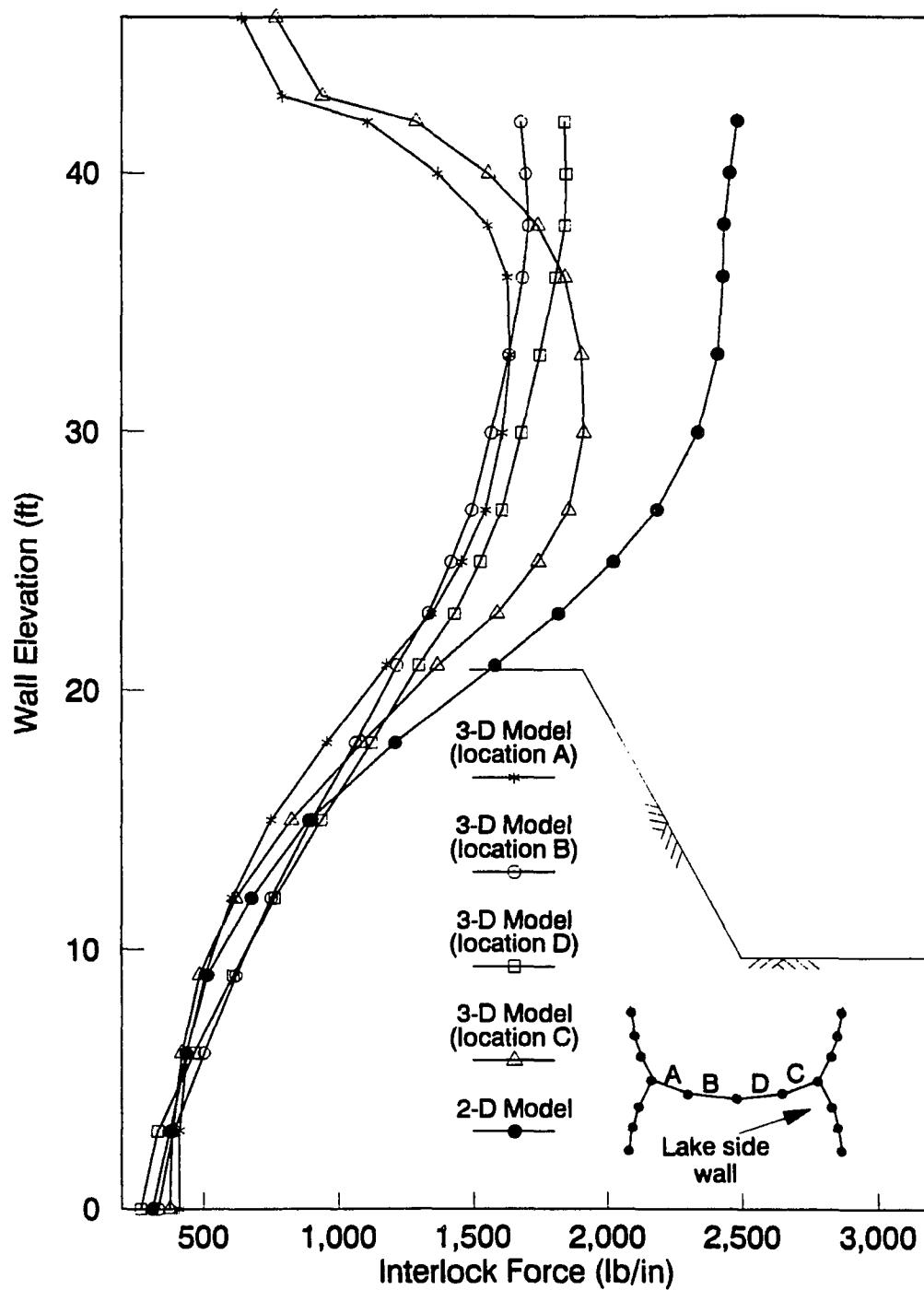
Figure 4.28   Interlock forces at the present structural state.
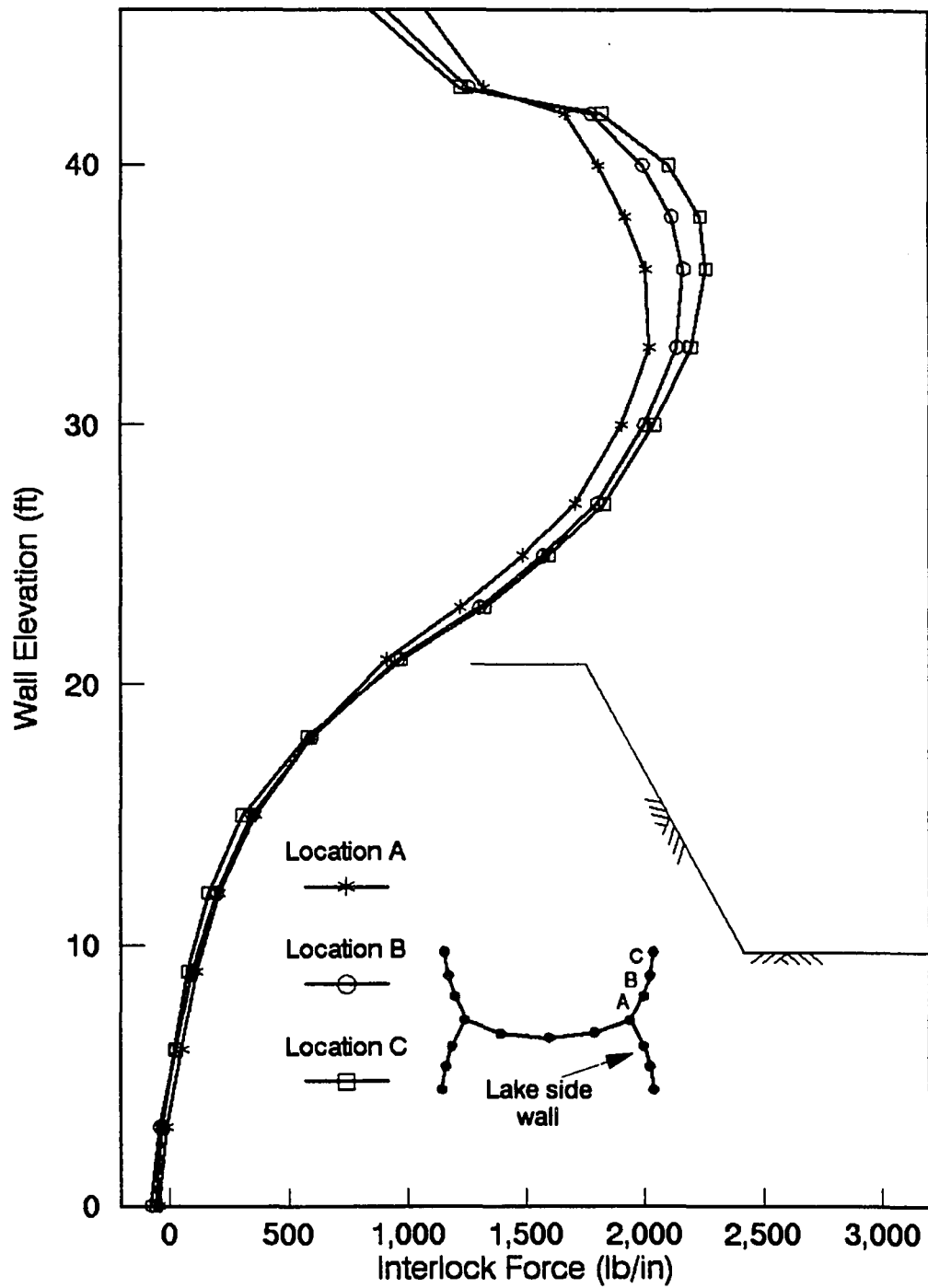
Figure 4.29 Variation of the interlock forces in the lake side wall sheeting at the present structural state.
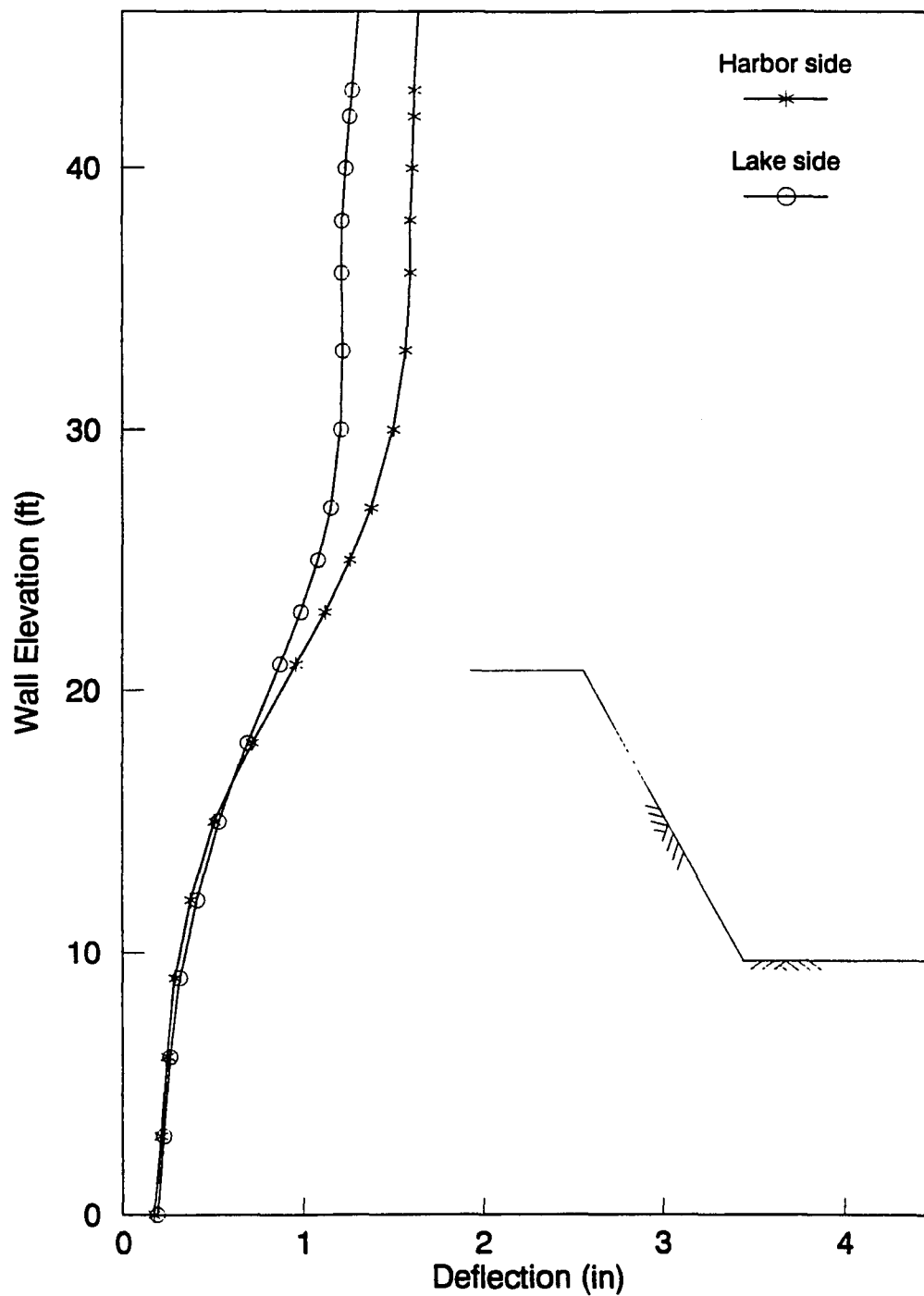
Figure 4.30 Displacements of the two-dimensional model at the present structural state.
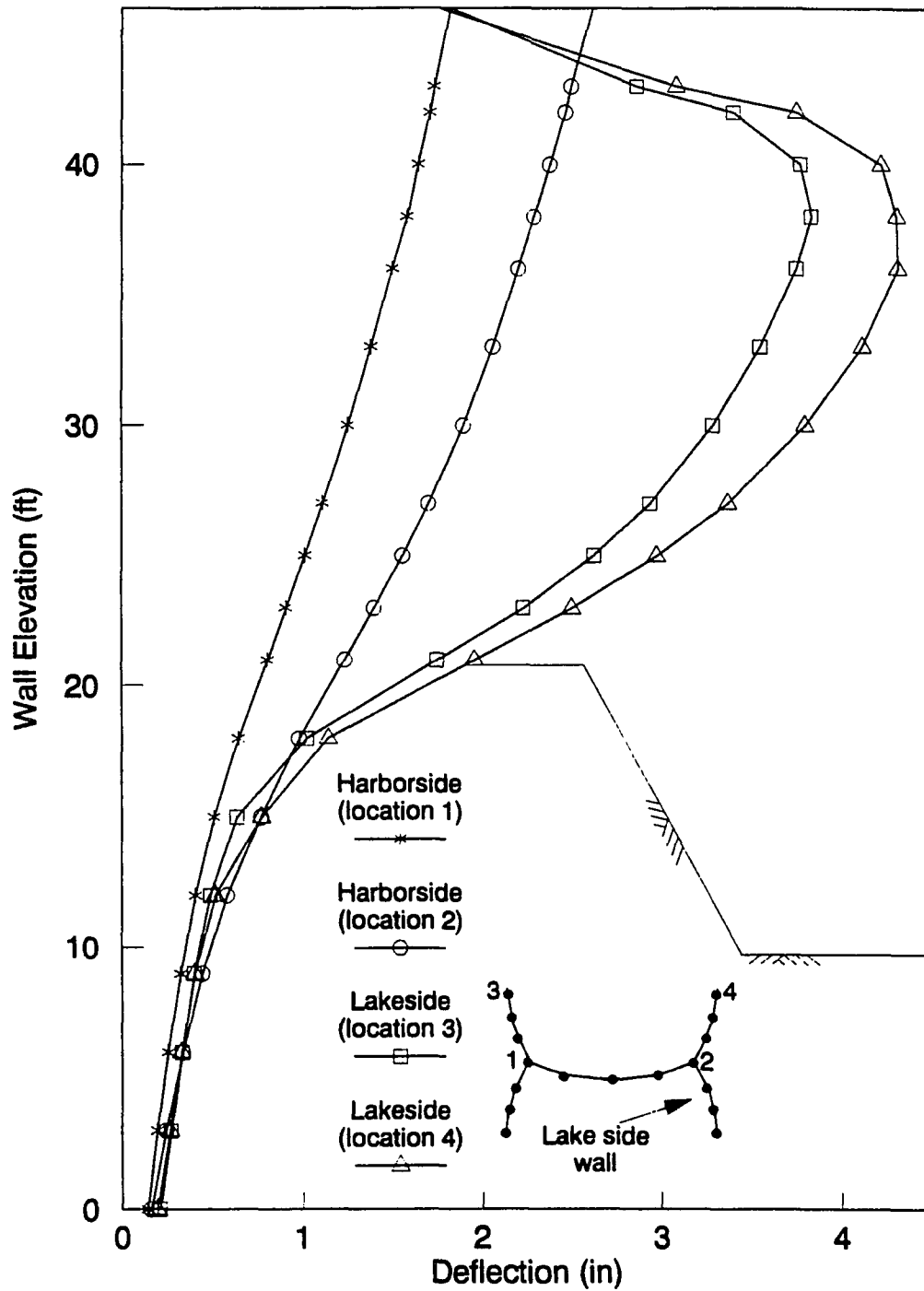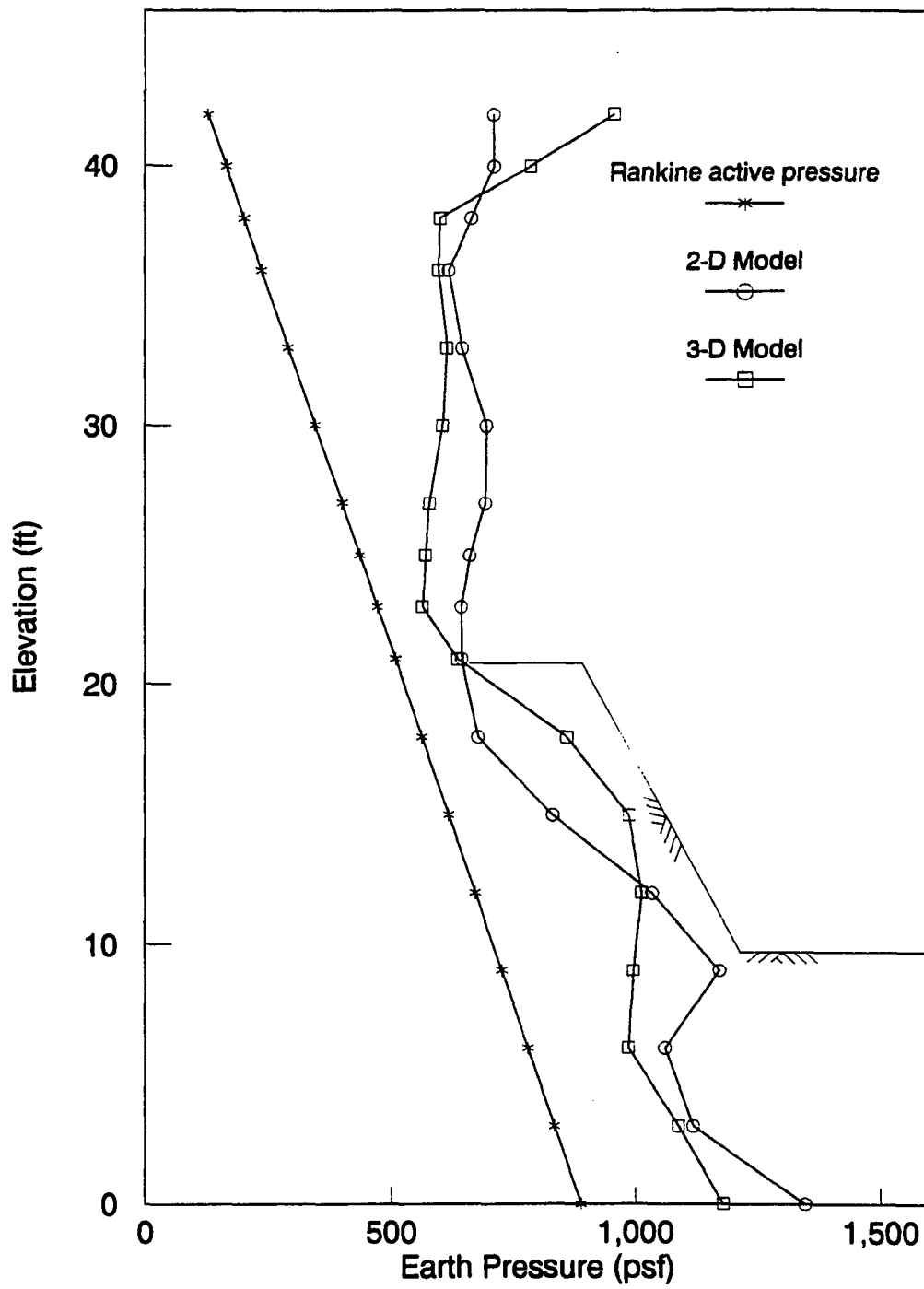
Figure 4.31 Displacements of the three-dimensional model at
the present structural state.

Figure 4.32   Lateral earth pressure distributions at the present structural state.

earth pressure distributions against the lake side sheeting predicted by both models show that the pressures were far larger than the Rankine active pressure values at the upper half of the structure (see Figure 4.32).

The displacement plots for both models and the interlock force plots for the three-dimensional model in the present condition show that the permanent effects were more predominant on the lake side of the structure than the harborside, as might be expected. The settlements for the present condition predicted along the mid-cell line at the top of the fill layer are plotted in Figure 4.33. The three-dimensional model results indicating 9.5 in. settlement on the harbor side and 12.5 in. on the lake side conform quite well with the previous site investigations reporting settlements exceeding 1 ft on the lake side [1].

4.7.3. Stage III: Wave load analysis

Wave statistics in the form of hindcast wave data were used to select the wave parameters. The wave pressures were generated according to the formulae for evaluation of the pressures on vertical walls for incident crest and trough conditions of the wave. For a detailed discussion of the methodology, the reader is urged to refer to the Chapter 5 of the final report, "Structural Analyses of Calumet Harbor Breakwater" [2]. The pressures on the lake side face of the breakwater due to individual waves were calculated at different elevations and concentrated at the nodes of the
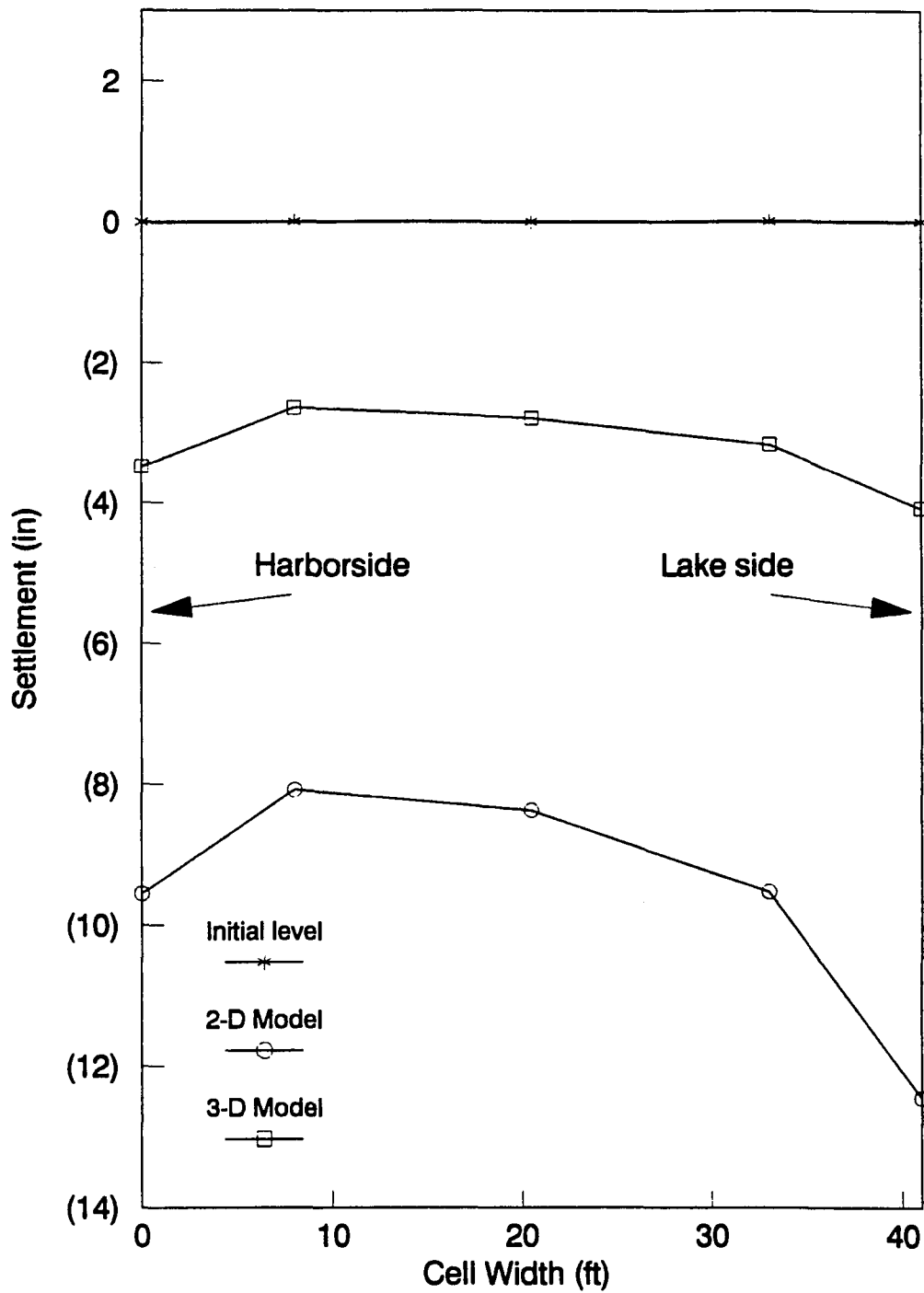
Figure 4.33   Settlements at the top of the fill layer at the
present structural state.

mesh. Description of the details and the assumptions are given in Appendix B.

Results of three wave applications on the finite element models are presented in this section. These waves are; 4 ft high from North-Northwest, 16 ft high from North-Northwest and 24 ft high from Northeast. In accordance with the descriptions and assumptions, crest and trough position loading for each wave was started from the present condition of the structure.

The interlock force predictions of the two- and three-dimensional models are shown in Figures 4.34 and 4.35, respectively. The general form of the plots are in accordance with the previous analyses results of the respective models. The two-dimensional model predicts maximum interlock forces near the top of the sheetpile. The three-dimensional model predicts maximum interlock forces around 33 ft level with sharp decreases through the top of the sheet piles.

The interlock force variation range (crest value to trough value) is negligible for a 4 ft wave cycle for either model. For the 16 ft wave cycle, the maximum interlock force ranges are 246 lb/in at the 42 ft level (shorter level at the diaphragm wall) and 312 lb/in at 36 ft level for the two- and three-dimensional models, respectively. For the 24 ft wave cycle, the maximum values increase to 1631 lb/in at the 42 ft level and 1304 lb/in at the 36 ft level, for two- and three-dimensional models, respectively.
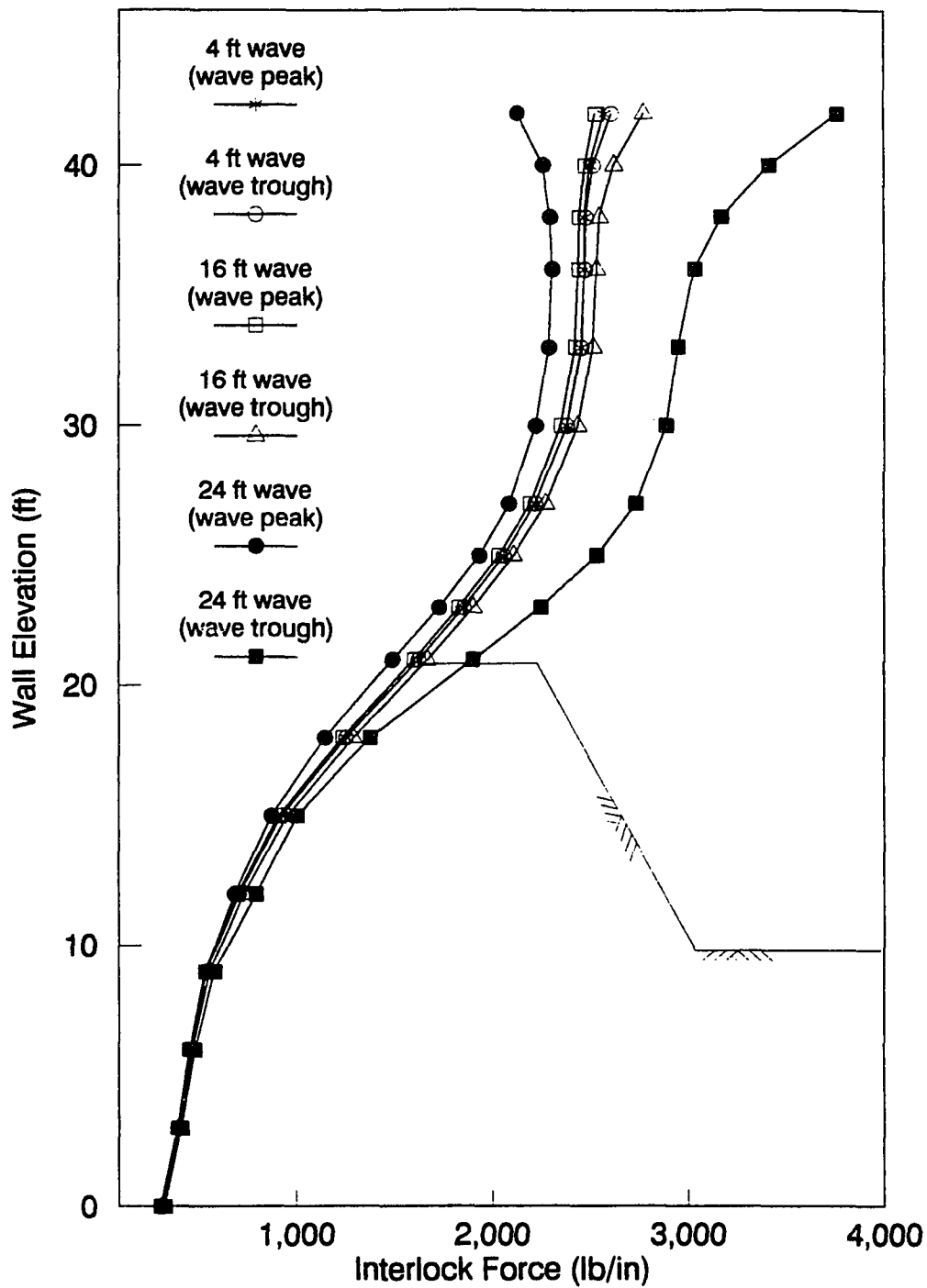
Figure 4.34 Interlock force variations of the two-dimensional model under wave action.
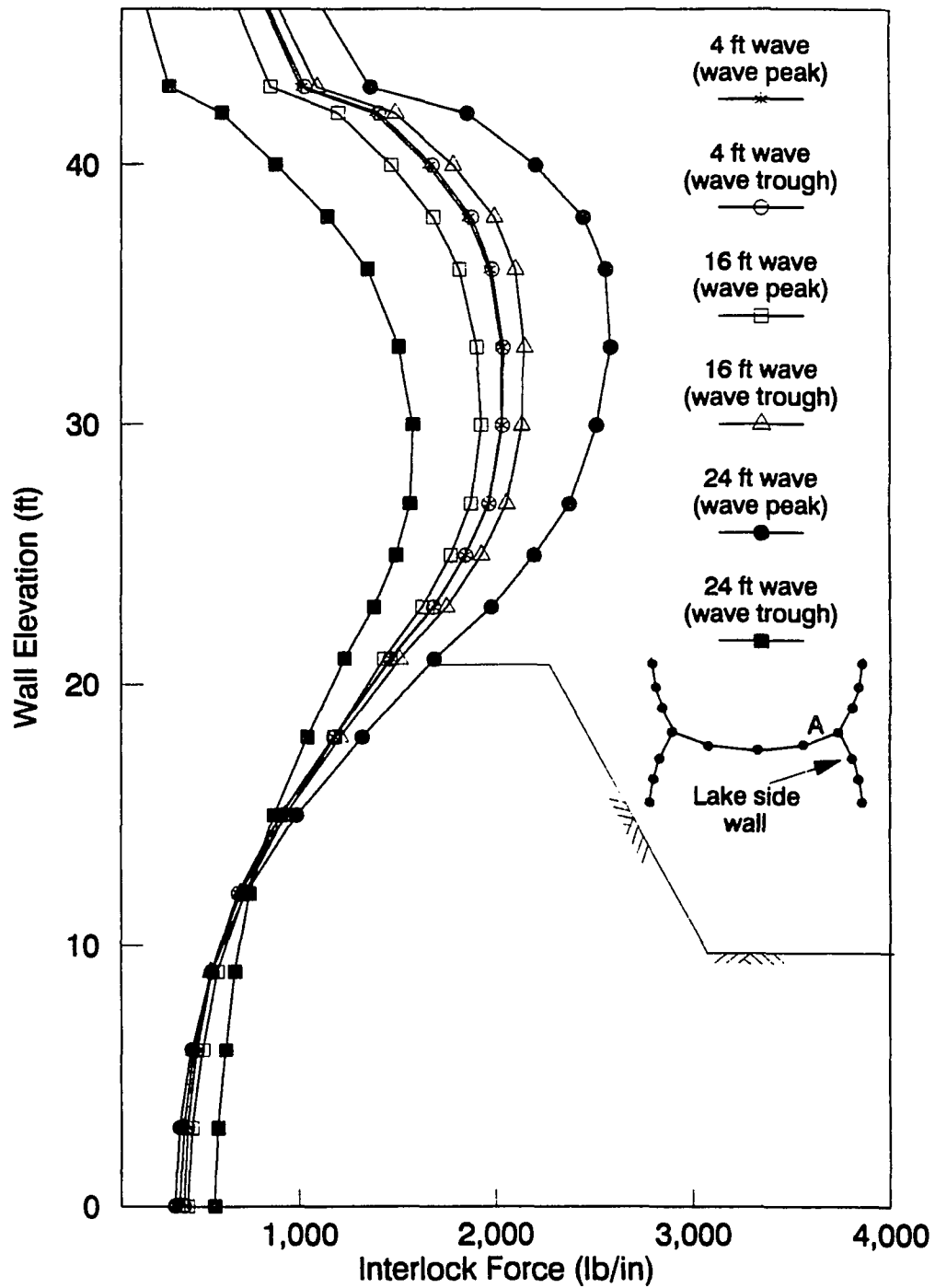
Figure 4.35   Interlock force variations of the three-dimensional model under wave action.

The displacement plots corresponding to the three waves are given in Figures 4.36 and 4.37. The maximum displacement ranges occur at the top of the sheetpiles for both of the models. Displacement ranges corresponding to the 4 ft wave cycle were insignificant for both models. The displacement range for the 16 ft wave cycle was predicted as 1 in. by both models, whereas, for the 24 ft wave cycle predictions were 6 in. and 3.4 in. by two- and three-dimensional models, respectively.

It should be noted that the displacements within the top 4 ft of the two-dimensional model are excessive for the 24 ft wave cycle compared to the three-dimensional model results. Two apparent reasons for this discrepancy are the lack of shear resistance provided by the diaphragm wall in the two dimensional model as mentioned in Section 4.7.2 and nonexistence of springs above 42 ft level due to the shorter diaphragm wall.

4.8. Comparisons with the Recorded Data

The field and the predicted data by the finite element models were compared at different elevations for fixed wave heights. The strains that were recorded on different days by using the data acquisition system were transformed into hoop force ranges with the aid of the diagnostic tests [2]. The wave properties for a specific period of recorded strain range variation were obtained from the Coastal Engineering Research Center (CERC) and the National Climactic Data Center. The
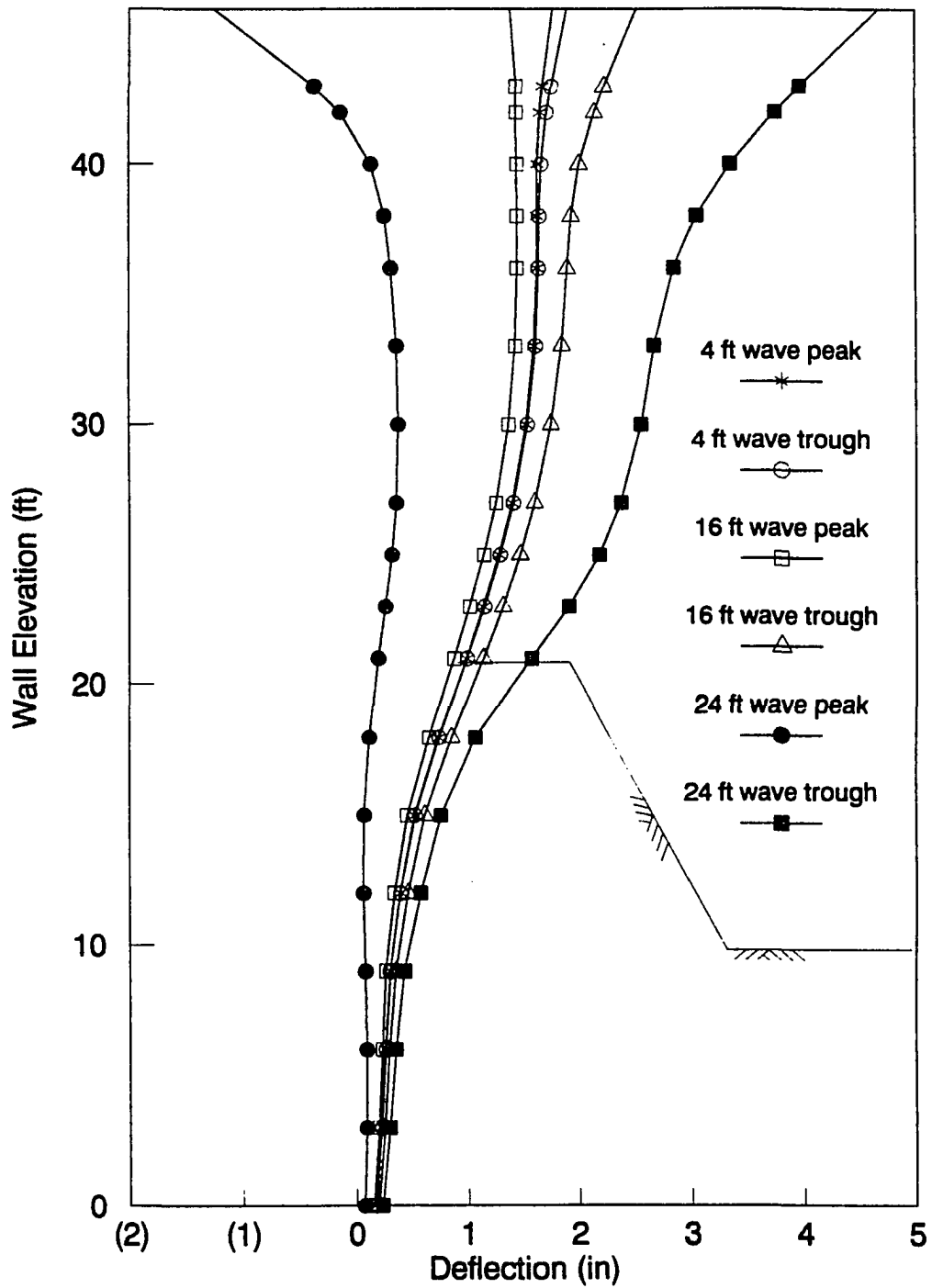
Figure 4.36   Displacements of the two-dimensional model at the lake side wall under wave action.
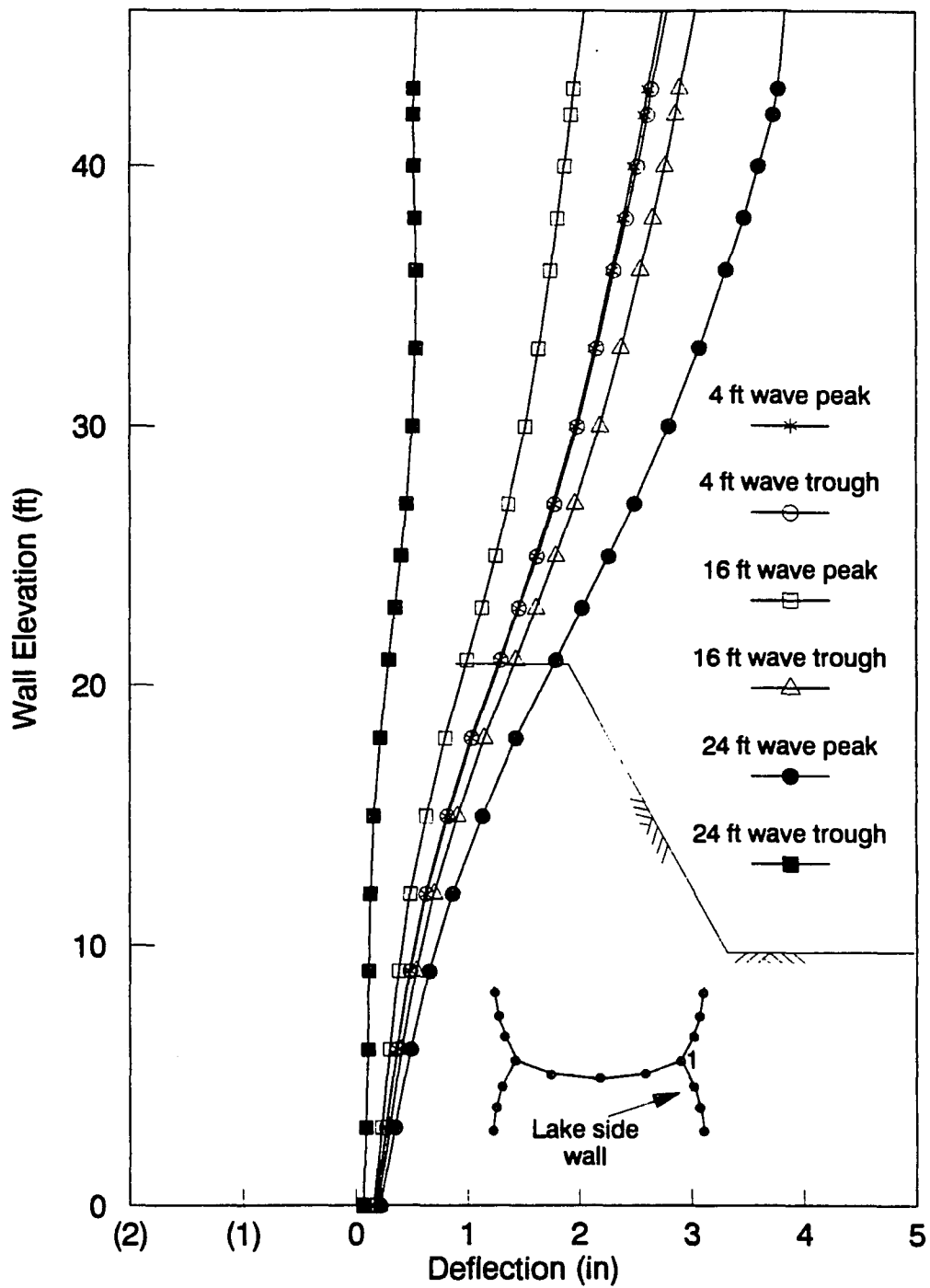
Figure 4.37   Displacements of the three-dimensional model
under wave action.

recorded field data were primarily from the NNW direction with a maximum wave height of 13.9 ft during the data collection period.

Four cases were selected for the correlation of the finite element and the field data. Table 4.2 indicates the time of wave record, maximum wave height, wind direction as recorded on the marine log, and the wave direction as per real-time wave statistics. Table 4.3 indicates the recorded hoop-force ranges.

The variation of the hoop forces at three locations on the lake side along the vertical profile of the structure are shown in Figures 4.38 through 4.41 for the four cases selected. The predicted values in Figure 4.40 are considerably above the recorded values. As mentioned earlier, Table 4.2 compares the marine log data with CERC data. From the Table for Feb. 2nd, the marine log data reads NW, while the CERC data indicates NNW direction. If the waves are predominant in the NW direction, the hoop force variations are considerably reduced with respect to those predicted on the basis of NNW direction. Both models predicted consistently greater ranges than measured at the top location, with the two-dimensional model values being closer to those recorded. However, at the other two locations three-dimensional values were in better agreement with the recorded data.

In Figures 4.38 through 4.41 it should be noted that the recorded interlock force ranges at the top location are

Table 4.2 Time, date, max. wave height in the record and
corresponding wind and wave directions.

Date	Time of record	Maximum wave height H_{max} (ft)	Wind dir. marine log	Wave dir. real-time statistics
Jan 12th	5:00 hrs	10.20	NW	WNW
Feb 2nd	13:59 hrs	6.00	NW	NNW
Feb 13th	20:49 hrs	12.00	NW	NNW
Feb 24th	14:27 hrs	13.90	NW	NNW

Table 4.3   Recorded hoop-force ranges - strain gauges 12,13
and 7.

Date	H_{max} (ft)	S.G. 12 (lb/in.)	S.G. 13 (lb/in.)	S.G.7 (lb/in.)
Jan 12th	10.20	135.28	327.52	71.84
Feb 2nd	6.0	46.70	50.92	20.84
Feb 13th	12.0	63.34	41.48	2.67
Feb 24th	13.90	167.42	667.70	122.91

Table 4.3   (continued) strain gauges 5,6,8,9 and 10.

Date	H_{max} (ft)	S.G.5 (lb/in.)	S.G.6 (lb/in.)	S.G.8 (lb/in.)	S.G.9 (lb/in.)	S.G.10 (lb/in.)
Jan 12th	10.20	124.92	24.00	34.97	18.53	73.54
Feb 2nd	6.0	28.85	36.00	10.05	40.00	45.82
Feb 13th	12.0	3.27	4.30	3.64	3.00	3.57
Feb 24th	13.90	123.24	48.16	47.83	22.36	106.65

Figure 4.38 Predicted and recorded interlock force ranges under wave action (data recorded on Jan. 12th).

Direction - NNW, Wave Height = 6.0 ft
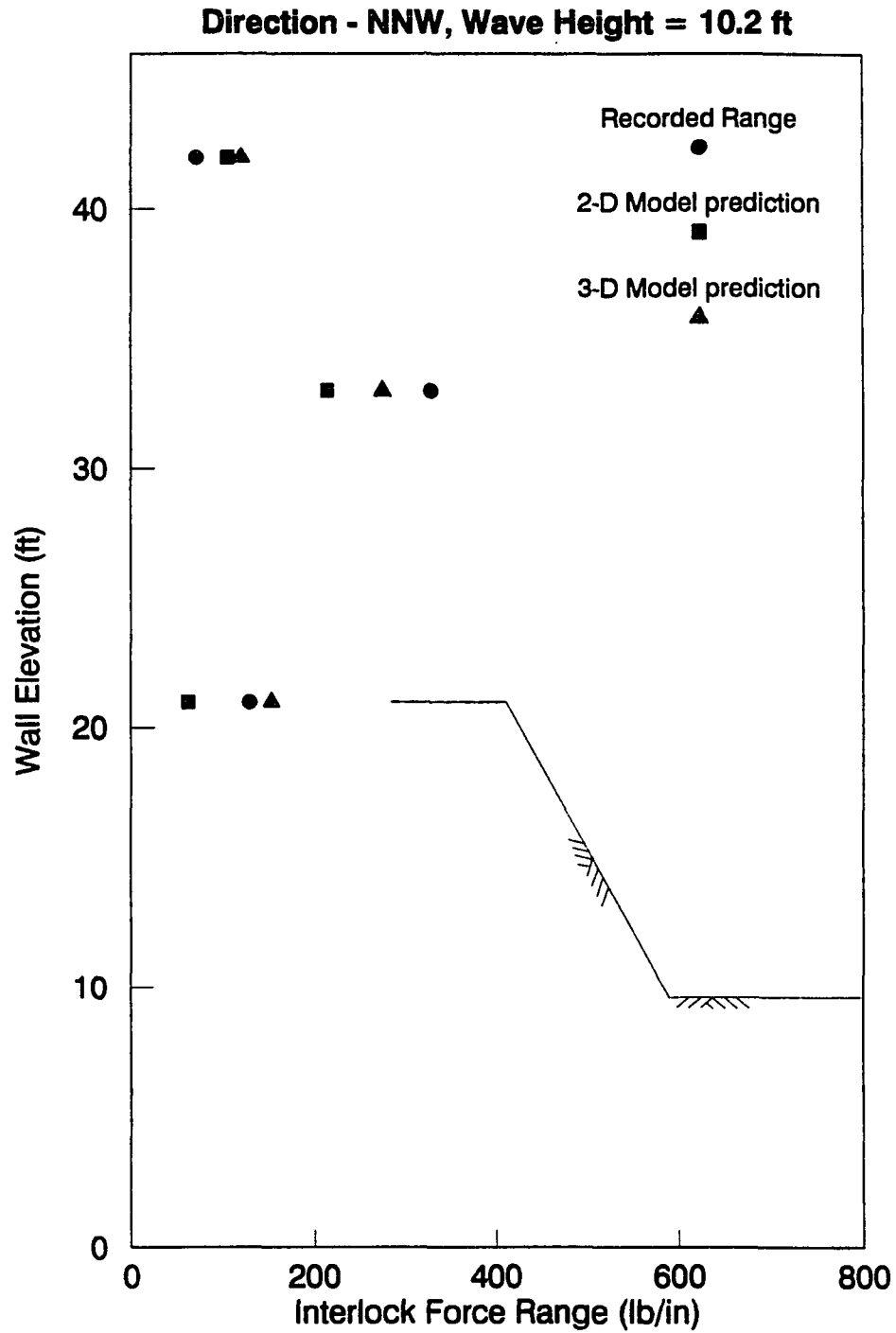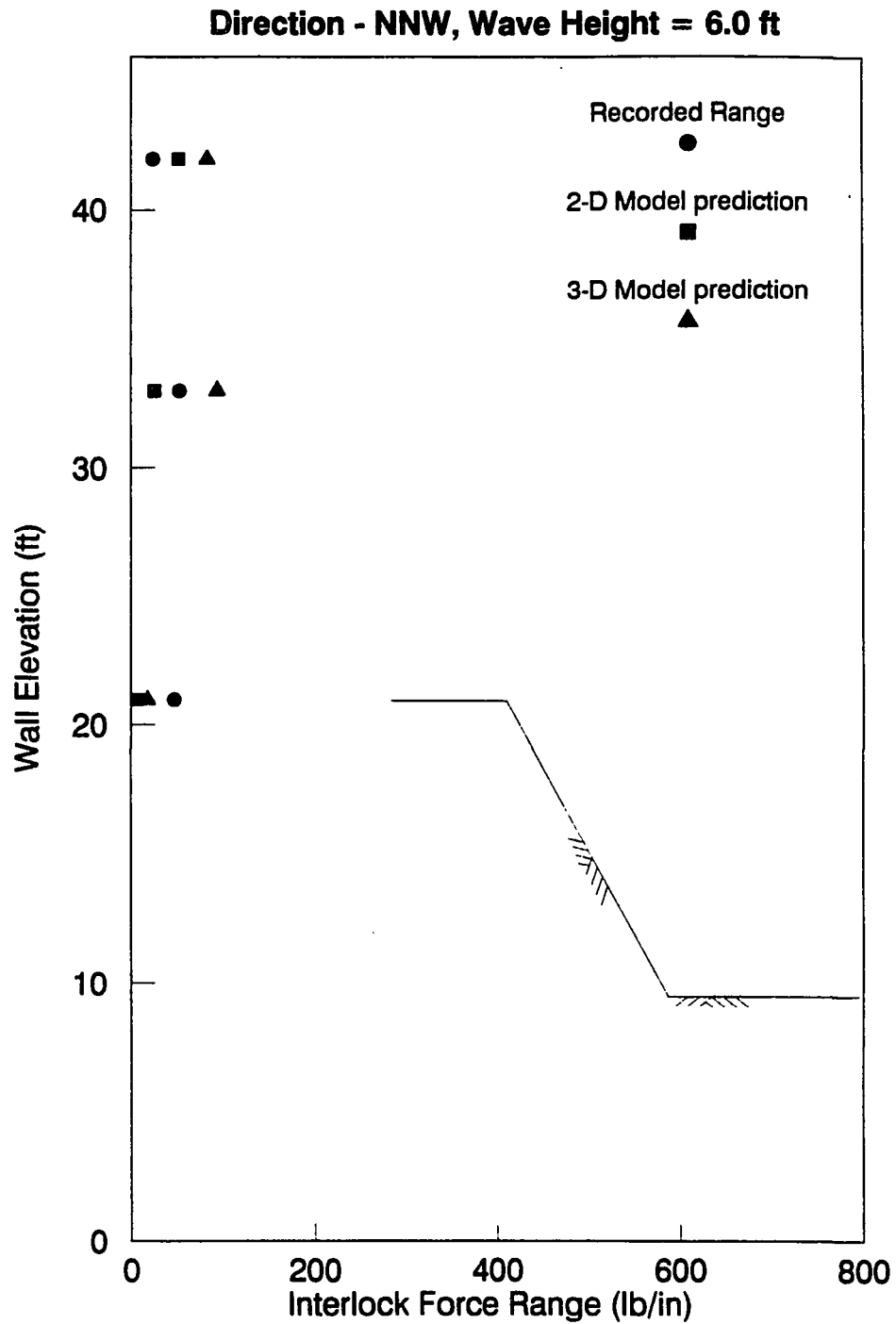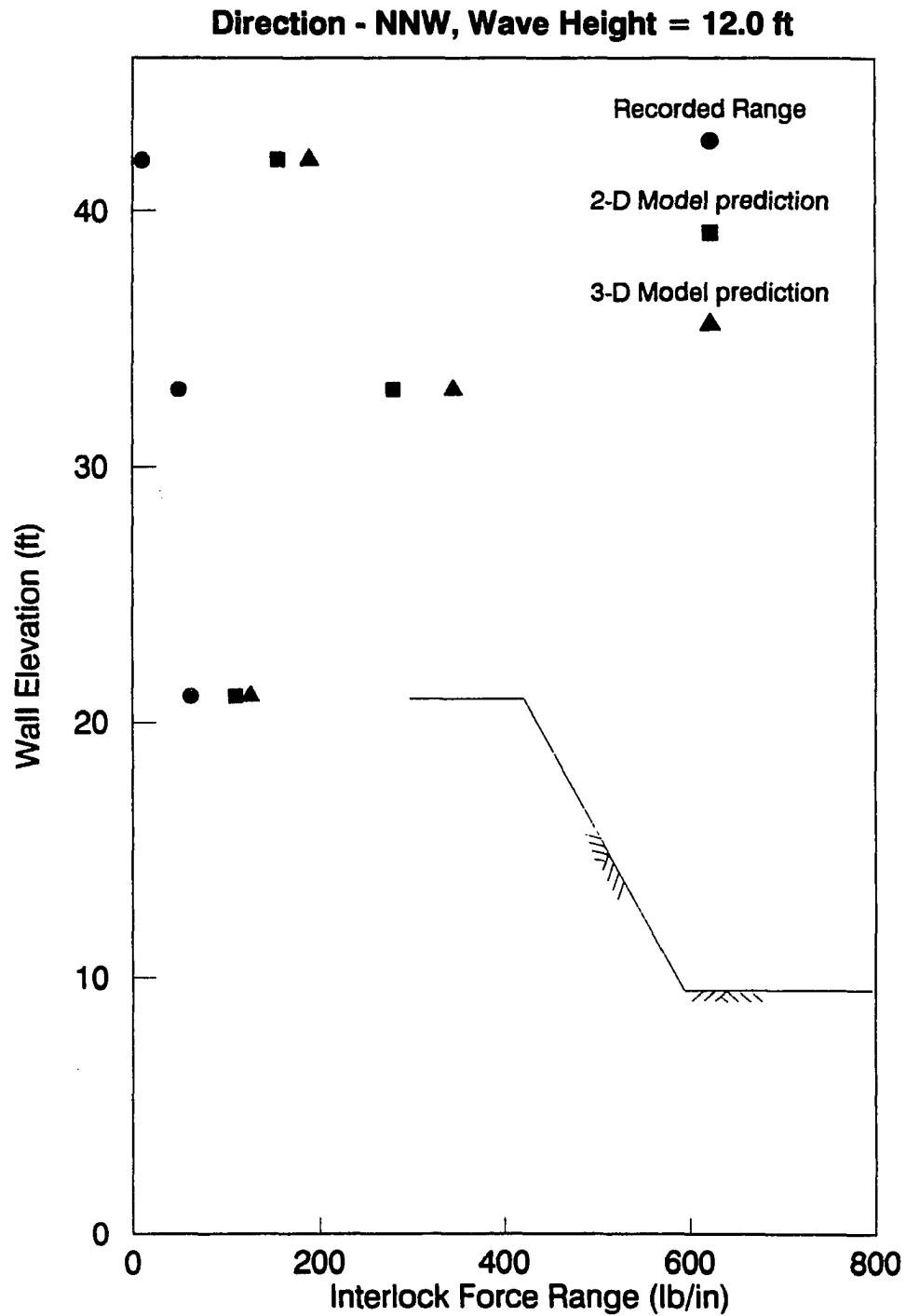
Figure 4.39   Predicted and recorded interlock force ranges under wave action (data recorded on Feb. 2nd).

Figure 4.40   Predicted and recorded interlock force ranges
under wave action (data recorded on Feb. 13th).

Direction - NNW, Wave Height = 13.9 ft
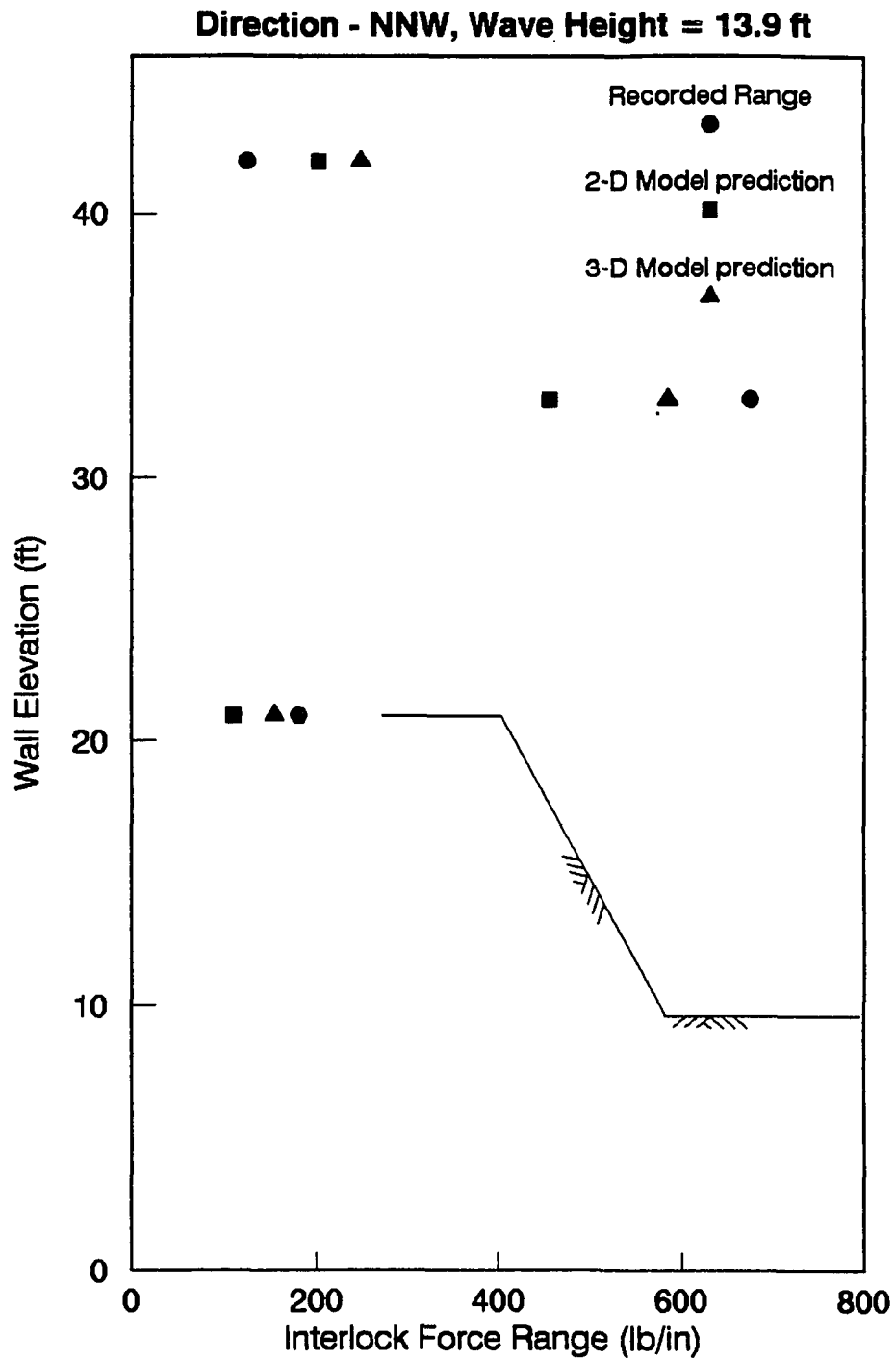
Figure 4.41   Predicted and recorded interlock force ranges
under wave action (data recorded on Feb. 24th).

consistently less than the finite element predictions.
Considering the dates on which the data were recorded (January
12th through February 24th), heavy ice formation at the top of
the sheetpiles, over the upper fill region and the capstones
is highly probable. Due to the frozen fill and the possible
ice build up between the capstones and the sheetpiles at the
top of the cell, lateral movement of the sheetpiles would be
constrained in this region. Also, due to the formation of ice
layer, the sheetpile response near the top of the cell would
become stiffer. Under such conditions, strain range readings,
and consequently the interpreted interlock force ranges would
be smaller at the top strain gauge location, which is 2 ft
above the still water level. It has been calculated that the
strains in the hoop direction would be reduced up to 20% due
to and ice layer formation of 1 in. on both sides of the
sheetpiles.

Another possible cause for the discrepancy between the
recorded data and the prediction of the finite element models
is related to the diagnostic tests performed on the sheetpile
coupons, regarding interlock force-strain calibrations. In
these tests, the coupons were loaded axially with the strain
gauges located on both sides of the webs and correlation made
with the associated interlock force. During wave action,
however, there exist fluctuating internal and external lateral
pressures on the sheetpiles which would generate additional
strains not accounted for in the diagnostic test set up. As a

result, the interpreted interlock force ranges would be somewhat greater than those actually exist over the sheetpiles on the breakwater. This argument would be insignificant for the top strain gauge location where such pressure fluctuations are minor.

4.9. Run Time Comparisons and Evaluation of ANSYS Package

Run time required for the three-dimensional model for one iteration was about twelve times of that required for the two-dimensional model. Moreover, for the load cases in this study, the number of iterations required for the three-dimensional model to achieve the same degree of convergence with the two-dimensional model was approximately three times as much. The apparent reason for this is the relatively larger deformations that occured in the three-dimensional model solutions. Consequently, the total required computer time becomes a considerable disadvantage for the three-dimensional model.

In general, ANSYS finite element package was found to be quite suitable for this study. Drucker-Prager material model as implemented in ANSYS performed satisfactorily as discussed in Chapter 3. Powerful pre- and post-processing routines were useful, especially for the three-dimensional model. Sliding surface elements could be more accurate to model the soil-structure interaction between the fill and the sheetpiles. However, this element was not available in ANSYS version 4.4. The only major problem faced regarding the use of ANSYS was

the wave front limitation (450) imposed by the supplier. The mesh for the three-dimensional model had to be reassembled several times in order not to exceed the wave front limitation.

5. SUMMARY AND CONCLUSIONS

5.1. Summary

Cellular structures initially were used basically as temporary systems to provide dry working environment for constructions inside shallow water. Later, the applications were extended to permanent structures such as retaining walls, breakwaters and navigation structures.

In the latter two cases, the metal fatigue can become a possible failure mode, if the structure is exposed to strong wave action and thus to extreme unbalanced lateral loads as in the case of South Chicago Harbor breakwater. Significant damage occurred in 1984 winter during a storm on the detached section of the above mentioned structure which was built in 1934. The investigation of the structure was conducted by the Structural Division of the Civil and Construction Engineering Department of the Iowa State University, starting in 1988, with the objectives to examine the possible failure modes and to evaluate the present condition of the structure as the basis for future rehabilitation. The project involved field investigation, laboratory testing, force field determination and finite element analyses. The study presented here covers a part of that investigation aimed at determination of the interlock forces caused by the wave action.

It has been well established that the conventional design methods for cellular structures which were essentially

developed in the 1940s and 1950s have substantial shortcomings. These methods are usually overconservative in predicting the interlock forces and none of them is capable of predicting deformations, a rather important parameter in evaluation of the performance of cellular structures. Also, these methods can not provide guidelines to handle irregular forces such as those would be imposed by the waves.

In the past 15 years the finite element method has been applied to the cofferdam problem. The method has the ability to deal effectively with problems involving soil-structure interaction, loading and geometric irregularities, as well as behavioral complexities of the materials. The past finite element work consisted of applications of two-dimensional model versions (axisymmetric, vertical slice and generalized plane strain) which were demonstrated to yield satisfactory results. However, all of these models require specific assumptions and simplifications regarding the loads and geometry, and they can provide only partial information regarding the structural behavior. These drawbacks can properly be eliminated by using three dimensional modelling. However, the disadvantage is complex and tedious modelling work, as well as considerable increases in run time and memory requirements.

The primary objective of this work was to investigate the structural response of the Calumet Harbor breakwater under forces caused by the wave action. The analyses were conducted

in parallel with two- and three-dimensional finite element models to evaluate the model performances on a comparative basis. The ANSYS finite element package is used throughout the analyses.

The prediction capability of the Drucker-Prager elastic-perfectly plastic model was tested as it is implemented in the ANSYS package by comparison to the results of triaxial tests. Dependence of the lateral earth pressures on the circumferential stiffness of the sheetpile wall was investigated using an axisymmetric model comparable to the cell size of the actual breakwater studied. The same model was used also for a series of parametric studies regarding several factors that are involved in the finite element modelling of cellular structures. These factors were the associativity parameter in the Drucker-Prager model, frictional coefficient between the wall and the fill material, sensitivity to the mesh density and the permanent effects of lateral loads.

Two-dimensional vertical slice and three-dimensional finite element models of the South Chicago Harbor breakwater structure were prepared using the ANSYS finite element package and utilized throughout this study. The first of the three stages of the load history was the simulation of the construction of the structure (the post-construction state). It was proposed that the present structural state of the breakwater would be considerably different from that of the

immediately after the completion of the construction due to
the wave load effects. The second load stage aimed at
determining this latter structural state (the present state).
In the final stage, the response of the structure was
investigated under wave loads. The structure was
quasistatically loaded by the pressures corresponding to the
imminent peak and trough positions of a specific wave acting
on the structure, assuming these pressures control the limits
of the deviation of structural response.

The predictions of both models were analyzed on a
comparative basis for each of the three load stages mentioned
earlier regarding deformations, interlock forces and earth
pressures on the sheetpiles. In addition, the performance of
the models under wave loading were compared with the recorded
field data.

5.2. Conclusions

5.2.1 Construction simulation

1. Where comparisons were possible, the two- and three-
    dimensional model predictions were consistent for the
    construction simulation stage regarding hoop forces
    in the sheetpiles. The displacements, however, were
    predicted to be consistently greater along the
    height of the structure by the three-dimensional
    model due to the geometric deformations in the curved
    interface wall.

2. Locations of the maximum interlock forces and

displacements were at about 18 ft depth measured from top of the sheetpiles following fill and berm placement. After the capstones were placed the locations were shifted upward by approximately 5 ft and the differences between the two model predictions increased slightly.

3. The hoop force predictions by the two models agreed within 8%.

4. The displacements predicted by the three-dimensional model were greater before and after the capstone placement (up to 70% before and up to 43% after).

5. In the middle of the cell, the outward deflections of the sheeting predicted by the three-dimensional model were approximately four times those predicted by the two-dimensional model at the Y-joints.

5.2.2 Simulation of the present condition

1. Displacements and hoop forces predicted by both models indicated a stabilization trend throughout the cyclic application of the hypothetical wave loads. The present structural state of the breakwater predicted by the two models was significantly different from the post-construction state with major increases in interlock forces, displacements and earth pressures.

2. The maximum hoop force location for the two-dimensional model occured at the shorter level of the

diaphragm wall, and at the 16 ft level for the three dimensional model.

3. Hoop forces predicted by the three-dimensional model were comparatively less up to 28%. Apparently, this discrepancy is due to the limited capabilities of the two-dimensional vertical slice model which can incorporate only those deformations at the Y-joints. The increased bending as predicted by the three-dimensional model in the external wall sheetpiles away from the Y-joints cause the reduced hoop forces.

4. Maximum displacements occured at the top for both models. However, the three-dimensional model values were up to 50% higher due to the additional geometric deformations in the curved interface wall.

5. At the top of the fill both models predicted larger settlements near the lake side sheetpiles. The settlement value was 12.5 in. for the three-dimensional model. This agreed well with the site observations that exceeded 1 ft. Corresponding two-dimensional model settlement was approximately 4 in.

6. The shapes and magnitudes of the lateral earth pressure distributions predicted by the two models deviated greatly from those of the post-construction state and from the linear distribution pattern of the classical theories.

5.2.3 Wave load analyses

1. Where comparisons were possible, hoop force and
    displacement response ranges of the two models were
    consistent for the waves analyzed.

2. Maximum hoop force ranges took place in the vicinity
    of the shorter level of the interface wall.

3. Maximum displacement ranges occured at the top of the
    sheetpiles for both models.

4. The hoop force and displacement response ranges
    for the two dimensional model were greater,
    especially near the top of the sheet piles, for the
    case of 24 ft wave which imposes the greatest
    lateral loads on the structure. This indicates that
    for larger unbalanced lateral loads the effect of the
    missing interface wall shear resistance in the two
    dimensional model becomes more significant.

5.2.4. Comparisons with the Recorded Data

1. The predicted ranges by both models were consistently
    greater with respect to those recorded at the top
    location (the depression level of the diaphragm
    wall).

2. At the other two locations which were at 13 and 25 ft
    depth levels, the three dimensional model values were
    in better agreement with the recorded data.

3. Limitations of the diagnostic tests regarding the
    interlock force-strain calibrations and the

possible ice formation at the top of the
breakwater during data recording are the potential
sources for the discrepancies between the finite
element predictions and the recorded data.

5.2.5. Model selection criteria

As discussed in Chapter 4 in detail, the discrepancies
between the two model results can be explained, in general, by
the limitations due to the two-dimensional idealization of the
vertical slice model. However, due to the certain
disadvantages involved (basically, the modeling complexities
and the major increases regarding computation time and memory
requirements), three-dimensional model application is rather
unpractical for cellular structures. For a specific case, the
model selection would depend on the factors such as the
geometry and the size of the structure, the importance of the
structure, the magnitude and characteristics of loads and the
type of information sought about the structural behavior.

REFERENCES

[1] U.S. Army Corps of Engineers, Chicago District.
     <u>Recoinassence Report, Major Rehabilitation, Calumet</u>
     <u>Harbor Breakwater, Illinois</u>. Chicago: U.S. Army Corps of
     Engineers, 1986.

[2] Wipf, T. J., Greimann, L. F., Challa, R. K., Bakir, B. S.
     and Wood, D. L. <u>Structural Failure Analysis of Calumet</u>
     <u>Harbor Breakwater</u>. Report submitted to U.S. Army Corps of
     Engineers, Chicago. C.C.E. Dept., Iowa State University,
     1989.

[3] Wilson, J.F., Editor. <u>Dynamics of Offshore Structures</u>.
     New York: John Wiley and Sons, 1984.

[4] Pennoyer, R. P. and Hockensmith, G. "Design of Sheet-
     piling Cofferdams." <u>Civil Engineering</u>, Vol. 5, 1935., pp
     19-23.

[5] Terzaghi, K. "Stability and Stiffness of Cellular
     Cofferdams." <u>Transactions</u>, ASCE, vol. 110, paper no.
     2253, 1945, pp 1083-1202.

[6] Cummings, E. M. "Cellular Cofferdams and Docks." <u>Journal</u>
     <u>of the Waterways and Harbors Division</u>, ASCE, vol, 83,
     proc. paper 1366, 1957, pp 13-15.

[7] Krynine, D.P. Discussion of "Stability and Stiffness of
     Cellular Cofferdams," by K. Terzaghi, <u>Transactions</u>, ASCE,
     vol. 110, paper no. 2253, 1945, pp 1175-1178.

[8] Hansen, J. B. "The Internal Forces in a Circle of
     Rupture." <u>The Danish Geotechnical Institute, Bulletin no.</u>
     <u>2</u>, Copenhagen, Denmark, 1957.

[9] Department of Navy, <u>Design Manual: Soil Mechanics,</u>
     <u>Foundations and Earth Structures</u>. Naval Facilities
     Engineering Command, Navdock DM-7, Washington, D.C.,
     1977.

[10] Schoroeder, W. L. and Maitland, J. K. "Cellular
     Bulkheads and Cofferdams." <u>Journal of the   Geotechnical</u>
     <u>Engineering Division</u>, ASCE, vol.105, no. GT7, 1979, pp
     823-837.

[11] Lacroix, Y., Esrig, M. I. and Lusher, U. "Design,
     Construction and Performance of Cellular Cofferdams."
     <u>Proceedings, ASCE Specialty Conference on Lateral</u>
     <u>Stresses in the Ground and Earth Retaining Structures</u>,
     ASCE, 1970, pp 271-328.

[12] Dismuke, T. D. "Cellular Structures and Braced Excavations." Foundation Engineering Handbook. Ed. H. F. Winterkorn, H. F. Fan. New York: Van Nostrand Reinhold Co., 1975, pp 445-480.

[13] Rossow, M., Demsky, E. and Mosher, R. Theoretical Manual for Design of Cellular Sheetpile Structures. Washington D.C.: U.S. Army Corps of Engineers, 1987.

[14] Swatek, E. P. "Design and Installation of Cellular Structures." Proceedings, Conference on Design and Installation of Pile Foundations and Cellular Structures, ASCE. Lehigh Univ., 1970, Ed. H. Y. Fang and T. D. Dismuke. Lehigh Valley, 1970, pp 413-423.

[15] Tenessee Valley Authority. Steel Sheet-piling Cellular Cofferdams on Rock. TVA Technical Monograph no. 75, vol. 1, 1957.

[16] Pennoyer, R. P. Discussion of "Stability and Stiffness of Cellular Cofferdams", by K. Terzaghi, Transactions, ASCE, vol. 110, paper no. 2253, 1945, pp 1124-1133.

[17] Maitland, J. K., and Schroeder, W. L. "Model Study of Circular Sheetpile Cells." Journal of Geotechnical Engineering Division, ASCE, vol. 105, no. GT-7, 1979, pp 805-821.

[18] White, A., Cheney, J. A. and Duke, M. "Field Study of a Circular Bulkhead." Journal of Soil Mechanics and Foundations Division, ASCE, vol. 87, no. SM4, paper no. 2902, 1971, pp 89-124.

[19] Clough, G. W. and Kuppusamy, T. "Finite Element Analysis of Lock and Dam 26 Cofferdam." Journal of the Geotechnical Engineering Division, ASCE, vol. 111, no.4, 1985, pp 521-544.

[20] Kittisatra, L. "Finite Element Analyses of Circular Cell Bulkheads." Diss. Oregon State University, 1976, Corvalis, OR.

[21] Clough, G. W., and Hansen, L. A. A Finite Element Study of the Behavior of the Willow Island Cofferdam. Technical Report, no. CE218. Department of Civil Engineering, Stanford University, Stanford, Calif.,1977. Technical Report, no. CE218.

[22] Clough G. W. and Duncan, J. M. "Finite Element Analyses of Retaining Wall Behavior." Journal of Soil Mechanics and Foundations, ASCE, vol. 97, no. SM12, 1971, pp 1657-

1673.

[23] Duncan, J. M., Bryne, P., Wong, K. S. and Mabry, P.
Strength, Stress-strain, and Bulk Modulus Parameters for
Finite Element Analyses of Stresses and Movements in Soil
Mases. University of California, Berkeley, Calif., 1980,
Report no. UCB/GT/80-01.

[24] Stevens, R. F. "Study of the Behavior of a Cellular
Cofferdam." Diss., Duke University, 1980, Durham, NC.

[25] Gallagher, R. H. Finite Element Analysis Fundamentals.
Englewood Cliffs, N.J.: Prentice - Hall, 1975.

[26] Shannon and Wilson Inc. Summary Report, Instrumentation
Data Analyses and Finite Element Studies for First Stage
Cofferdam, Lock and Dam 26 (Replacement). Department of
the Army, St. Louis District, Corps of Engineers, 1983.

[27] Wipf, T. J., Greimann, L. F., Challa, R. K., Wood, D. L.
Status of Experimental Phase of Calumet Harbor Breakwater
Study. C.C.E. Dept., Iowa State University, 1989.

[28] DeSalvo, G. J. and Swanson, J. A. ANSYS Engineering
Analysis System - User Manuals I and II, Theoretical
Manual and Examples Manual. Houston, Pa.: Swanson
Analysis Systems Inc., 1985.

[29] Hill, R. The mathematical Theory of Plasticity. London:
Oxford University Press, 1950.

[30] Drucker, D. C. "Some Implications of Work Hardening and
Ideal Plasticity." Quart. Appl. Math., vol. 7, 1950, pp.
411-418.

[31] Prager, W. "Recent Developments in Mathematical Theory
of Plasticity." J. Appl. Phys., vol. 20, No. 3, 1949,
pp. 235-241.

[32] Drucker, D. C. "Coulomb Friction, Plasticity and Limit
Loads." Jnl. Appl. Mech. Vol. 21, 1954, pp 71-74.

[33] Desai, C. S. and Sirivardane, H. J. Constitutive Laws
for Engineering Materials with Emphasis on Geologic
Materials. Englewood Cliffs, New Jersey: Prentice-Hall,
Inc., 1984.

[34] Bridgeman, P. W., Studies in Large Plastic Flow and
Fracture with Special Emphasis on the Effects of

Hydrostatic Pressure. New York: McGraw-Hill Book Co., 1952.

[35] Mandelson, A. Plasticity: Theory and Applications. New York: McMillan Publishing Co., 1968.

[36] Zienkiewicz, O. C. Humpeson, C. and Lewis, R. W. "Associated and Nonassociated Visco Plasticity and Plasticity in Soil Mechanics." Geotechnique, Vol. 25, no.4, 1975, 671-689.

[37] Davis, E. H. "Theories of Plasticity and the Failure of Soil Masses." Soil Mechanics: Selected Topics. Ed. I. K. Lee. London: Butterworth, 1980, 341-380.

[38] Drucker, D. C. and Prager, W. "Soil Mechanics and Plastic Analysis of Limit Design." Q. Appl. Math., vol. 10, no.2, 1952, pp 157-165.

[39] Desai, C. S. and Christian, J. T. Numerical Methods in Geotechnical Engineering. New York: McGraw Hill Book Co., 1977.

[40] Craig, R. F. Soil Mechanics. 2nd ed. London: Van Nostrand Reinhold Company, 1980.

[41] Sarpkaya, T. and Isaacson, M. Mechanics of Wave Forces on Offshore Structures. New York: Van Nostrand Reinhold Co., 1981.

[42] U.S. Army Corps of Engineers, Chicago District. General Design Memorandum and Environmental Assessment - Major Rehabilitation. Chicago: U.S. Army Corps of Engineers, 1988.

[43] Bowles, J. E. Foundation Analysis and Design. 4th ed. New York: McGraw-Hill Book Co., 1988.

[44] Lambe, T. W., Whitman, R. V. Soil Mechanics. New York: John Wiley and Sons, Inc., 1969.

APPENDIX A

A repetitive pattern of the structure of rectangular cells was used in the assessment of the bar element stiffnesses. The repetitive pattern has the dimensions of a single cell and contains a diaphragm wall as shown in Figure 4.6. An equal and opposite pressure distribution was assumed to be acting on diaphragm wall from the neighboring cells. Therefore the diaphragm walls in the cell will be stationary, whereas the lake and harbor sides of a cell will move relative to each other because of the difference in internal and external pressure distributions. The stiffness of the diaphragm which acts as a stiff spring connecting the two walls was calculated by considering a unit relative outward movement of harbor and lake side walls as follows:

$$K_t = \frac{AE_c}{W} \qquad (A.1)$$

where,

K_t = total stiffness of the diaphragm of the equivalent rectangular cell

A = cross-sectional area of the diaphragm wall

E_c = elastic modulus of sheetpiles in the circumferential direction

W = diaphragm length of the equivalent rectangular cell (Figure 4.6.(b))

Since the width of PS23 piles is 0.375 inches and the height of the diaphragm wall is 42 feet (diaphragm wall is 4 feet

shorter than the outer walls), the total cross-sectional area
of the diaphragm is:

$$A = 42 * (0.375/12) = 1.31 ft^2 \qquad (A.2)$$

The length of the diaphragm in the equivalent breakwater is 36
feet and the elastic modulus in the circumferential direction
has been determined to be 0.0265 with respect to that of steel
in Section 4.4. Using these data in the total stiffness
equation (Equation A.1):

$$K_t = 9.48 * 10^{-4} * E_{steel} \qquad (A.3)$$

This term was first divided by the cell length (38 feet) to
find the stiffness of the unit slice and then by the cell
height (42 feet) to determine the stiffness per unit height of
the unit slice:

$$K_u = \frac{K_t}{(38 * 42)} = 2565 \, lb/ft \qquad (A.4)$$

where,

K_u = stiffness per unit height of the unit slice

The individual stiffnesses of the bar elements (K_i) were
determined by multiplying K_u, by the respective representative
height for each bar element. As seen in Figure A.1, the bar
elements were spaced nonuniformly in order to match the nodes
with the strain gauge locations. The cross-sectional areas of
individual bar elements which are required as input then
calculated by:
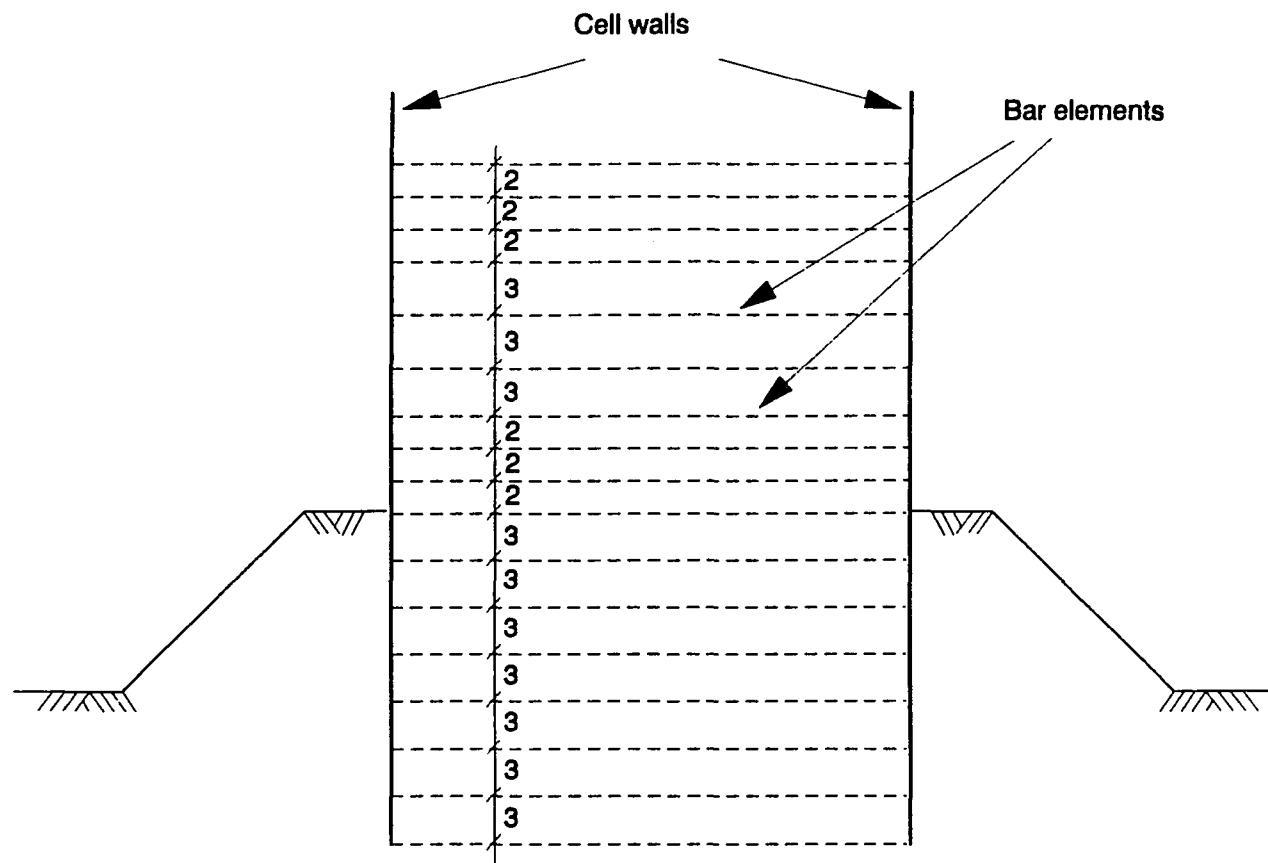
Figure A.1   Location of bar elements.

$$A_i = \frac{K_i L}{E}$$ (A.5)

where,

A_i = cross-sectional area for a bar element

K_i = stiffness of a bar element

The results of the above calculations for the five different contributory lengths are tabulated in Table A.1.

Table A.1 Areas of the bar elements.

Type	Representative Height H_i (ft)	Bar Element Stiffness $K_i = K_u * H_i$ (lb/ft²)	Bar Element Area $A_i = (K_i * L)/E_c$ (ft²)
A	1.0	2565.0	0.822E-3
B	2.0	5130.0	0.164E-2
C	2.5	6412.0	0.206E-2
D	3.0	7695.0	0.247E-2
E	1.5	3847.5	0.123E-2

APPENDIX B

B.1. Determination of Wave Forces on the Breakwater

The wave pressures were assumed to be acting directly over the lake side wall of the breakwater above the lake bed. Water level inside the cell is assumed to be at the top of the sheetpiles during wave action. Accordingly, the net pressure on the lake side wall is the algebraic addition of the inside hydrostatic pressure and the external pressure. The external pressure consists of the dynamic component of the wave and the hydrostatic component. The variation of the total wave pressure profiles of the 24 ft wave is shown in Figures B.1 and B.2. Applied pressure profiles of the same wave is given in Figures B.3 and B.4. The wave pressures calculated at each node were transformed into forces acting at that node considering the contributory area for that node. The contributory area is defined as the area bounded by the midpoints between nodes of the finite element mesh. To calculate the force at a node, the pressures calculated at the mode are multiplied by the contributory area for that mode. Figures B.5 and B.6 indicate the nodal force profiles for the 24 ft wave as applied to the two dimensional model. The calculated forces were transformed into ANSYS input modes for application on two- and three-dimensional finite element models. Reference [2] should be referred for further details.

WAVE HEIGHT = 24 ft
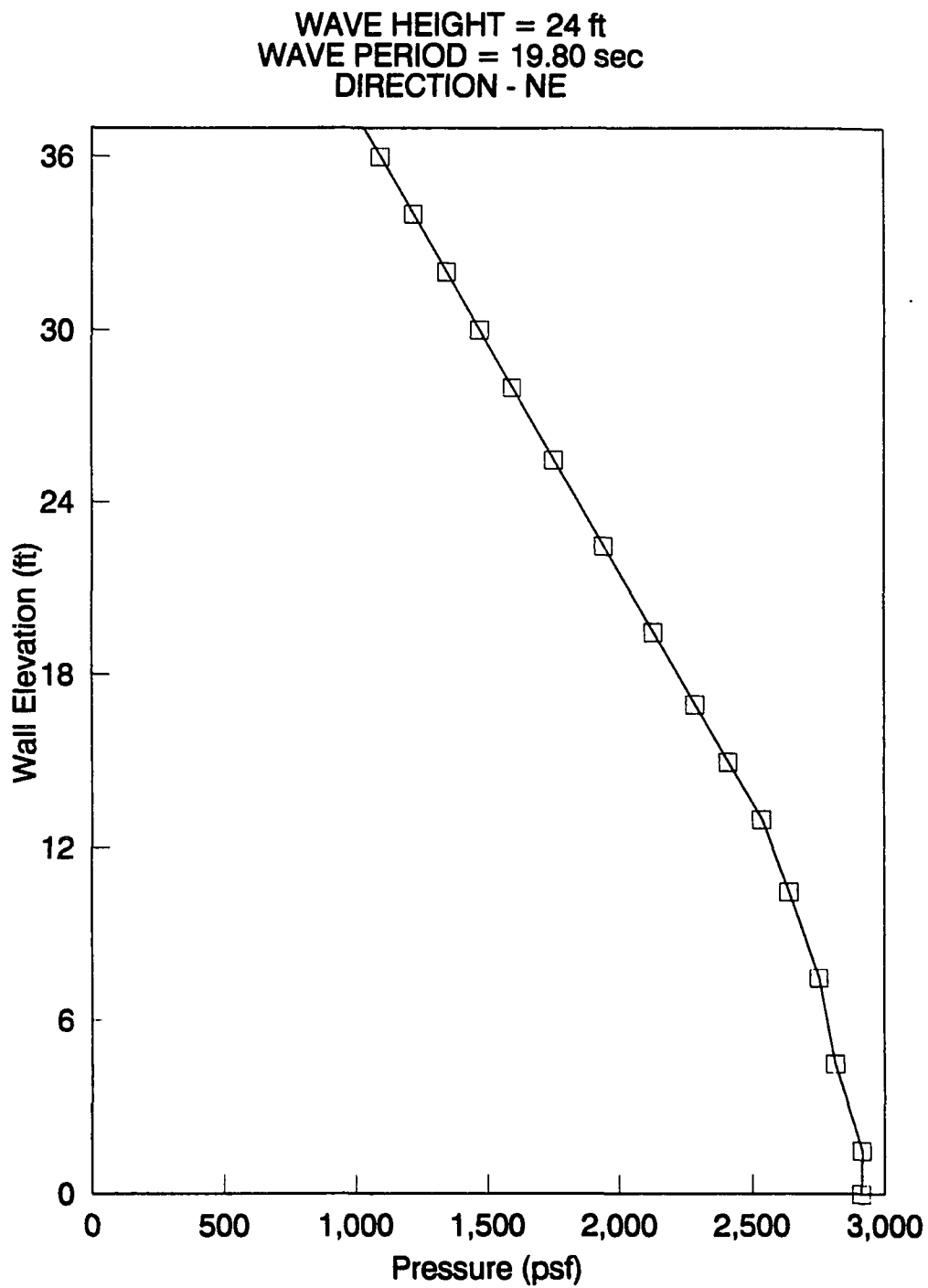WAVE PERIOD = 19.80 sec
DIRECTION - NE

Figure B.1   Typical variation of total pressure
(static+dynamic) along the elevation of the
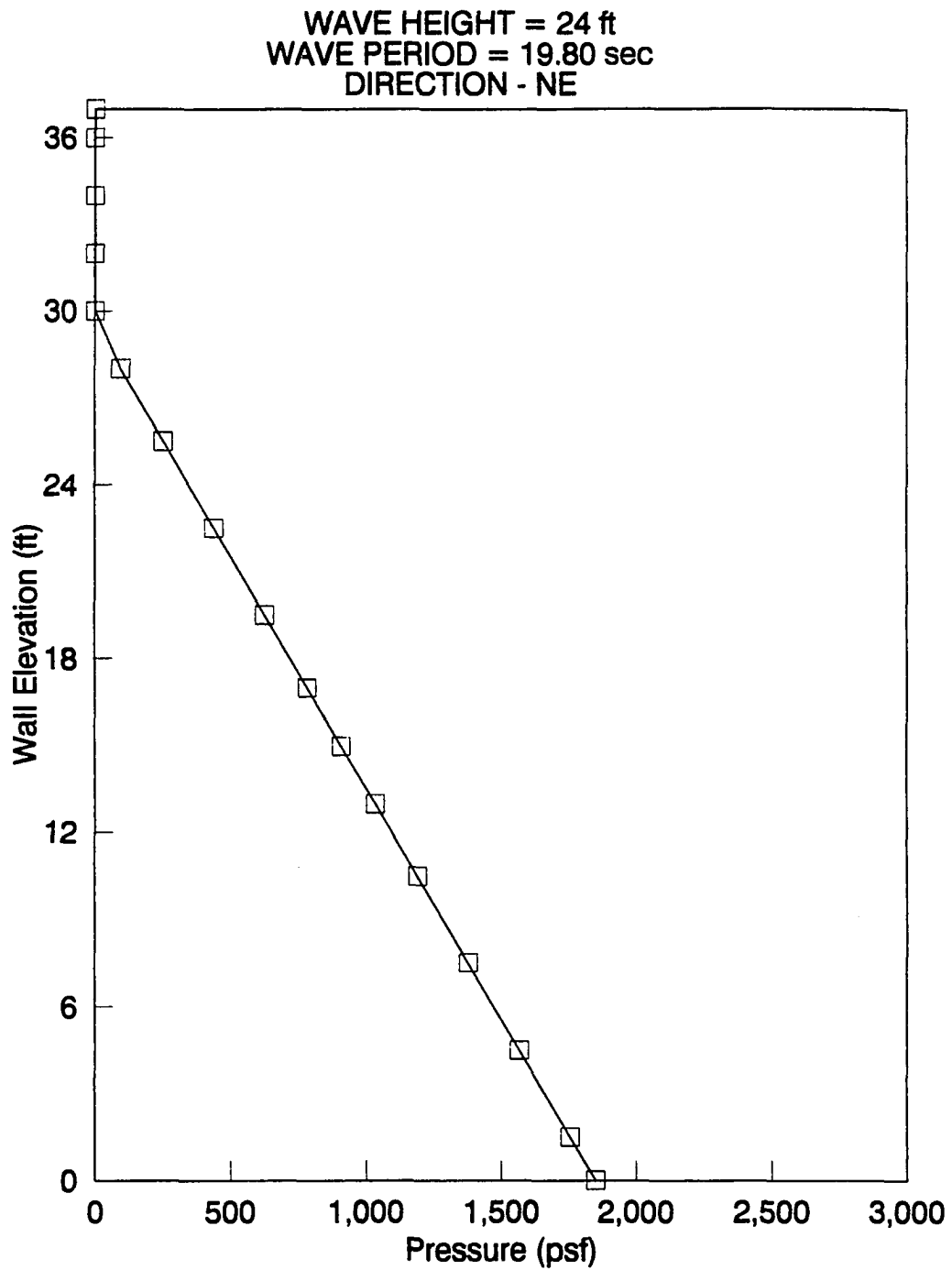breakwater - Cnoidal wave theory - wave peak.

Figure B.2 Typical variation of total pressure
(static+dynamic) along the elevation of the
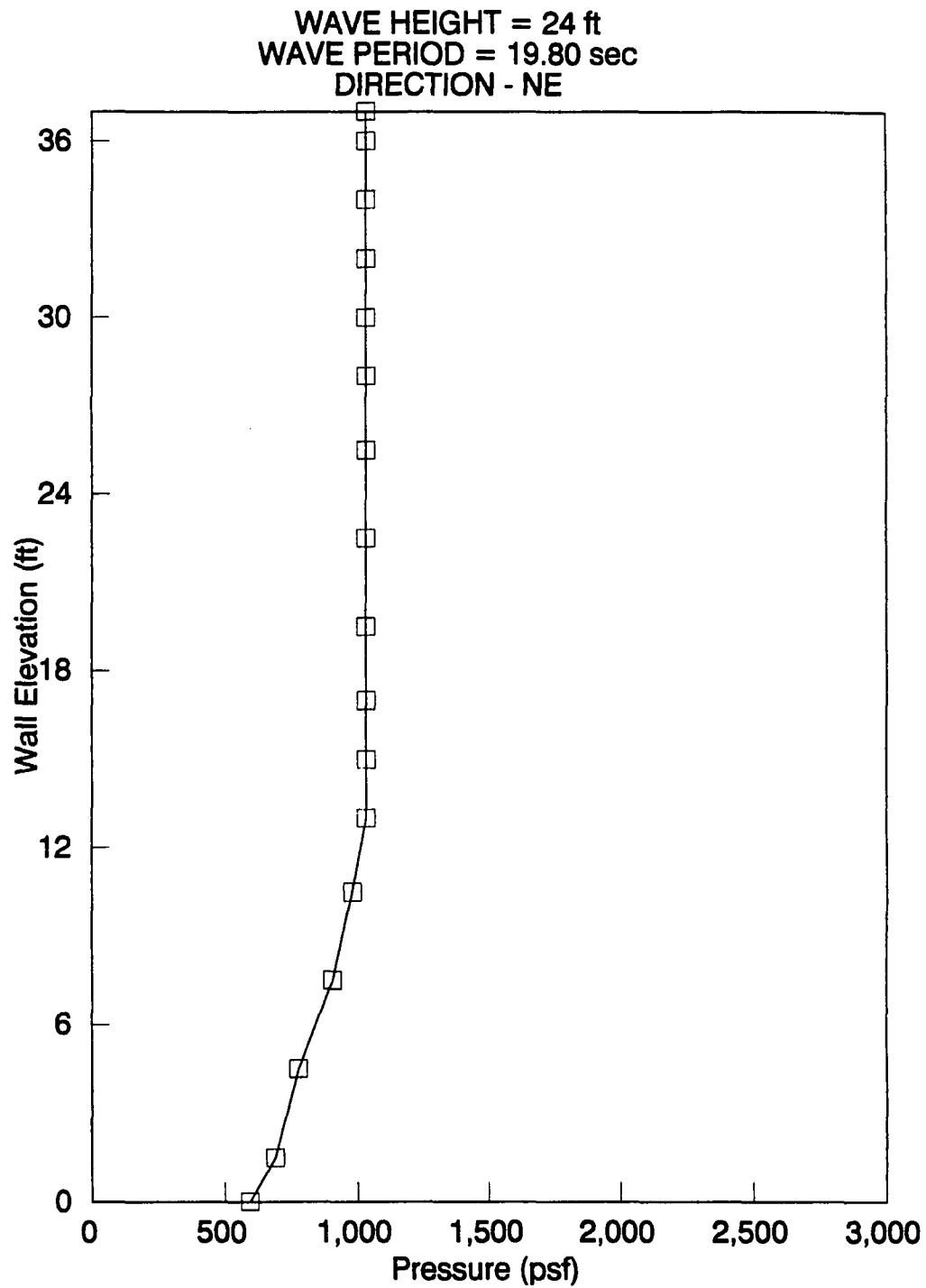breakwater - Cnoidal wave theory - wave trough.

Figure B.3 Typical applied pressure variation along the
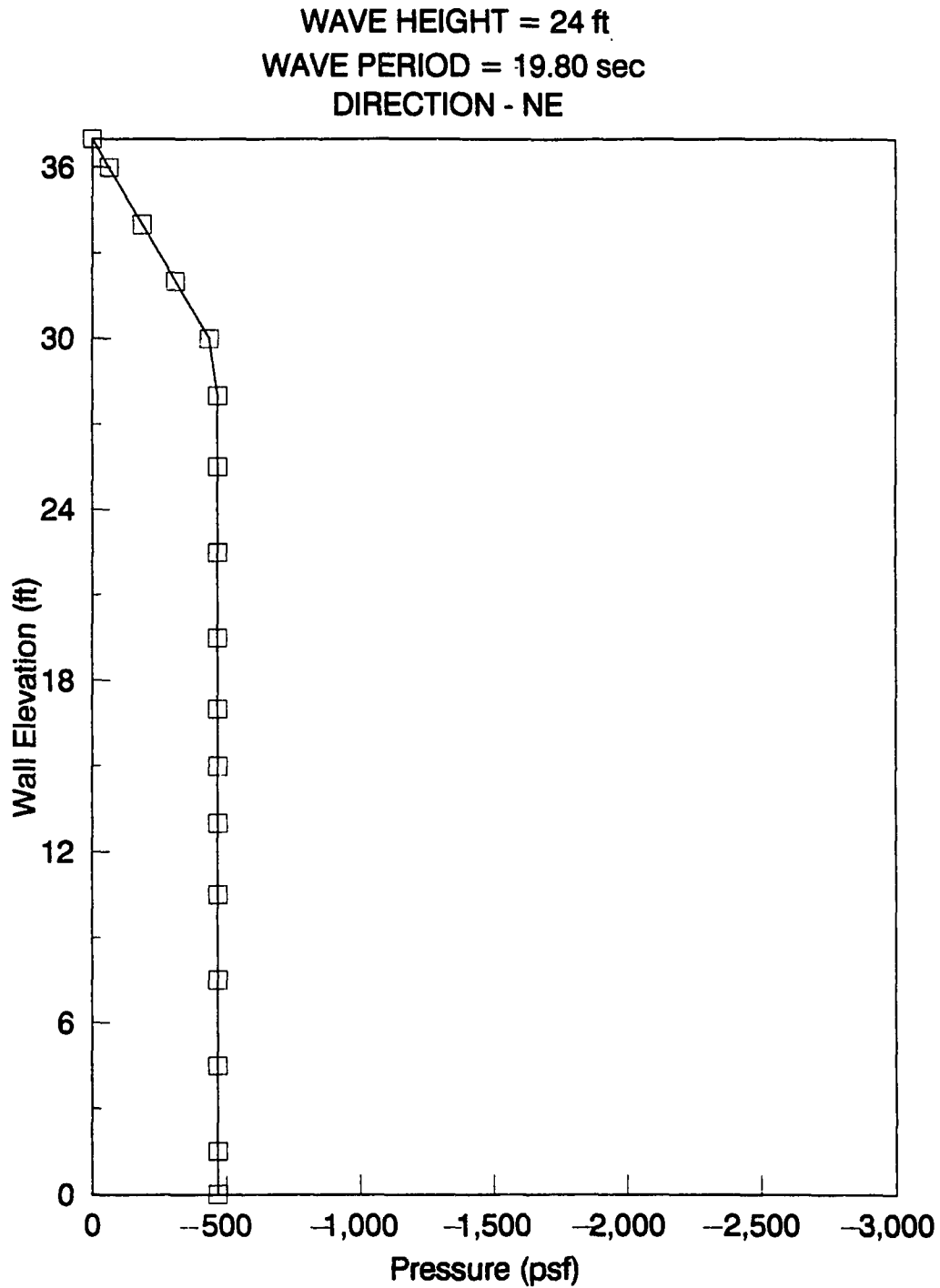elevation of breakwater - Cnoidal wave theory -
wave peak.

Figure B.4   Typical applied pressure variation along the
elevation of breakwater - Cnoidal wave theory -
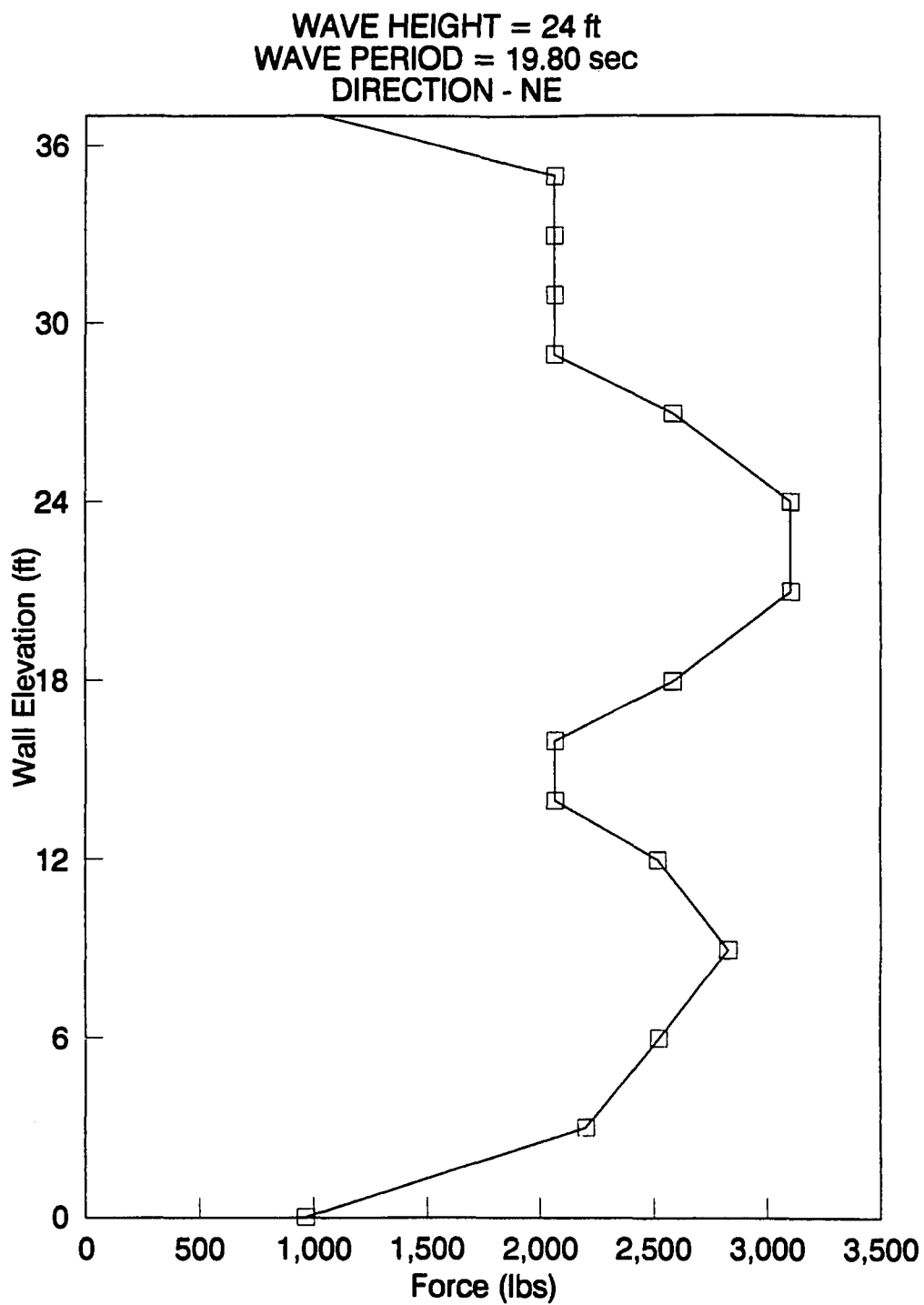wave trough.

Figure B.5   Typical nodal force variation along the elevation
of the breakwater - Cnoidal wave theory - wave
peak.

WAVE HEIGHT = 24 ft
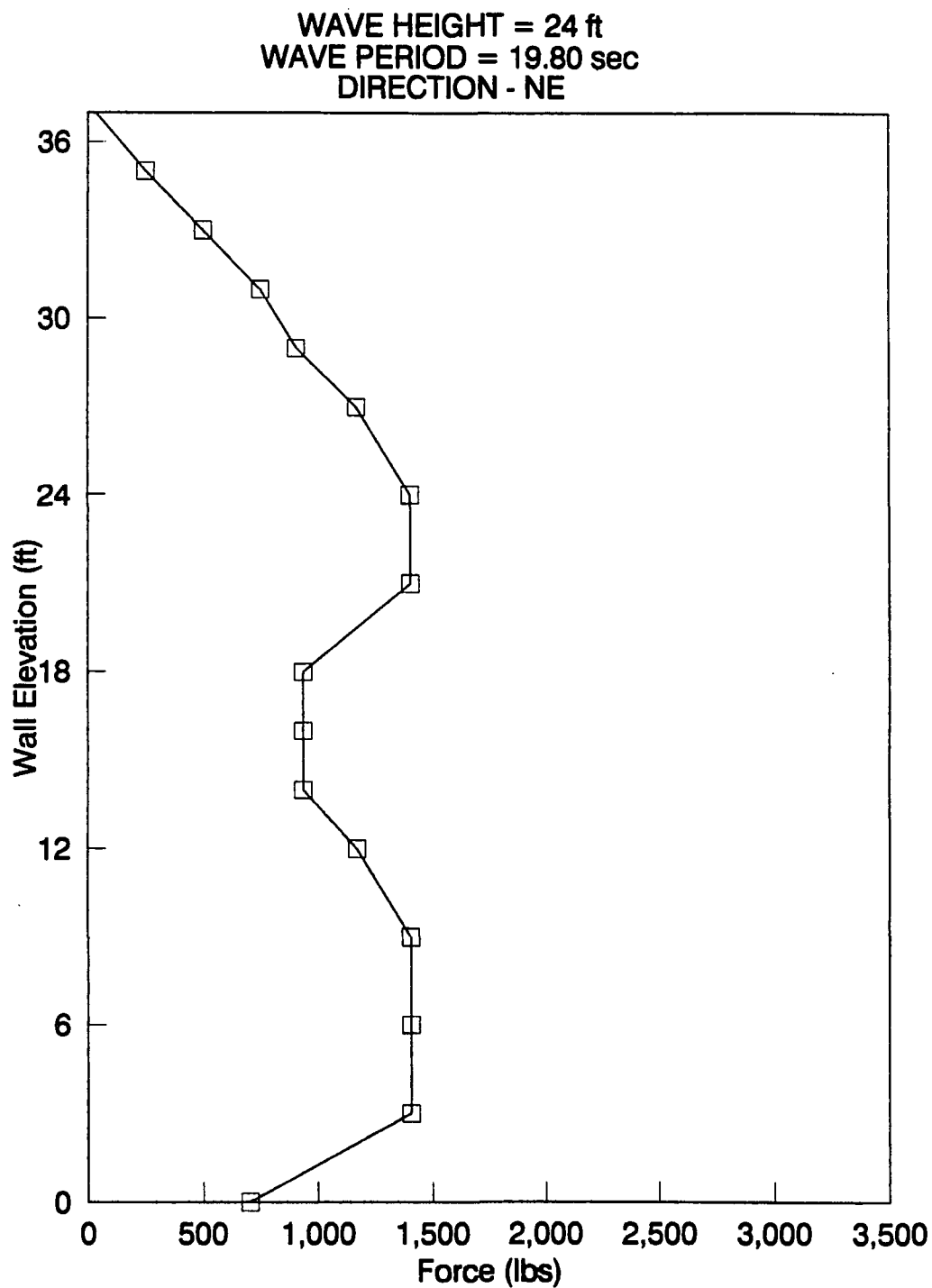WAVE PERIOD = 19.80 sec
DIRECTION - NE

Figure B.6   Typical nodal force variation along the elevation
of the breakwater - Cnoidal wave theory - wave
trough.